NASA TECHNICAL NOTE

NASA TN D-5942

NASA TN D-5942

WIND-TUNNEL INVESTIGATION OF A V/STOL TRANSPORT MODEL WITH FOUR POD-MOUNTED LIFT FANS

by William A. Newsom, Jr.

Langley Research Center
Hampton, Va. 23365

NATIONAL AERONAUTICS AND SPACE ADMINISTRATION • WASHINGTON, D. C. • AUGUST 1970

ERRATA

NASA Technical Note D-5942

WIND-TUNNEL INVESTIGATION OF A V/STOL TRANSPORT MODEL WITH FOUR POD-MOUNTED LIFT FANS

Completed 20 Oct 70 DW

By William A. Newsom, Jr.

August 1970

Because of incorrect plotting of figure 38, corrections to NASA TN D-5942 are necessary.

First page after the cover: The last three lines of the "Abstract" (item 16 in the standard title page) should be replaced by the following:

"terms of dynamic pressure and downwash factor, and there was a favorable sidewash effect."

Page 1: The last four lines of the "Summary" should be replaced by the following:

"planes in terms of dynamic pressure and downwash factor, and there was a favorable sidewash effect."

Page 13, fourth line from bottom: In the equation, $C_{n_{\beta,v}}$ should read $\Delta C_{n_{\beta,v}}$.

Pages 13 and 14: The last three lines on page 13 and the first three lines on page 14 should be replaced by the following:

"These data show a favorable sidewash at the tail and show that the sidewash was more favorable when the flap was deflected."

Page 14: The fifth result listed in the "Summary of Results" section should be replaced by the following:

"5. There was a favorable sidewash at the tail, and the sidewash was more favorable when the flap was deflected."

Page 76, figure 20(c): The scale values for C_{Y_β} (top plot) should be 0, -.02, and -.04 instead of 0, -.002, and -.004.

Page 102: Figure 38 should be replaced by the attached figure.

1. Report No.	2. Government Accession No.	3. Recipient's Catalog No.
NASA TN D-5942		

4. Title and Subtitle

WIND-TUNNEL INVESTIGATION OF A V/STOL TRANSPORT MODEL WITH FOUR POD-MOUNTED LIFT FANS

5. Report Date: August 1970

6. Performing Organization Code:

7. Author(s)

William A. Newsom, Jr.

8. Performing Organization Report No.: L-7199

9. Performing Organization Name and Address

NASA Langley Research Center
Hampton, Va. 23365

10. Work Unit No.: 721-01-11-03

11. Contract or Grant No.:

12. Sponsoring Agency Name and Address

National Aeronautics and Space Administration
Washington, D.C. 20546

13. Type of Report and Period Covered: Technical Note

14. Sponsoring Agency Code:

15. Supplementary Notes

16. Abstract

The investigation included force and moment measurements over a range of angles of attack and sideslip through the transition speed range for several power conditions. The static longitudinal, lateral, and directional stability characteristics were determined for several configurations, and lift-fan thrust performance was measured. The model had an increase in lift with increasing airspeed and showed lateral and directional stability for all test conditions but longitudinal stability for only the higher test speeds. Flow conditions at the tail for the powered-lift condition were similar to those of conventional airplanes in terms of dynamic pressure and downwash factor, ~~but~~ and there was a ~~decidedly adverse~~ favorable sidewash effect. ~~The adverse sidewash was compensated to a considerable extent, however, by the~~ fact that the model ~~was~~ about neutrally stable, ~~rather than unstable, with the vertical tail off~~.

17. Key Words (Suggested by Author(s))	18. Distribution Statement
Lift-fan V/STOL transport Transition tests	Unclassified – Unlimited

19. Security Classif. (of this report)	20. Security Classif. (of this page)	21. No. of Pages	22. Price*
Unclassified	Unclassified	102	$3.00

*For sale by the Clearinghouse for Federal Scientific and Technical Information
Springfield, Virginia 22151

WIND-TUNNEL INVESTIGATION OF A V/STOL TRANSPORT MODEL WITH FOUR POD-MOUNTED LIFT FANS

By William A. Newsom, Jr.
Langley Research Center

SUMMARY

Static force tests of a model of a transport type V/STOL airplane with four lift fans mounted in nacellelike pods on the wings have been made in the Langley full-scale tunnel. The investigation was made for a range of angles of attack and sideslip through the transition speed range. Power conditions included accelerating and decelerating as well as drag-trimmed flight. The model had an increase in lift with increasing airspeed in the transition speed range. This increase in lift was caused mainly by the normal increase in wing lift with increasing speed, but there was also some additional lift induced on the wing as a result of fan operation. The model showed lateral and directional stability for all test conditions but longitudinal stability for only the higher test speeds. The flow conditions at the tail for the powered-lift condition were similar to those of conventional airplanes in terms of dynamic pressure and downwash factor, ~~but~~ and there was a ~~decidedly~~ favorable ~~adverse~~ sidewash effect. ~~This adverse sidewash was compensated to a considerable extent, however, by the basic stability of the model, which was about neutrally stable, rather than unstable, with the vertical tail off.~~

INTRODUCTION

Lift-fan configurations are of considerable interest for possible application to future V/STOL transport airplanes. Large-scale wind-tunnel investigations of a number of different configurations have been made at the NASA Ames Research Center to determine static aerodynamic and stability and control characteristics; and the results of some of these investigations have been published in references 1 and 2. The NASA Langley Research Center is extending this research to determine the dynamic stability and control characteristics of a similar series of configurations. The Langley models are based on some later design studies than those used for the Ames models and are consequently not exact small-scale models of the large-scale Ames models although the general configurations are the same. As a preliminary step in such dynamic stability investigations, the static stability characteristics of the models are usually determined in conventional wind-tunnel tests. Since these static aerodynamic data are of value in themselves and show the

effects of some test variables not covered in the Ames investigations, the data from the first series of such tests (six-fan configuration) are presented in reference 3 and the data from the second series of tests are presented herein.

The particular configuration discussed herein has four lift fans mounted in nacelle-like pods on a relatively straight wing. Test conditions covered the transition speed range and a range of values of fan-exit-vane deflection, angle of attack, and angle of sideslip. The exit-vane deflections and tip-speed ratios included those for accelerating and decelerating transition conditions as well as those for drag-trimmed level flight. The investigation was made in the Langley full-scale tunnel, but was of fairly small scale because of the small size of the dynamic models.

SYMBOLS

All longitudinal forces and moments are referred to the stability-axis system, and lateral forces and moments are referred to the body-axis system.

A	aspect ratio, $\frac{b^2}{S_w}$
b	wing span, ft (m)
b_e	effective span factor
c	local wing chord, ft (m)
$\bar{c}$	mean aerodynamic chord, ft (m)
C_D	drag coefficient, $\frac{F_D}{qS_w}$
$C_{D,i}$	induced drag coefficient, $\frac{C_L{}^2}{e\pi A}$
C_L	lift coefficient, $\frac{F_L}{qS_w}$
C_l	rolling-moment coefficient, $\frac{M_X}{qS_w b}$
C_m	pitching-moment coefficient, $\frac{M_Y}{qS_w \bar{c}}$
C_n	yawing-moment coefficient, $\frac{M_Z}{qS_w b}$

C_Y	side-force coefficient, $\frac{F_Y}{qS_w}$
$C_{m_{i_t}}$	horizontal-tail-effectiveness parameter, $\frac{\partial C_m}{\partial i_t}$, per deg
C_{m_α}	static longitudinal stability parameter, $\frac{\partial C_m}{\partial \alpha}$, per deg
C_{l_β}	effective-dihedral parameter, $\frac{\Delta C_l}{\Delta \beta}$ for values of β of $\pm 5^o$, per deg
C_{n_β}	directional-stability parameter, $\frac{\Delta C_n}{\Delta \beta}$ for values of β of $\pm 5^o$, per deg
$\Delta C_{n_{\beta,v}}$	change in directional stability due to presence of vertical tail
$C_{n_{\delta_v}}$	change in yawing moment due to vertical-tail deflection, $\frac{\partial C_n}{\partial \delta_v}$, per deg
C_{Y_β}	lateral-stability parameter, $\frac{\Delta C_Y}{\Delta \beta}$ for values of β of $\pm 5^o$, per deg
e	span efficiency factor
F_D	drag, lb (N)
F_L	lift, lb (N)
F_Y	side force, lb (N)
i_t	horizontal-tail incidence, deg
M_X	rolling moment, ft-lb (m-N)
M_Y	pitching moment, ft-lb (m-N)
M_Z	yawing moment, ft-lb (m-N)
q	free-stream dynamic pressure, $\frac{1}{2}\rho V^2$, lb/ft^2 (N/m^2)
q_t	dynamic pressure at tail, lb/ft^2 (N/m^2)
r	fan radius, ft (m)

S_h horizontal-tail area, ft^2 (m^2)

S_v vertical-tail area, ft^2 (m^2)

S_w wing area, ft^2 (m^2)

T lift-fan thrust, lb (N)

T_s static lift-fan thrust, lb (N)

T_z vertical component of T, lb (N)

V free-stream tunnel velocity, ft/sec (m/sec)

V_j fan-exit velocity, ft/sec (m/sec)

α angle of attack, measured between free stream and fuselage reference line, deg

β angle of sideslip, measured between free stream and fuselage reference line, deg

β_v fan-exit-vane deflection, measured rearward from fan axis, deg

δ_f flap deflection, deg

δ_v vertical-tail deflection, deg

ϵ downwash angle, deg

μ tip-speed ratio, $\frac{V}{\omega r}$

ρ air density, slugs/ft^3 (kg/m^3)

σ sidewash angle, deg

ω fan rotational speed, rad/sec

$1 - \frac{d\epsilon}{d\alpha}$ downwash factor

$1 - \frac{d\sigma}{d\beta}$ sidewash factor

MODEL

Photographs of the model used in the investigation are shown as figure 1, and a three-view drawing of the model is shown in figure 2. A list of the geometric characteristics of the model is presented in table I. The four lift fans mounted in nacellelike pods on the wing were driven by compressed air exhausting through turbine blades fixed on the circumference of the rotor. Each fan (the direction of rotation of which is indicated in fig. 2) was provided with a set of louver-type vanes mounted across the fan exits as shown in figure 3. These exit vanes were used to redirect the fan slipstream for propulsion through the transition speed range. The wing trailing edge on each side of the fan pods was fitted with a single-slotted flap, as shown in figure 3(a). The T-mounted horizontal tail was fitted with tip extensions which permitted tests of two horizontal-tail sizes.

The pressure-survey rakes used in some of the tests were composed of 68 tubes per fan and were mounted beneath the two fans on the right-wing pod. The tubes were placed in the spaces between the fan exit vanes and were distributed evenly over the entire fan area so that an integration of the fan slipstream could be obtained. The survey rakes were constructed so that they could be moved and tilted as the fan exit vanes were deflected. With this feature it was possible to keep the survey tubes alined with the flow and in the same relative part of the slipstream.

TESTS

The investigation was made in the Langley full-scale tunnel. The forces and moments were measured on an internally mounted strain-gage balance. Power-on tests were run at certain nominal values of fan tip-speed ratio μ, as indicated by tachometers measuring the rotational speed of the model fans and the wind-tunnel drive motors. The actual values of μ for each test were later calculated for the presentation of the data from the value of free-stream dynamic pressure measured during the tests. Maximum free-stream velocity during the tests was approximately 73 ft/sec (22 m/sec), which corresponds to a Reynolds number of about 900 000 based on $\bar{c}$. Because of the small size of the model in relation to the size of the tunnel test chamber, no corrections to the data were necessary to account for tunnel effects.

Fan Thrust

The power-on tests of the model were made at a constant fan speed of 6960 rpm. In order to determine the fan thrust characteristics over the range of model operating conditions, fan-efflux wake surveys were made with the survey rakes mounted under the right-hand fans to obtain measurements of fan-slipstream dynamic pressure for tip-speed ratios (μ) ranging from 0 to about 0.3 at fan-exit-vane deflections (β_V) from 0^o to 45^o. The tests were made at angles of attack from -10^o to 20^o with flap deflected as well as undeflected.

Clean Configuration

Preliminary tests were made of the model in the clean (fans covered) configuration to determine characteristics of the configurations for the conventional flight mode. The tests covered both tail-off and tail-on conditions with $\delta_f = 0^o$ and $\delta_f = 40^o$ for an angle-of-attack range of -10^o to 25^o.

Transition Configuration

Longitudinal aerodynamic characteristics.- Tests were made for a range of angles of attack from -10^o to 25^o for nominal tip-speed ratios of 0.10 to 0.30 with fan-exit-vane deflections of 0^o to 45^o to determine the lift, drag, and pitching-moment characteristics. Tests of the model with the tail on were made to determine the effects of flap deflection and horizontal-tail size on the longitudinal stability characteristics. Tests of the model with the tail off were made for both $\delta_f = 0^o$ and $\delta_f = 40^o$ over the complete test range to provide data for analysis. Horizontal-tail incidence in the tail-on tests generally was set to give approximately zero tail lift, as indicated by comparison of the pitching moments with those determined in the tail-off tests. A limited number of tests were made over a range of horizontal-tail incidence angles from 0^o to 20^o, however, to obtain data for determination of the downwash and dynamic-pressure characteristics in the vicinity of the horizontal tail.

Lateral-directional stability characteristics.- Tests were made at $\beta = \pm 5^o$ over an angle-of-attack range from -10^o to 25^o to determine the static lateral-directional stability characteristics of the model. The free-stream tunnel velocity was selected to give $F_D/F_L = 0$ (i.e., drag trimmed) at $\alpha = 0^o$, $F_D/F_L = -0.15$ at $\alpha = 0^o$, $F_D/F_L = 0.15$ at $\alpha = 0^o$, or drag trimmed at $\alpha = 10^o$ for the various values of β_V. Tests were made with $\delta_f = 40^o$ for both tail-on and tail-off conditions. A limited number of tests were made to determine the linearity of the lateral-directional characteristics with sideslip angle. These tests were made for a range of sideslip angles from -20^o to 20^o with drag trimmed at both $\alpha = 0^o$ and $\alpha = 10^o$. To obtain data for analysis of the sidewash at

the tail, a limited number of tests were made in which the deflection angle of the vertical tail was varied from -20° to 20°.

RESULTS

All forces and moments are referred to the assumed center-of-gravity location ($0.384\bar{c}$). This center-of-gravity location is at the center of thrust of the fans for the hovering condition. (See fig. 2.) An index to the data figures is given in table II.

Fan Characteristics

Measurements of the fan thrust obtained by pressure-survey rakes mounted under the fans in the right wing pod are presented in figures 4 to 6. The data of figure 4 show the static thrust of the fans for exit-vane deflections from 0° to 45°. It should be noted that the fan thrust shown in figure 4 is that measured by the surveys of the fan efflux with the survey tubes alined with the fan exit vanes and is not the fan lift component. To determine the accuracy of the thrust measured in these surveys, the data for $\beta_V = 0^{\circ}$ and zero airspeed were compared with the lift of the complete model as measured by a strain-gage balance. These two measurements agreed within 2 percent. The data of figure 4 show slight changes of fan thrust as the vanes are deflected but the thrust of the front fan generally increases whereas that of the rear fan decreases.

The data of figures 5 and 6 show variation of fan thrust for tip-speed ratios ranging from 0 to about 0.3 for values of β_V from 0° to 45°. In general, the data show the usual steady loss of thrust with increasing forward speed that has been indicated by the data for the large-scale model of reference 2 and the small-scale model of reference 3. The rear-fan thrust shows the slight increase at the lower speeds that all fans experienced in reference 3. The front fan, however, possibly due to its location ahead of the wing and a different inflow pattern shows a decrease in thrust at almost all speeds. This difference in variation of thrust with forward speed was also shown in unpublished data, obtained at the Ames Research Center, where the rear fan thrust remained constant up to almost $\mu = 0.30$ but the front fan thrust decreased steadily to a 20-percent loss in thrust at $\mu = 0.30$. Figure 6 indicates a somewhat lower amount of thrust for the rear fan when the flap is deflected. This result is probably caused by the effects of inflow changes on fan thrust.

All power-on data presented are shown in terms of the lift-fan tip-speed ratio μ, but the relationship between the tip-speed ratio and the ratio of the free-stream velocity to the fan-exit velocity is presented in figure 7 so that the data may be also analyzed in terms of V/V_j.

Clean Configuration

The results of the tests made to determine the model characteristics in the conventional flight mode are presented in figures 8 and 9. These figures show the basic stability characteristics of the model with fans inoperative and covered, and thus with no fan flow to affect the aerodynamic characteristics of the model.

Longitudinal stability characteristics.- Figure 8 shows that with the small horizontal-tail configuration $S_h/S_W = 0.25$, which was used for most of the tests, the model was longitudinally unstable. The tail configuration had been selected originally during the model tests of reference 3 but the present model configuration evidently had substantially different aerodynamic characteristics. With the tip extensions added to the horizontal tail, longitudinal stability was attained but with a static margin of only 2 percent of the mean aerodynamic chord.

Lateral-directional stability characteristics.- Figure 9 shows that the model had static lateral-directional stability below the stall with the vertical tail $\left(S_V/S_W = 0.15\right)$ used in the tests. Deflecting the flap, as shown by the data of figure 9(b), had a small effect on the static lateral-directional stability of the model.

Transition Configuration

Longitudinal aerodynamic characteristics.- The data from the longitudinal tests for the transition configuration are presented in figures 10 to 18. Detailed inspection of these figures may show some discrepancies in the levels of C_L, C_D, and C_m for nominally similar conditions or closely comparable conditions. This situation results from small inaccuracies in setting airspeed (or μ) and vane angle β_V because small changes in β_V cause large changes in C_D and because small differences in μ cause large changes in all three aerodynamic coefficients $\left(C_L,\ C_D, \text{ and } C_m\right)$, particularly at low values of μ. The accuracy with which μ was set is indicated by the scatter in the actual values for a given nominal condition shown in figures 10 to 15, and β_V could be set only to an accuracy of about $\pm 1^\circ$. The inaccuracies in setting the values of μ and β_V change the absolute values of the aerodynamic coefficients significantly but do not cause important changes in the variations of these coefficients with α, i_t, and μ on which analysis of stability and control characteristics is based.

Figures 10 to 13 present the results of tests made with the horizontal tail off to determine the longitudinal aerodynamic chararacteristics for various fan-exit-vane deflection angles over a range of tip-speed ratios. Figure 10 (flap-undeflected configuration) and figure 11 (flap-deflected configuration) show the data as a function of angle of attack. Data for airplane configurations having lift fans for propulsion are frequently presented as a function of tip-speed ratio for $\alpha = 0^\circ$; so figure 12 (flap undeflected) and

figure 13 (flap deflected) present the data in this form. These figures were based on the data of figures 10 and 11.

The results presented in figures 14 to 18 show the longitudinal aerodynamic characteristics of the model with the horizontal tail on. The tests of figure 14 (flap undeflected) and figure 15 (flap deflected), made with the small horizontal tail, cover a wide range of vane angles and tip-speed ratios and are useful for examining stability for a wide range of accelerating and decelerating conditions. No effort was made to determine the optimum tail incidence for each test condition; but, as pointed out previously, for each value of β_V, the tail incidence was set to give approximately zero tail lift at the condition of drag trimmed for zero angle of attack to try to avoid tail stall and its effects on longitudinal stability. These data, which were obtained with the small horizontal tail $\left(S_h/S_W = 0.25\right)$, show that the model was longitudinally unstable for all test conditions, just as it was for the clean configuration.

The data presented in figure 16 cover tests made through the transition speed range with drag trimmed at $\alpha = 0^O$ with the larger $\left(S_h/S_W = 0.30\right)$ horizontal tail on the model. These data show that the model became neutrally stable or slightly stable at $\beta_V = 30^O$.

The effectiveness of the horizontal tail in trimming the model is shown in figures 17 (flap undeflected) and figure 18 (flap deflected). Both sets of data were obtained with the model with the small tail for conditions of drag trimmed at $\alpha = 0^O$.

Lateral-directional stability characteristics.- Figure 19 presents the results of the tests made with tails off to determine the static lateral-directional stability characteristics at each fan-exit-vane deflection angle through the transition speed range. These data are for drag trimmed at $\alpha = 0^O$.

The results presented in figures 20 to 23 show the lateral-directional stability and trim characteristics of the model with the tails on. Figure 20 presents data for conditions of accelerating and decelerating as well as drag-trimmed flight. In general, the model was laterally and directionally stable over the complete test angle-of-attack range for all power conditions.

The results of tests made to show the linearity of the lateral data are presented in figure 21. These data obtained with drag trimmed at $\alpha = 0^O$ and at $\alpha = 10^O$ show the variation of rolling-moment, yawing-moment, and side-force coefficients with sideslip angle for various values of β_V through the transition speed range. Reasonably linear variations of these quantities with β are indicated.

The data of figures 22 and 23 are from tests made with drag trimmed to provide basic data for analysis of the sidewash and dynamic pressure at the tail. The horizontal tail was mounted with $i_t = 0^O$ for all tail-on tests.

ANALYSIS OF DATA

The results of the present tests for a small-scale model are compared in several respects with the unpublished results of an Ames investigation. The Ames model, as shown in figure 24, was a large-scale model of a somewhat similar configuration with four pod-mounted fans. The geometry of the two models differed in many respects, since the configurations represented different designs; therefore, the results would not be expected to compare exactly but might be expected to show similar trends. The models differed particularly in aspect ratio, wing sweep, fan location, airfoil section, and flap size.

Lift and Drag Characteristics

Figure 25 shows the variation of lift and drag through the transition speed range for the present small-scale model and the large-scale Ames model. Most of the data are for $\beta_V = 0^O$ but small-scale model data are also presented to show the change for a drag-trimmed condition. Three pertinent remarks can be made from the data of figure 25. First, all the data show an increase in lift with increasing forward speed, as might be expected. Second, when the fan exit vanes are deflected rearward to trim the model in drag, there is a substantial loss in lift at the higher vane angles required for higher forward speeds. And third, the present small-scale model had a higher value of the ratio of lift to static thrust in the transition speed range than did the large-scale model. The higher lift of the smaller model resulted mainly from the fact that it had much larger flaps than the larger model. A comparison of the fan-thrust characteristics of the two models is shown in figure 26. These data show that the fan-thrust ratio T/T_S for the present small-scale model is higher than that for the large-scale model through the speed range. This difference in fan thrust would account for a small part of the difference in lift shown in figure 25. As noted in reference 3, the fact that the thrust of the present small-scale fans increases with increase in speed in the low velocity range probably indicates that they are not properly designed for static thrust and that a small amount of forward speed improves their operation. The fan-exit-velocity surveys indicated that forward speed probably eliminated a stalled flow condition at the roots of the fan blades.

A lift analysis for the small-scale model in terms of fan thrust, power-off lift, and total lift is presented in figures 27 and 28 as a function of the ratio of free-stream velocity to fan-exit velocity for the configurations with $\delta_f = 0^O$ and $\delta_f = 40^O$. The data of figure 27 are for an untrimmed condition of $\beta_V = 0^O$ and show the induced lift as the difference between the measured total lift and the curve constructed from the sum of the power-off lift and the pure fan-thrust lift. For example, at $V/V_j = 0.4$ for the configuration with $\delta_f = 40^O$, the induced lift was about 0.4 times the fan thrust. The data of figure 28 are similar to those of figure 27 except that they are for drag-trimmed test

conditions. This figure shows that little or no induced lift is actually achieved in this condition of steady level flight.

A comparison of the additional wing lift induced by the operation of the fans for the present model and the large-scale model is shown in figure 29. The induced lift for the present model is generally less than that for the large-scale model. This difference probably occurs largely because the present model had less wing area ahead of the rear fan than did the large-scale model; also, the front fan was closer to the wing leading edge and thus would cause more downwash on the wing than the front fan of the large-scale model.

Figure 30 shows a comparison of the lift characteristics of the present model with those of the model of reference 3 which had six fans spread spanwise across the wing. The comparison is for the drag-trimmed condition. It is apparent that the lift of the two configurations is very similar. This result might be considered surprising since one might anticipate that the six-fan configuration would have a more uniform spanwise distribution of lift and would be more efficient. Apparently the fans of the present model produce no net induced lift on the wing but they do not interfere with the operation of the flap; therefore, the total lift is about equal to the fan lift plus the basic lift of the wing and flaps. As explained in reference 3, the fans of the six-fan model induced lift on the wing but interfered with the operation of the flap to such an extent that they negated the induced lift; therefore, in that case too, the total lift was equal to the fan lift plus the basic lift of the wing and flaps.

Figure 31 shows how efficiently the present four-fan configuration produces lift by presenting the variation with speed of the thrust required for drag-trimmed level flight over the transition speed range. The experimental data are compared with the thrust required as calculated from the momentum considerations as outlined in reference 4. Two calculated curves are shown – one for an effective span equal to the wing span, which is something of an ideal condition, and one for an effective span equal to 0.70b, which corresponds to a value of airplane span efficiency factor $e = 0.50$ in the usual induced-drag equation $C_{D,i} = \frac{C_L^2}{e\pi A}$. The thrust required for the present model is about the same as that for the condition of an effective span equal to 0.70b; and, the effective span is low compared with that of the system described in reference 5, where the effective span was approximately equal to the geometric span. A possible reason for this result is suggested by the discussion of span loading in references 6 and 7.

The lift and drag characteristics of the configuration also determine to a considerable extent the technique that would be required to achieve the transition from lift-fan-supported flight to completely wing-supported flight. As shown in figure 18(d), the model would have a lift coefficient of 2.0 at $\alpha = 0^o$ with drag trimmed at $\beta_v = 45^o$ (maximum

vane angle) with flap deflected. If the lift fans were inoperative and covered, it would be necessary, as shown by the data in figure 8(b), to increase the angle of attack to about 11.5° in order to attain the lift needed for steady level flight. At that attitude, the configuration would be almost at the stall angle (about 3° below) and operating at only about 102 percent of the stall speed. The transition could be accomplished much more successfully with the configuration having the flap undeflected. For example, figure 17(d) shows that a lift coefficient of 0.8 at $\alpha = 0^\circ$ would be obtained for $\beta_V = 45^\circ$ with drag trimmed, flap undeflected. If the lift fans were inoperative and covered, it would be necessary, as shown by the data in figure 8(a), to increase the angle of attack to about 6.5° in order to attain the lift needed for steady level flight. At this attitude the configuration would still be well below the stall angle (about 15° below) and operating at an airspeed of about 140 percent of the stall speed. Closer analysis of the data could possibly reveal an optimum transition technique involving a combination of flap-position configurations.

Longitudinal Stability

Figure 32 presents curves of the variation of model pitching-moment coefficient with angle of attack for drag-trimmed test conditions through the transition speed range. The data, which were taken from figures 16(b) and 18, show that the model with the small horizontal tail was unstable for the entire transition speed range. However, even with the large horizontal tail, stability was achieved only for $\beta_V = 30^\circ$ and $\beta_V = 45^\circ$.

Figures 33 to 36 present information pertinent to longitudinal stability and trim. Figure 33 shows the downwash angles at the horizontal tail as determined from the tail incidence required to produce the same pitching moment as that for the tail-off condition. Since the tail must produce a nose-down moment for trim, it is evident that a variable-incidence tail or other moment-producing device must be used.

One possible stability problem that may be encountered when the horizontal tail is used to reduce the untrimmed values of pitching moment is discussed in reference 8 and illustrated in figure 34. The data at the top of figure 34(a) indicate the variation with airspeed of the untrimmed pitching moment (tail off) for various values of β_V at an angle of attack of 0° and for a value of lift of 80 pounds (355 N) at the value of forward speed corresponding to drag trim for each value of β_V. The dashed line intersects each curve at the value of velocity for drag trim at $\alpha = 0^\circ$. As can be seen, positive increments of pitching moment are produced by an increase in speed from the drag-trimmed speed at constant power for each value of β_V. As discussed in reference 8, if the configuration were trimmed with a device producing a moment which is invariant with airspeed (such as a reaction jet), the positive variations of moment with velocity indicate that the configuration will be stable with respect to speed. On the other hand, if a horizontal tail is used to reduce the untrimmed pitching moments, increasingly negative

pitching moments are produced by the tail with increase in airspeed. If the variation of the negative contribution of the tail to pitching moment with speed is larger than the positive variation of the tail-off configuration, speed instability will result. Tail contributions have been calculated and added to the tail-off data of figure 34(a) to give the tail-on characteristics shown at the bottom of the figure. For each value of β_V, the largest tail incidence that could be used without stalling the tail was assumed in the calculations. These calculated tail-on data show that the resulting configuration is unstable with respect to speed. The data of figure 34(b) indicate that a slightly worse situation exists for the flap-deflected configuration since the tail-off variation of pitching moment with speed is about zero or slightly negative. Speed instability combinated with low values of angle-of-attack stability can result in dynamic longitudinal instability and poor flight characteristics as discussed in reference 8.

Figure 35 shows the variation of downwash factor with fan-exit-vane deflection as determined from tail-incidence tests. These data show that the value of $1 - \frac{d\epsilon}{d\alpha}$ was approximately the same as the value considered normal for conventional airplanes (i.e., 0.5). Figure 36 shows the variation of dynamic pressure at the horizontal tail for $\alpha = 0^o$ as determined from

$$\frac{q_t}{q} = \frac{\left(C_{m_{i_t}}\right)_{\text{power on}}}{\left(C_{m_{i_t}}\right)_{\text{power off}}}$$

These data show that the dynamic pressure at the tail was constant through the transition speed range and was about 20 percent less than the free-stream value.

Lateral-Directional Stability

Figure 37 shows the static lateral and directional stability through the transition speed range. The plots were constructed from the data of figure 20 and show that the model was stable for all test conditions and that the vertical tail gives a degree of directional stability which has proved to be generally satisfactory in the past.

Figure 38 shows the variation of the sidewash factor $1 - \frac{d\sigma}{d\beta}$ at the vertical tail with β_V for drag-trimmed flight at various speeds. These sidewash data were determined from the relative effectiveness of the vertical tail in sideslip and incidence; that is,

$$1 - \frac{d\sigma}{d\beta} = \frac{\Delta C_{n_{\beta,v}}}{C_{n_{\delta_v}}}$$

These data show ~~adverse~~ favorable sidewash at the tail and show that the sidewash was more ~~adverse~~ favorable when the flap was deflected. ~~for the flap-deflected condition than for the flap-undeflected condition. For the complete model, however, this adverse sidewash and consequent low vertical-tail~~

~~effectiveness were compensated, to some extent, because the model was much less unstable with the tail off than might have been expected. In fact, it was about neutrally stable with the tail off.~~

SUMMARY OF RESULTS

Static force tests of a model of a transport-type V/STOL airplane with four lift fans mounted in nacellelike pods on the wings yielded the following results:

1. The model had an increase in lift with increasing airspeed in the transition speed range. This increase in lift with increasing speed resulted mainly from the normal increase in wing lift with increasing speed, but there was also some induced lift on the wing as a result of fan operation.

2. The model with the small horizontal tail was longitudinally unstable for the entire transition speed range. Even with the large horizontal tail, the model showed static longitudinal stability $\left(-C_{m_\alpha}\right)$ only at the higher test speeds.

3. The values of dynamic pressure and downwash factor at the tail in the powered-lift condition were approximately the same as those for conventional airplanes; that is, the dynamic pressure was generally within about 20 percent of the free-stream value, and the value of downwash factor $\left(1 - \frac{d\epsilon}{d\alpha}\right)$ was about 0.5.

4. The model had a level of static lateral and directional stability which has in the past proved generally satisfactory.

5. There was a ~~decidedly adverse~~ favorable sidewash at the tail, ~~which was compensated somewhat because the model with the vertical tail off was much less unstable than might be expected. In fact, it was about neutrally stable with the tail off.~~ and the sidewash was more favorable when the flap was deflected.

Langley Research Center,
National Aeronautics and Space Administration,
Hampton, Va., June 12, 1970.

REFERENCES

1. Hall, Leo P.; Hickey, David H.; and Kirk, Jerry V.: Aerodynamic Characteristics of a Large-Scale V/STOL Transport Model With Lift and Lift-Cruise Fans. NASA TN D-4092, 1967.

2. Kirk, Jerry V.; Hodder, Brent K.; and Hall, Leo P.: Large-Scale Wind-Tunnel Investigation of a V/STOL Transport Model With Wing-Mounted Lift Fans and Fuselage-Mounted Lift-Cruise Engines for Propulsion. NASA TN D-4233, 1967.

3. Newsom, William A., Jr.; and Moore, Frederick L.: Wind-Tunnel Investigation of a V/STOL Transport Model With Six Wing-Mounted Lift Fans. NASA TN D-5695, 1970.

4. Heyson, Harry H.: Nomographic Solution of the Momentum Equation for VTOL-STOL Aircraft. NASA TN D-814, 1961.

5. Newsom, William A., Jr.: Wind-Tunnel Investigation of a Deflected-Slipstream Cruise-Fan V/STOL Aircraft Wing. NASA TN D-4262, 1967.

6. Campbell, John Paul: Vertical Takeoff and Landing Aircraft. Macmillan Co., c.1962, pp. 56, 57.

7. Kuhn, R. E.; and McKinney, M. O.: Factors Involved in Selection of VTOL Transport Configuration. [Preprint] 337D, Soc. Automot. Eng., 1961.

8. Kelly, Mark W.; and Holzhauser, Curt A.: Aerodynamic Characteristics of Subsonic V/STOL Transport Airplanes. Pap. No. 61-105-1799, Inst. Aerosp. Sci., June 1961.

TABLE I.- GEOMETRIC CHARACTERISTICS OF THE MODEL

Fuselage:	
Length	7.33 ft (223.4 cm)
Cross-sectional area, maximum	1.34 ft^2 (1244.9 cm^2)
Wing:	
Area	13.85 ft^2 (12 866.6 cm^2)
Span	7.48 ft (228.0 cm)
Aspect ratio	4.05
Mean aerodynamic chord	1.89 ft (57.6 cm)
Tip chord	1.39 ft (42.4 cm)
Root chord	2.32 ft (70.7 cm)
Taper ratio	0.60
Dihedral angle	0^o
Thickness ratio	0.15
Airfoil section	Clark YH
Aileron, each:	
Chord	0.20c
Area	0.37 ft^2 (343.7 cm^2)
Flap, each:	
Type	Single slotted
Chord	0.30c
Span:	
Inboard section	0.88 ft (26.7 cm)
Outboard section	1.35 ft (41.1 cm)
Fan:	
Diameter	0.667 ft (20.3 cm)
Exit vane chord	0.092 ft (2.8 cm)
Number of vanes	9

TABLE I.- GEOMETRIC CHARACTERISTICS OF THE MODEL – Concluded

	Small	Large
Vertical tail:		
Area	2.08 ft^2 (1932.3 cm^2)	
Span	1.60 ft (48.8 cm)	
Aspect ratio	1.23	
Root chord	1.63 ft (49.7 cm)	
Tip chord	0.98 ft (29.9 cm)	
Airfoil section	NACA 0012	
Rudder:		
Chord	0.29 ft (8.8 cm)	
Span	1.52 ft (46.3 cm)	
Tail length, center of gravity to 0.25 mean aerodynamic chord	3.10 ft (94.5 cm)	
Horizontal tail:		
Area	3.46 ft^2 (3214.3 cm^2)	4.16 ft^2 (3864.6 cm^2)
Span	3.80 ft (115.8 cm)	4.83 ft (147.2 cm)
Aspect ratio	4.18	5.60
Root chord	1.17 ft (35.7 cm)	1.17 ft (35.7 cm)
Tip chord	0.70 ft (21.3 cm)	0.55 ft (16.8 cm)
Taper ratio	0.58	0.47
Dihedral angle	0^o	0^o
Pivot position	0.25$\bar{c}$	0.39 root chord
Airfoil section	NACA 0012	NACA 0012
Elevator, each:		
Root chord	0.35 ft (10.7 cm)	0.35 ft (10.7 cm)
Tip chord	0.21 ft (6.4 cm)	0.21 ft (6.4 cm)
Span	1.86 ft (56.7 cm)	1.86 ft (56.7 cm)
Tail length, center of gravity to 0.25 mean aerodynamic chord	3.38 ft (103.0 cm)	3.43 ft (104.5 cm)

TABLE II.- INDEX TO BASIC DATA FIGURES

Type of data	Figure	F_D/F_L	δ_f, deg	S_h/S_w	S_v/S_w
Fan thrust	4	Variable	0	Off	Off
	5	↓	0	↓	↓
	6		40		
Longitudinal	8(a)	Power off	0	Variable	0.15
	8(b)	Power off	40	Variable	.15
Lateral-directional	9(a)	Power off	0	Off	Variable
	9(b)	Power off	40	Off	Variable
Longitudinal	10	Variable	0	Off	0.15
	11	↓	40	↓	↓
	12		0		
	13		40		
	14		0	0.25	
	15		40	.25	
	16(a)	0	0	0.30	0.15
	16(b)	↓	40	.30	.15
	17		0	.25	.15
	18		40	.25	.15
Lateral-directional	19	0	40	Off	Off
	20	0, -0.15, 0.15	40	0.25	0.15
	21	0	40	↓	↓
	22	↓	0		
	23		40		

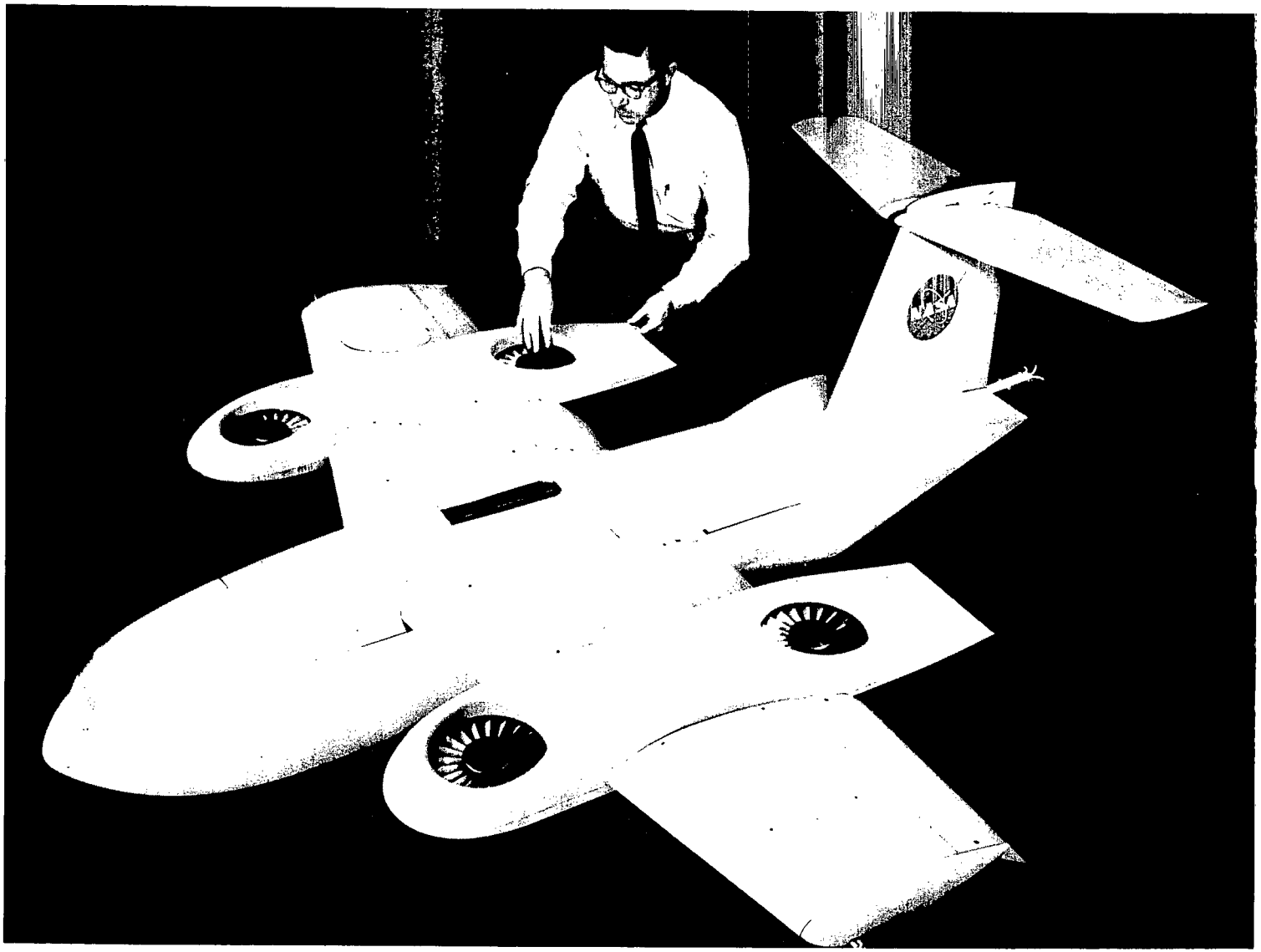

(a) Three-quarter front view. L-67-7754

Figure 1.- Photographs of model.

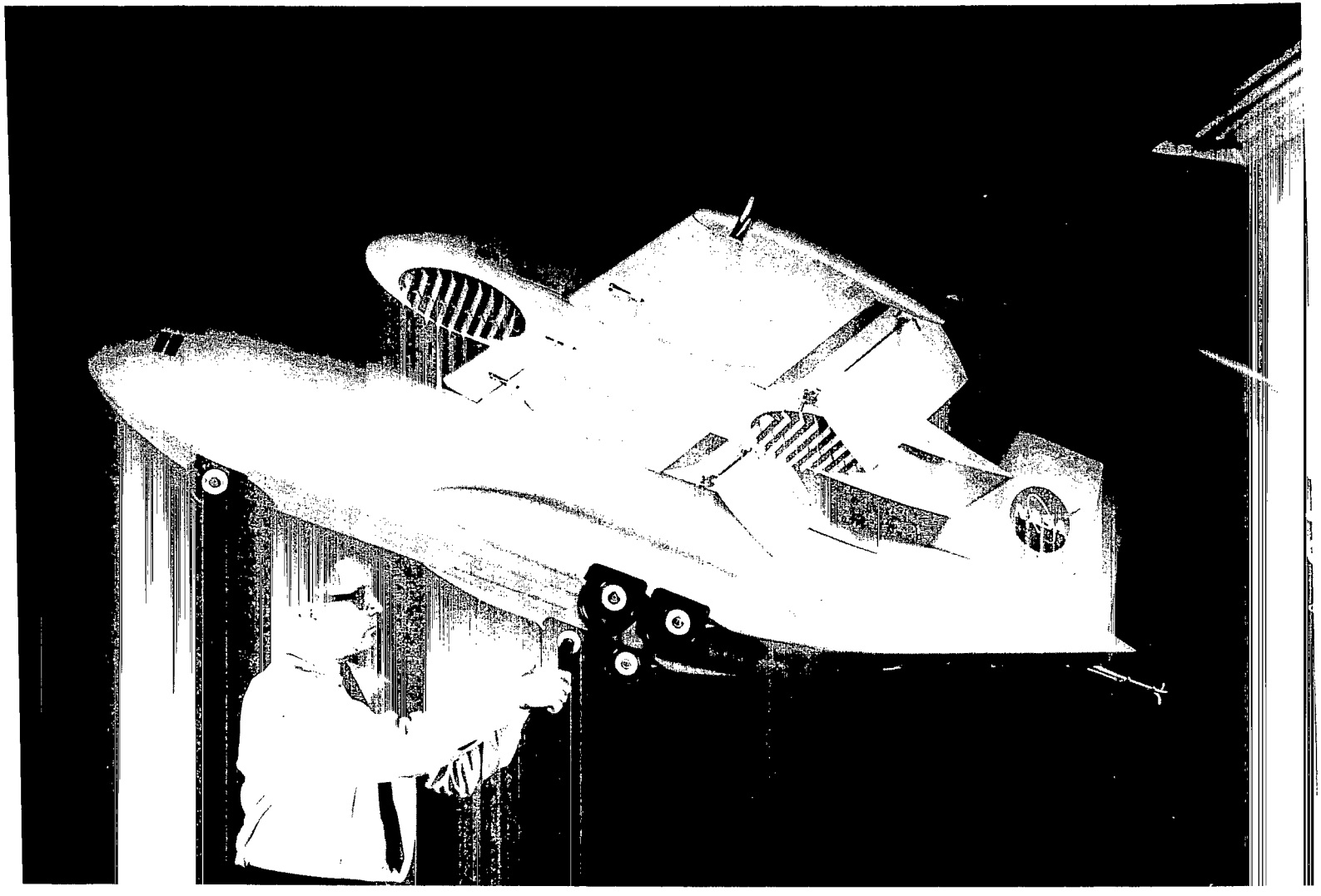

(b) Bottom view. L-67-7757

Figure 1.- Concluded.

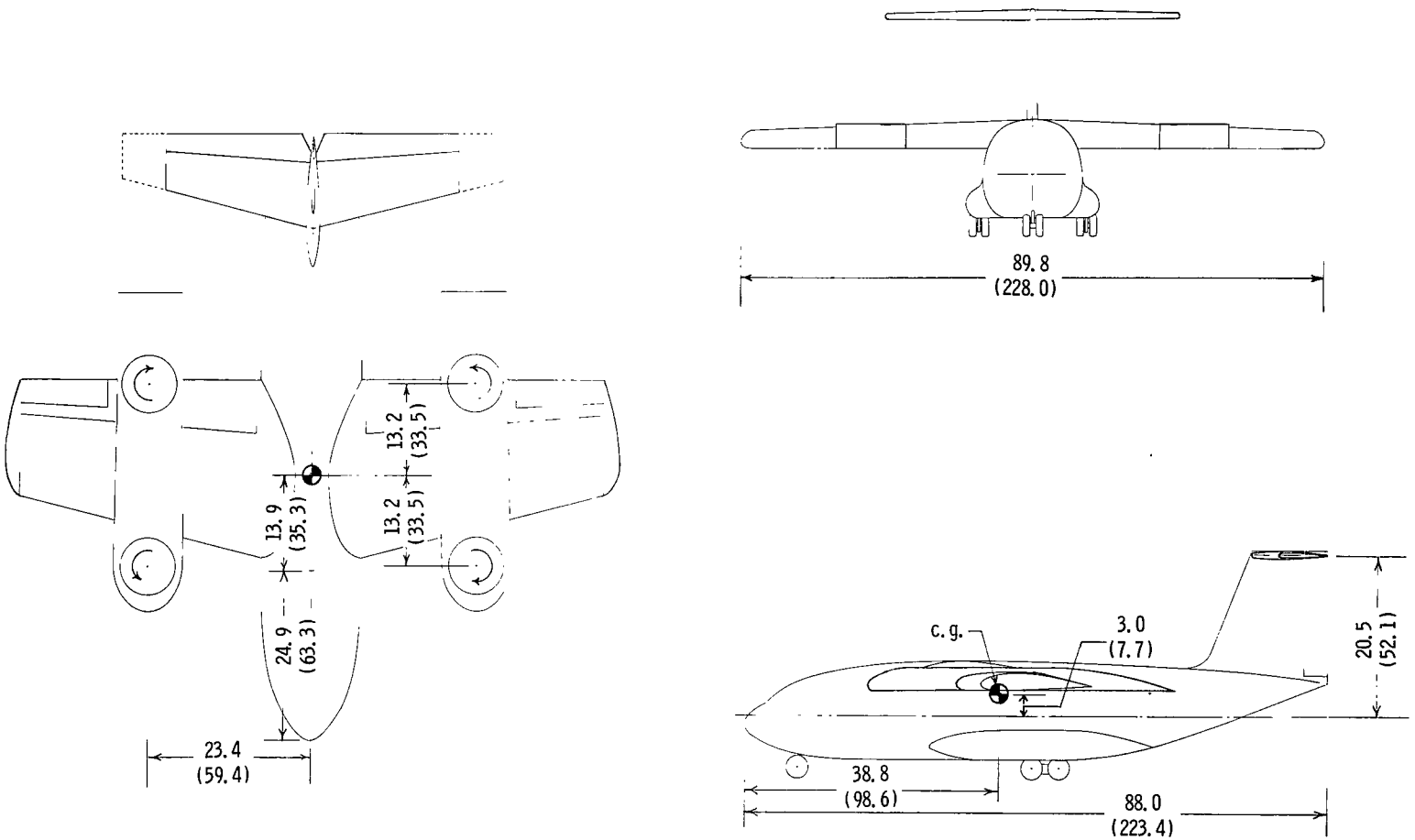

Figure 2.- Sketch of model. (Dimensions are given first in inches and parenthetically in centimeters.)

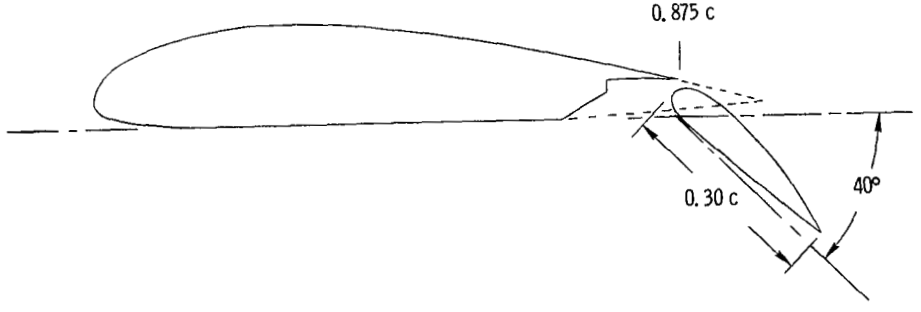

(a) Typical section through wing showing flap detail.

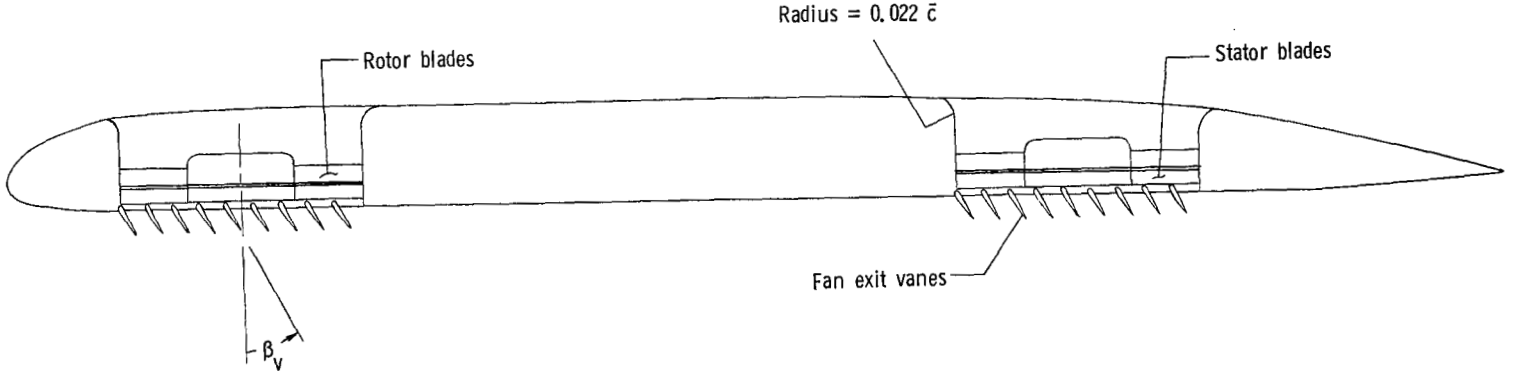

(b) Section through pod showing lift-fan position.

Figure 3.- Sketch showing wing and lift-fan pod details.

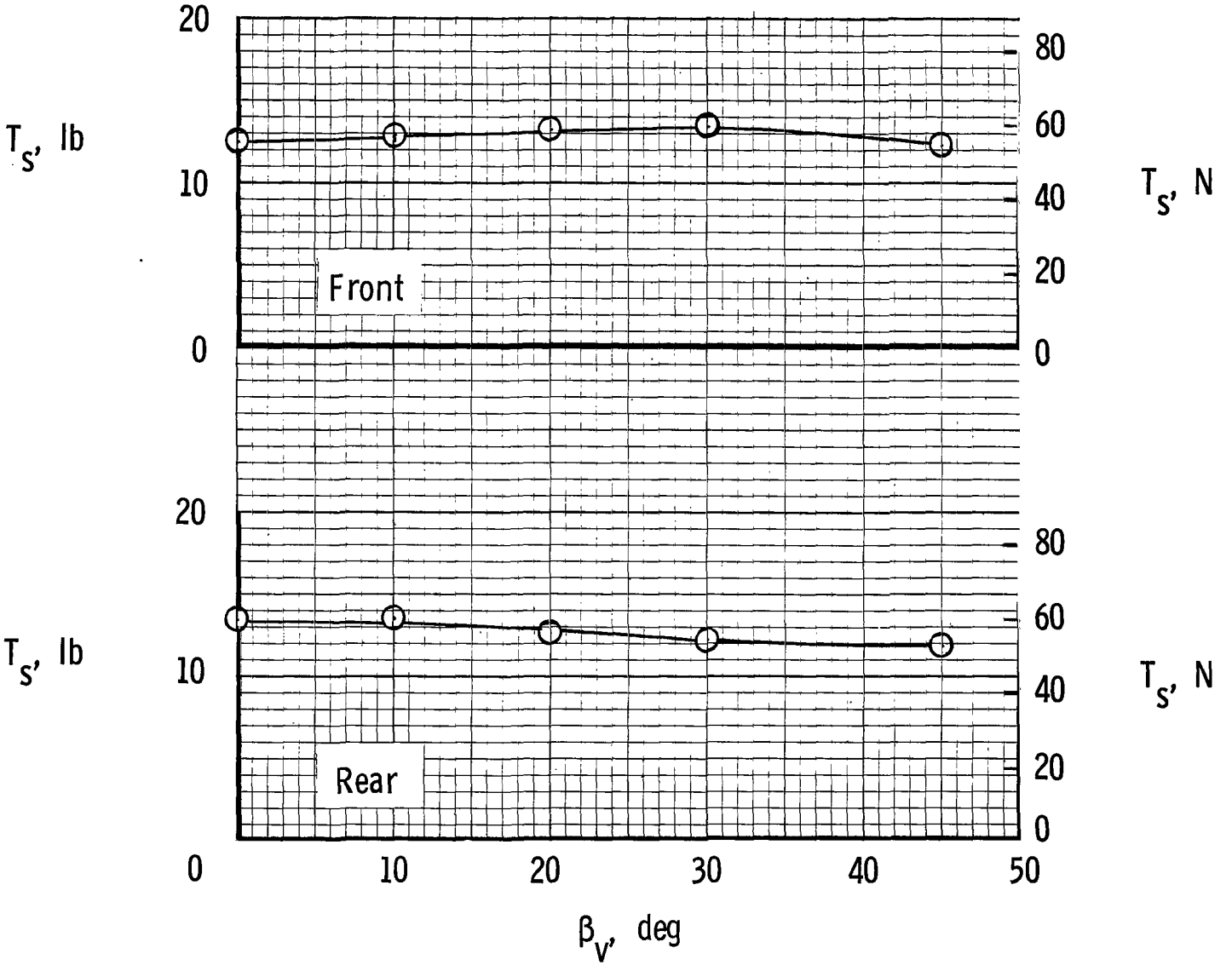

Figure 4.- Variation of static thrust of individual fans with exit-vane deflection.

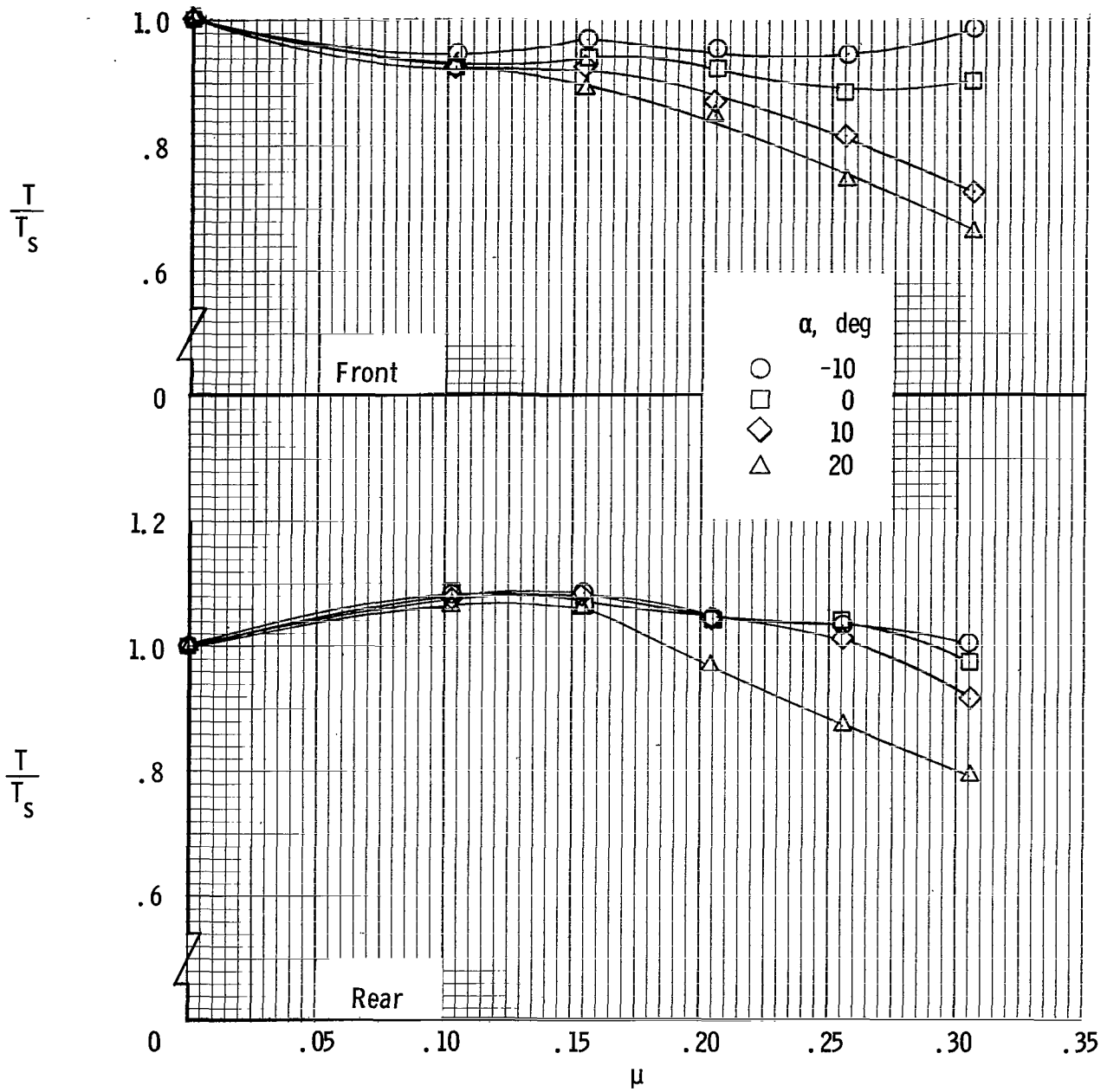

(a) $\beta_V = 0^0$.

Figure 5.- Variation of fan thrust with tip-speed ratio for $\delta_f = 0^0$. Tails off.

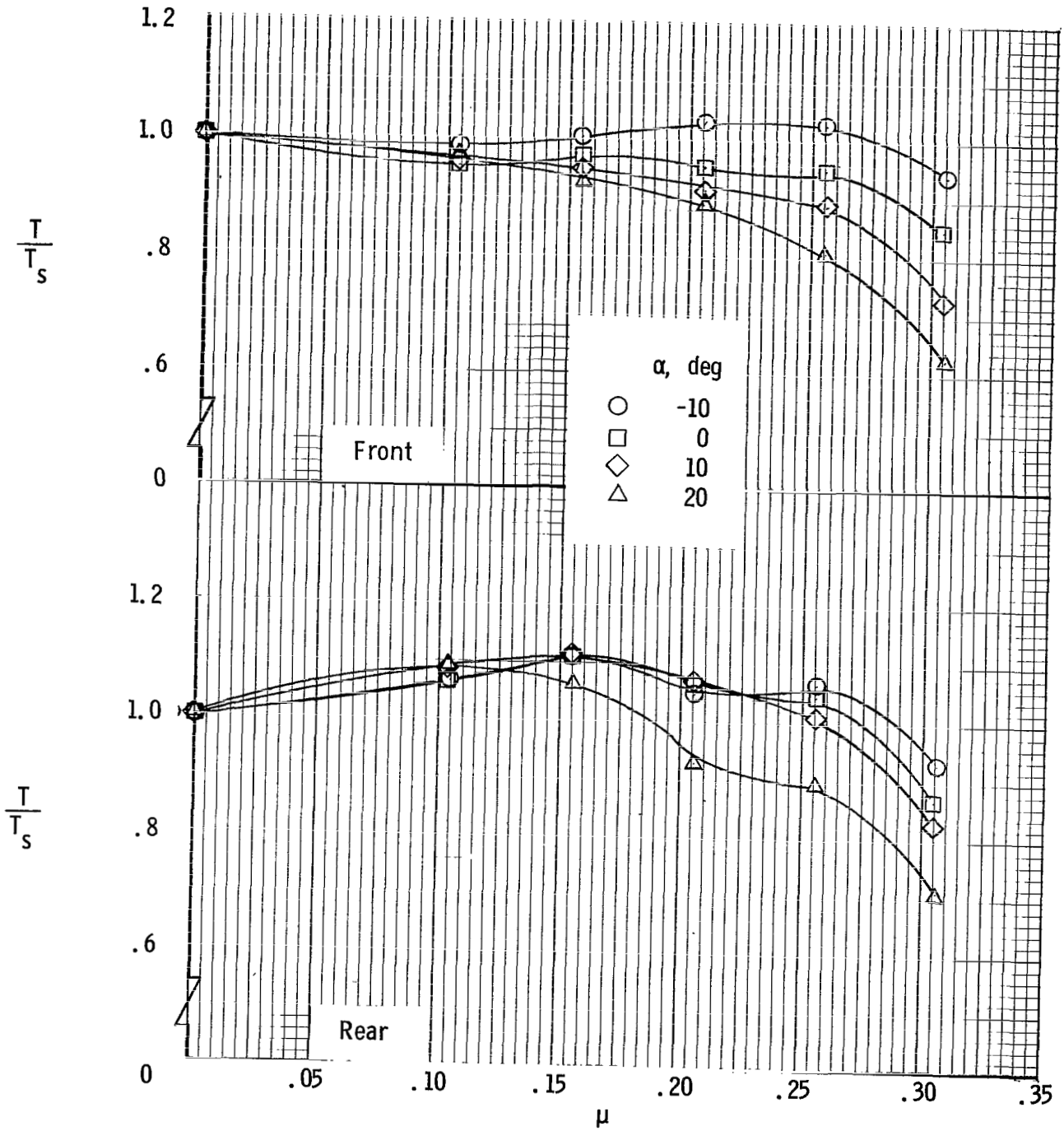

(b) $\beta_V = 10^o$.

Figure 5.- Continued.

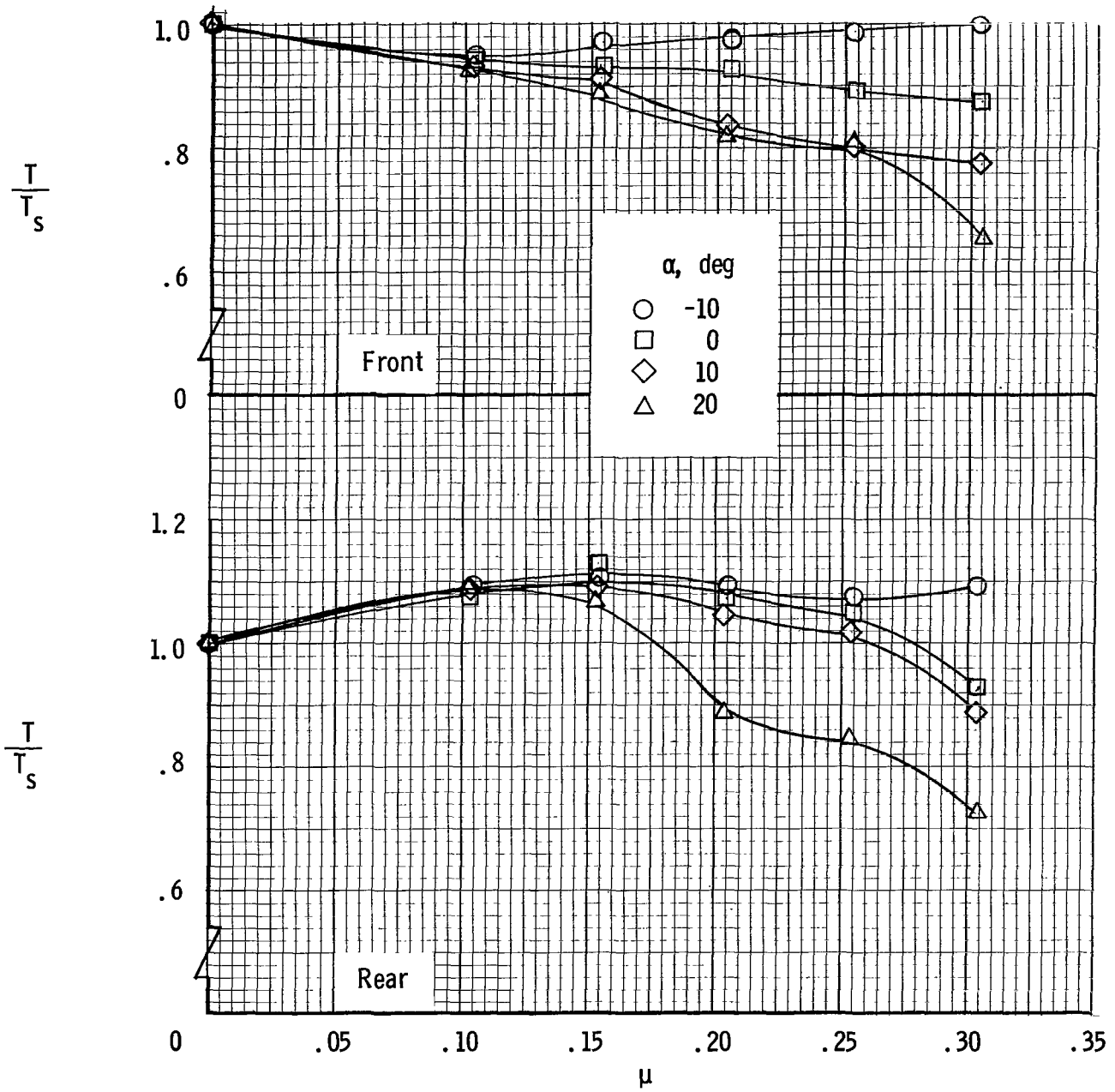

(c) $\beta_v = 20^0$.

Figure 5.- Continued.

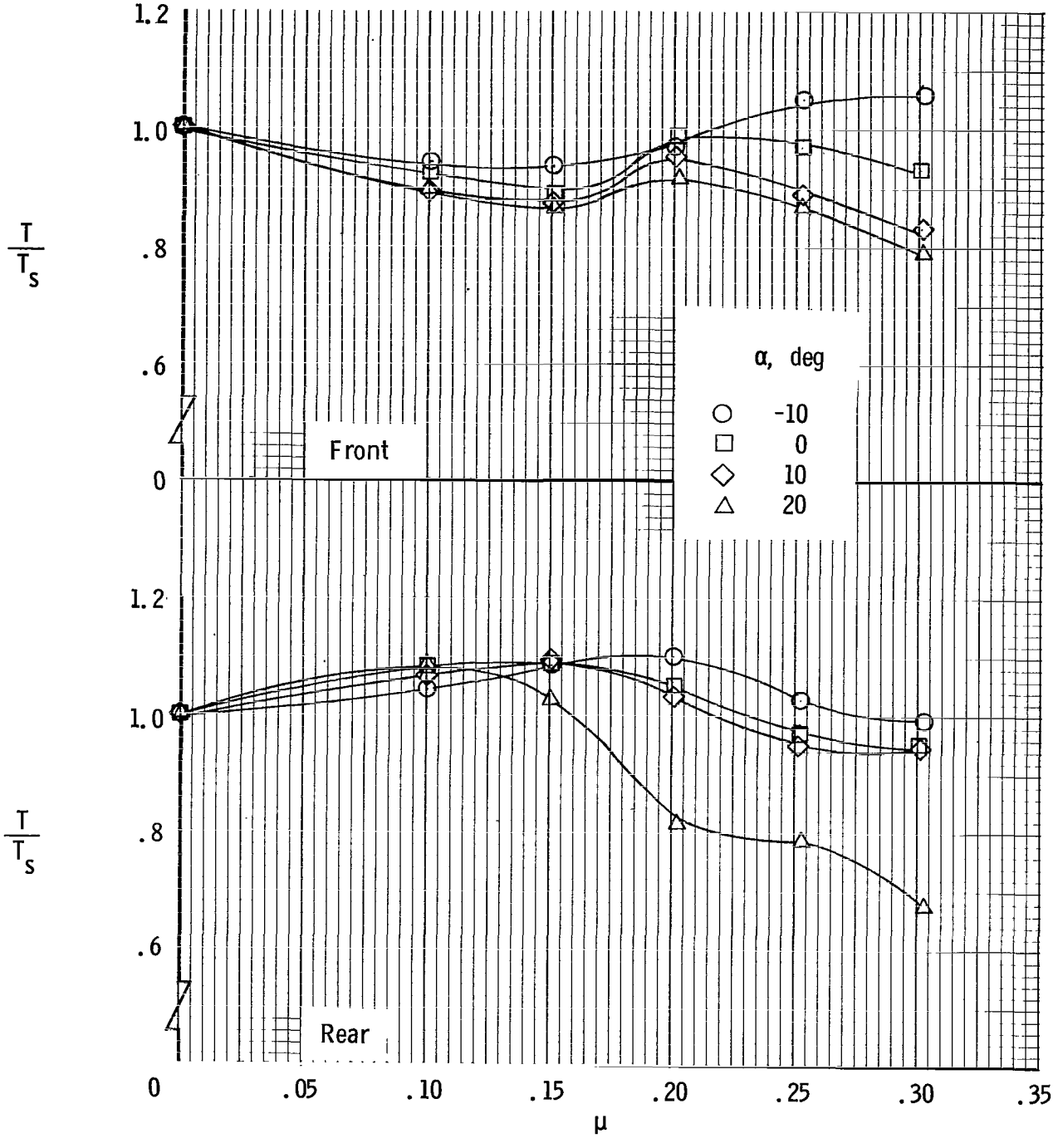

(d) $\beta_V = 30^0$.

Figure 5.- Continued.

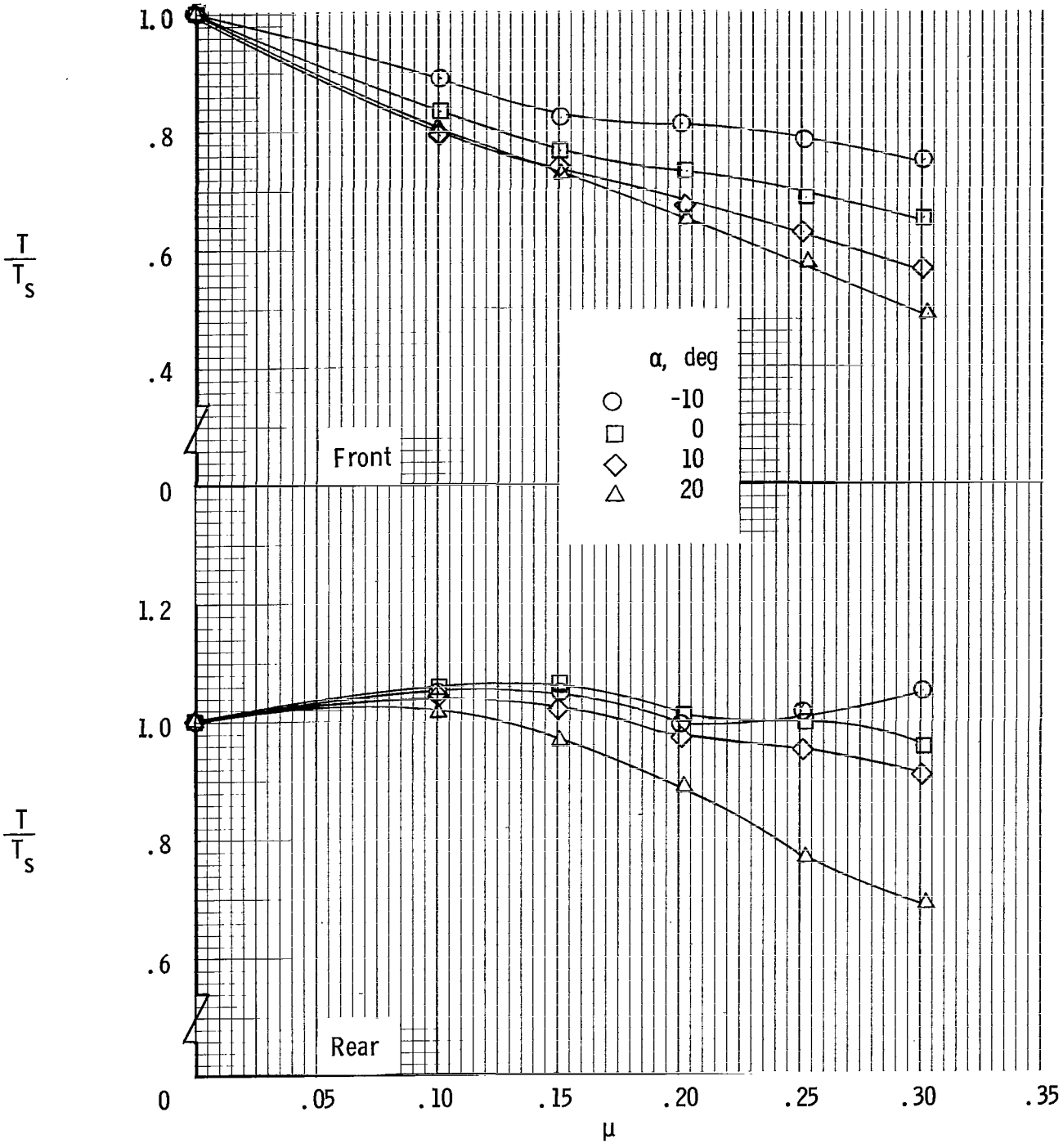

(e) $\beta_v = 45^0$.

Figure 5.- Concluded.

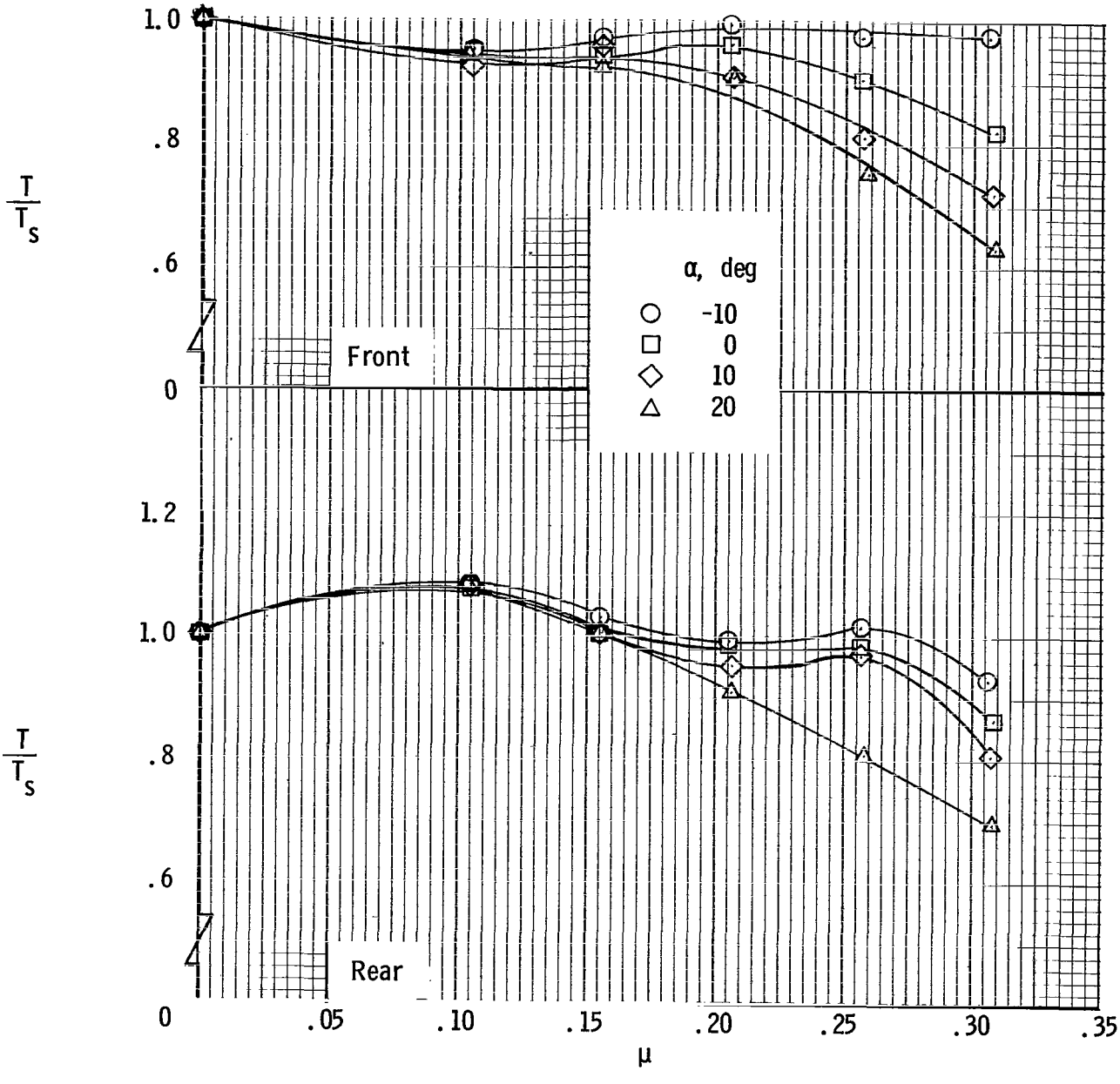

(a) $\beta_V = 0^0$.

Figure 6.- Variation of fan thrust with tip-speed ratio for $\delta_f = 40^0$. Tails off.

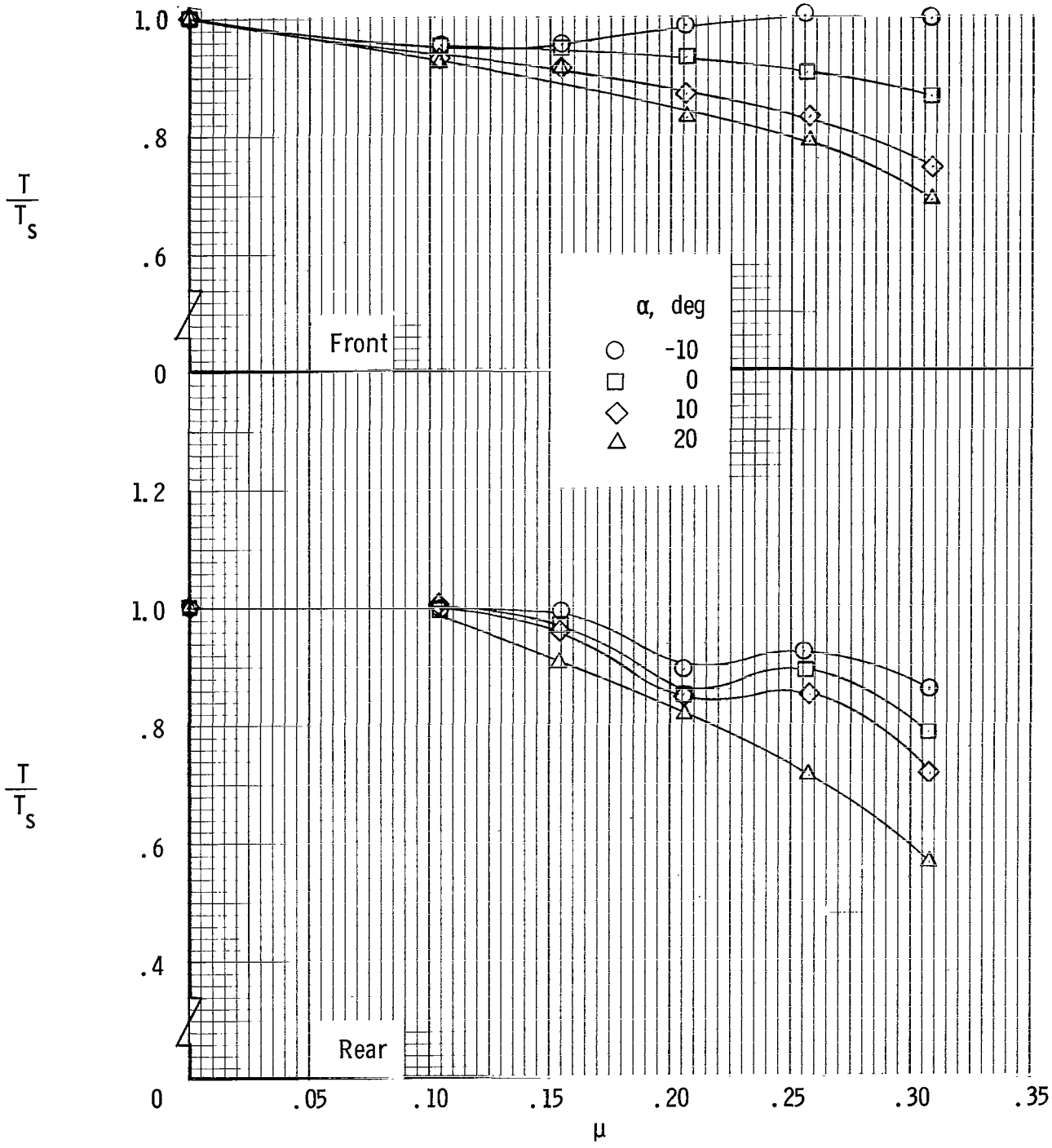

(b) $\beta_V = 10^0$.

Figure 6.- Continued.

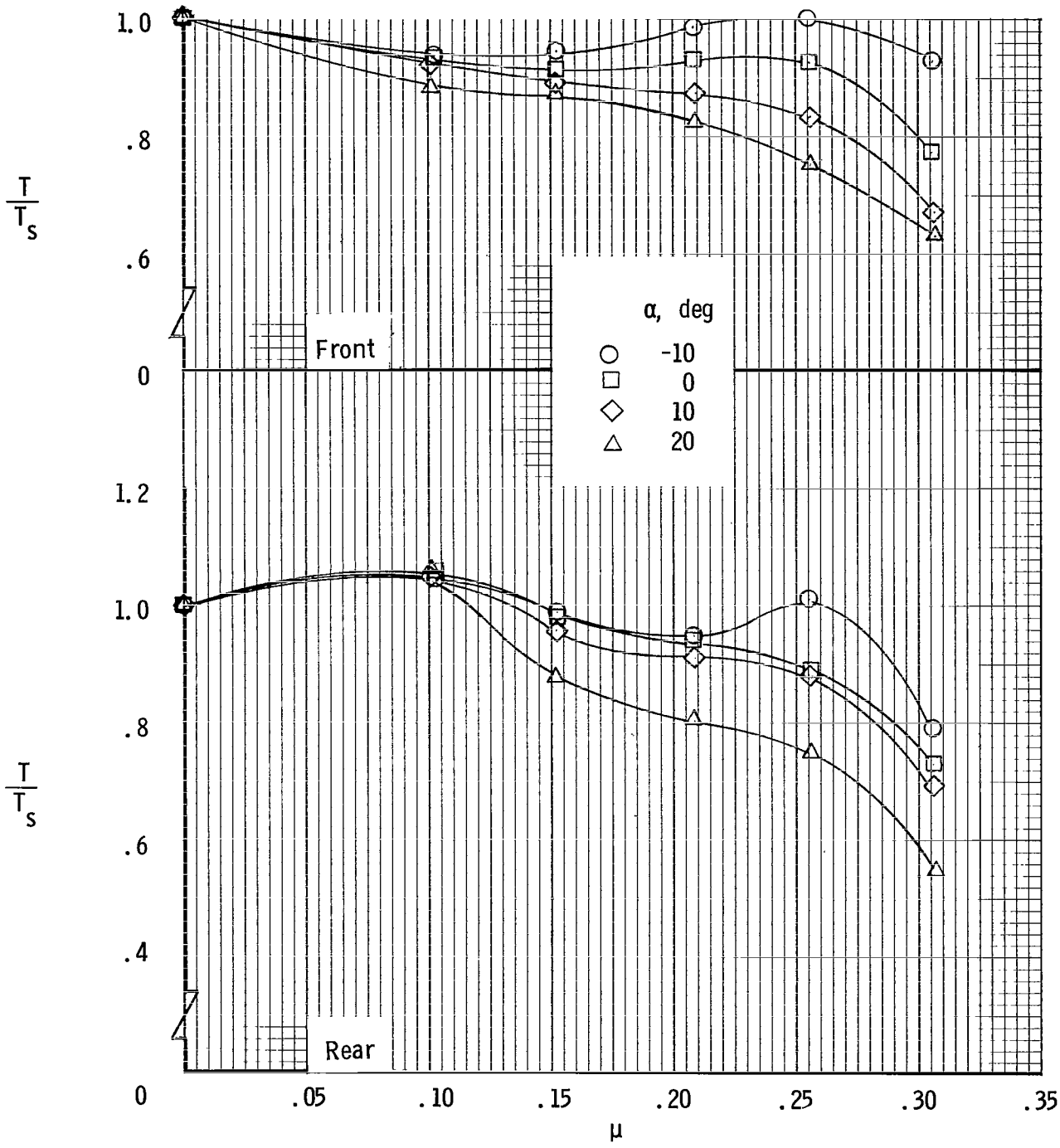

(c) $\beta_V = 20^o$.

Figure 6.- Continued.

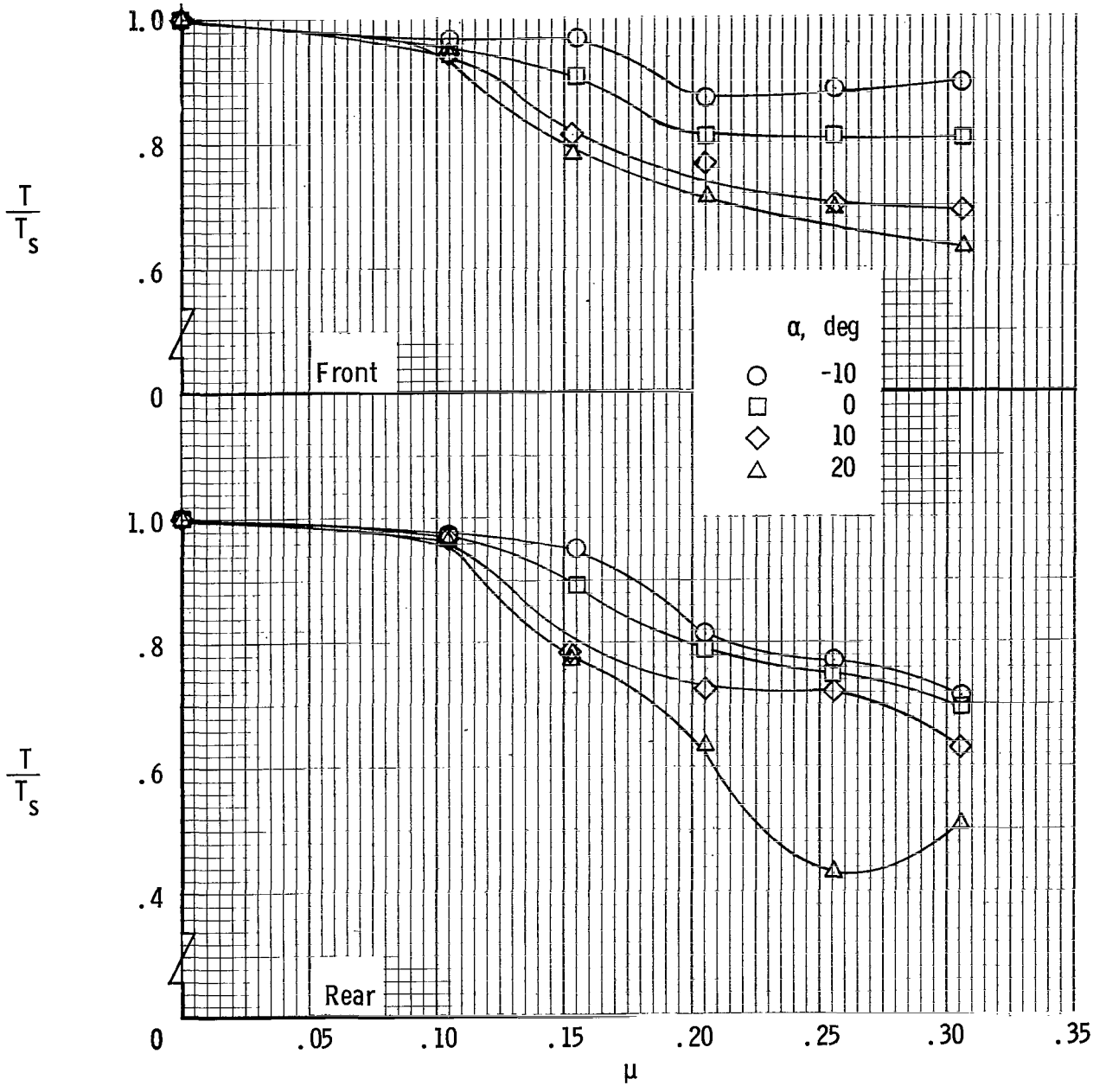

(d) $\beta_V = 30^0$.

Figure 6.- Continued.

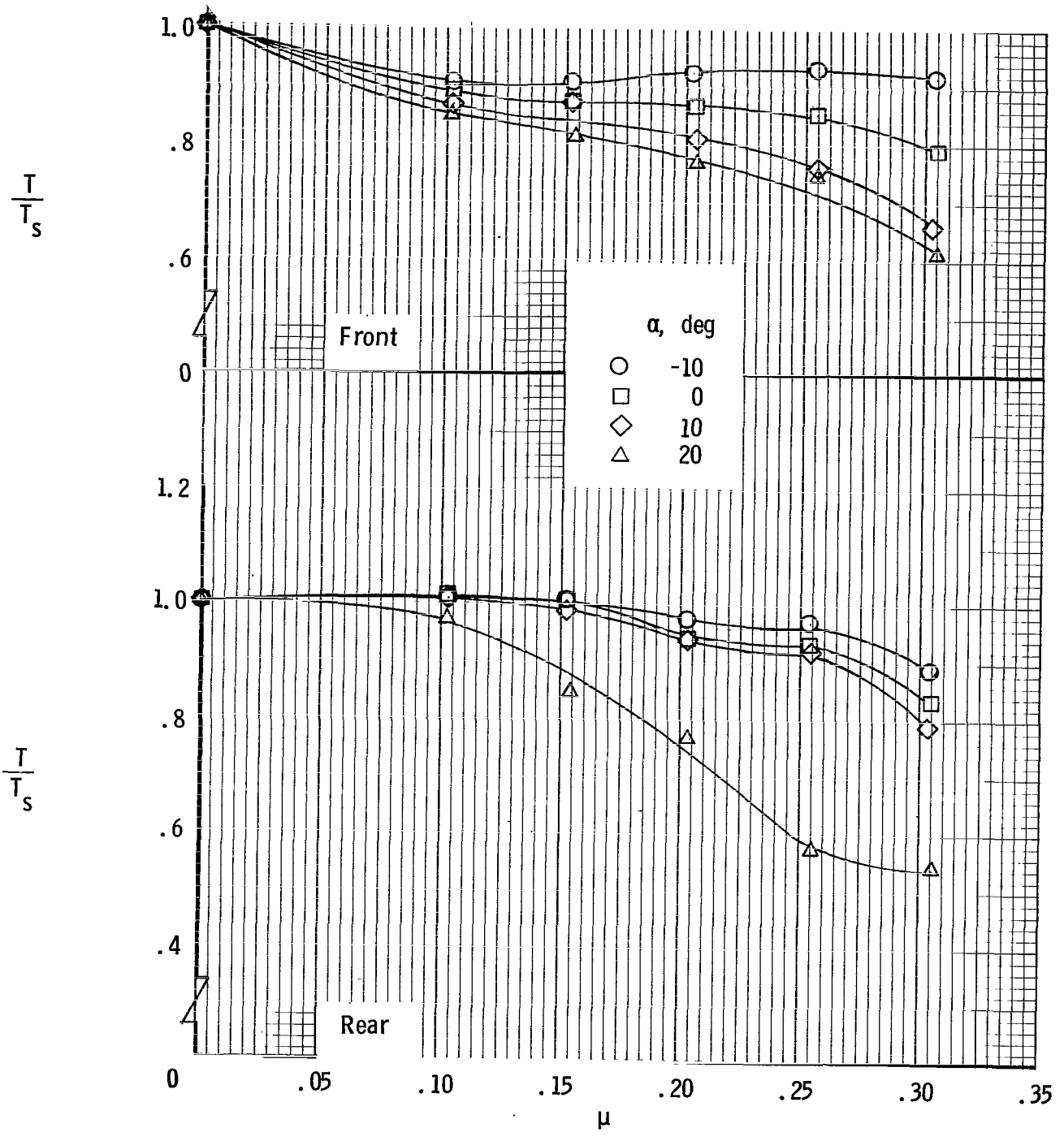

(e) $\beta_V = 45^0$.

Figure 6.- Concluded.

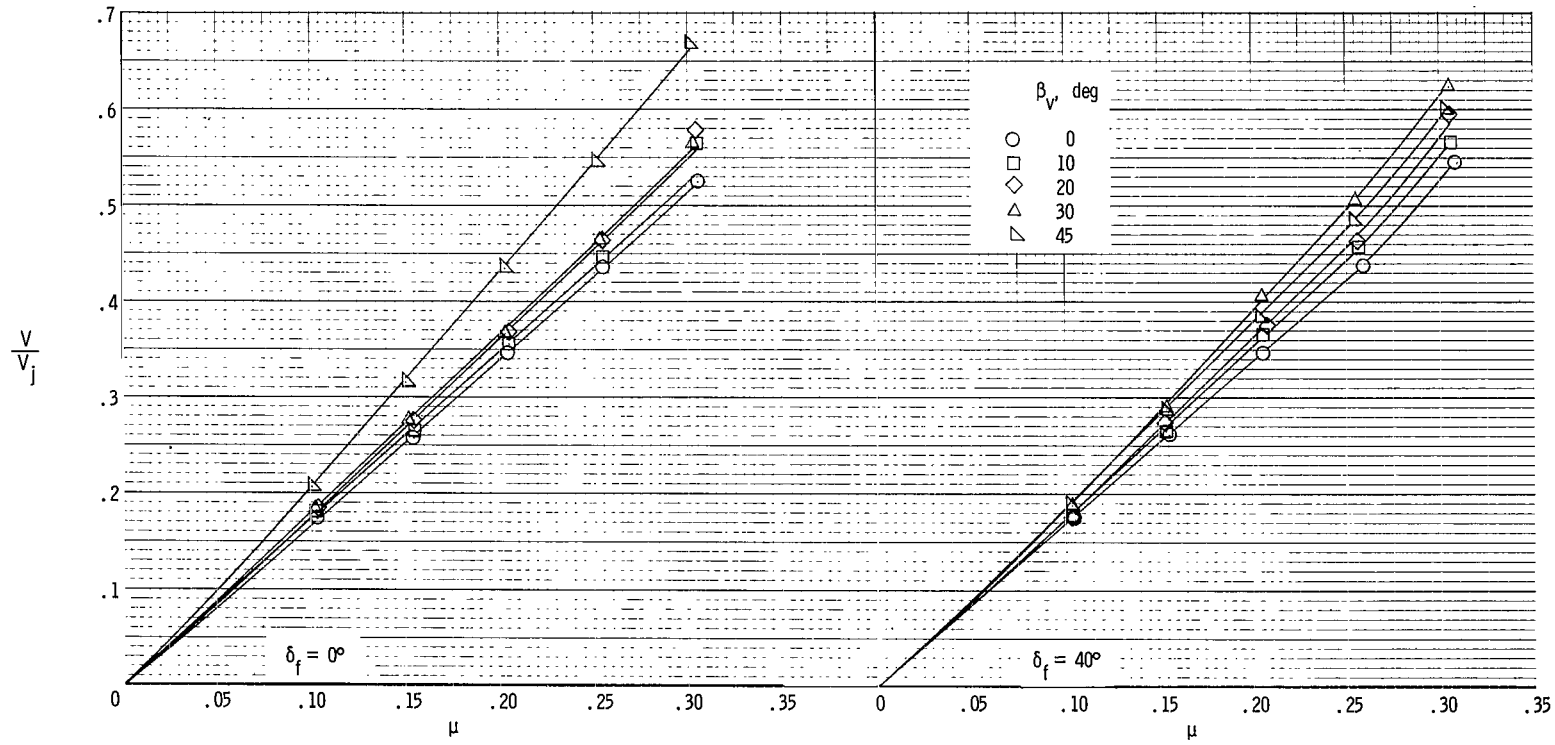

Figure 7.- Variation of average velocity ratio with tip-speed ratio. $\alpha = 0^0$.

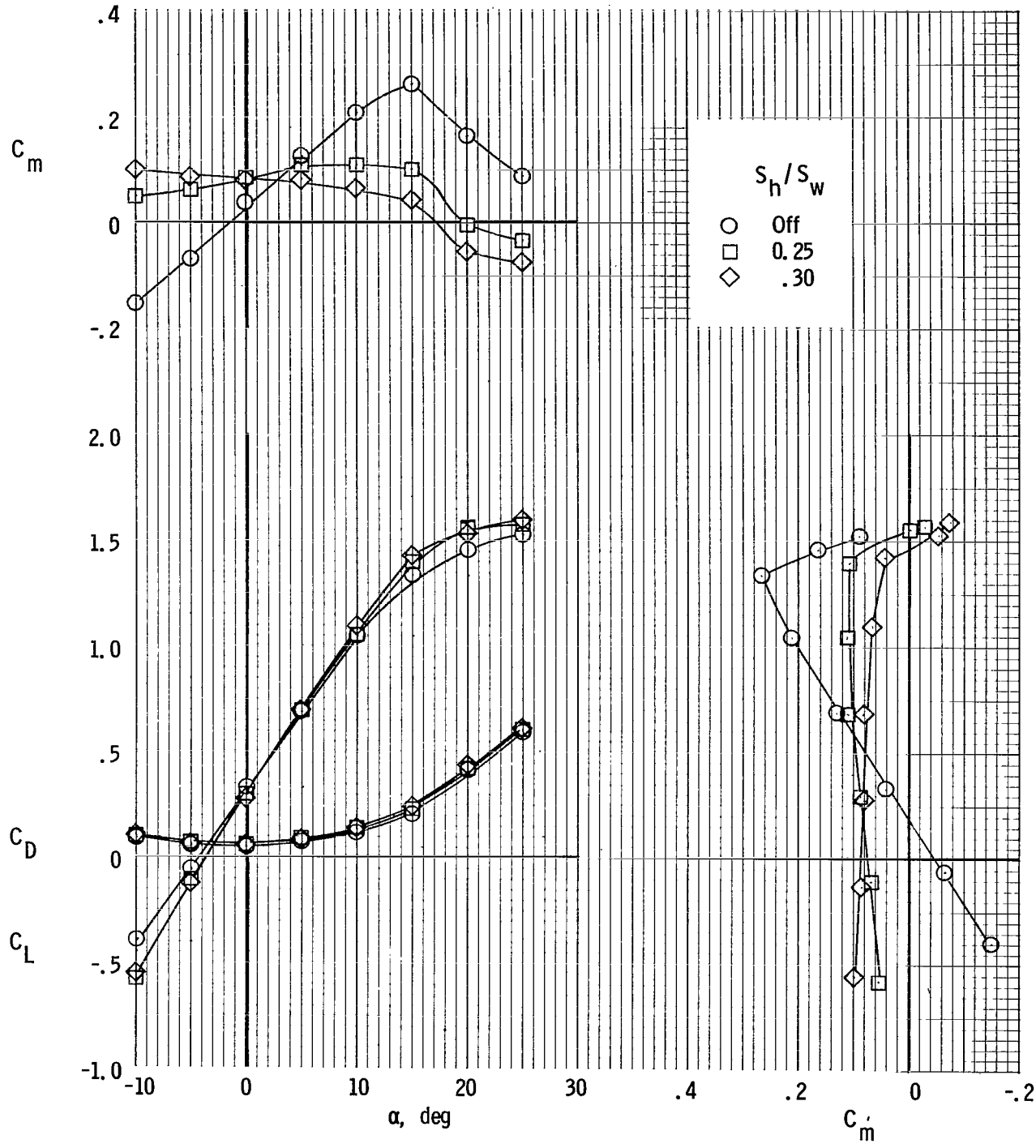

(a) $\delta_f = 0^0$.

Figure 8.- Effect of horizontal-tail area on longitudinal characteristics of model. Fans covered; $i_t = 0^0$.

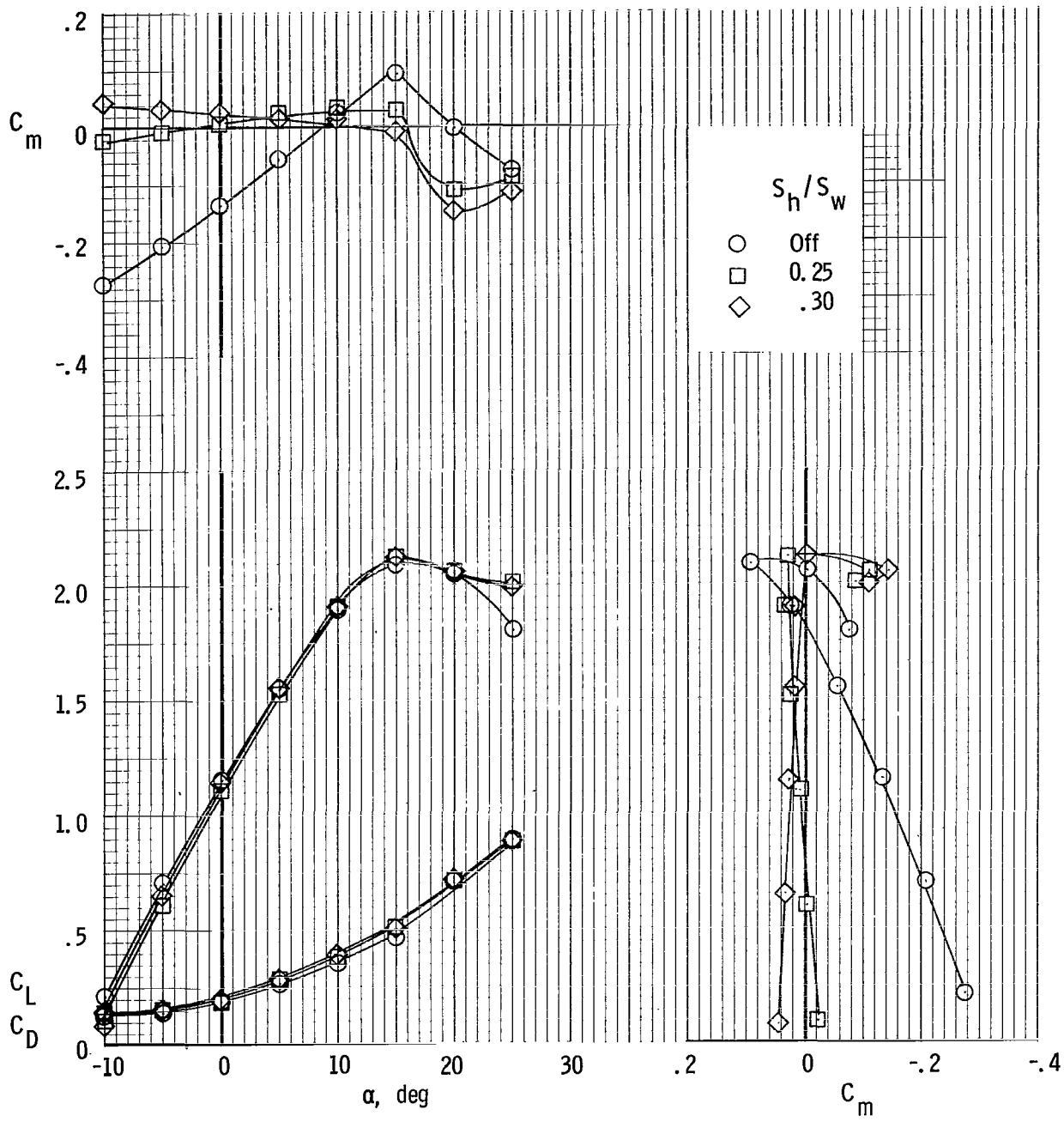

(b) $\delta_f = 40^0$.

Figure 8.- Concluded.

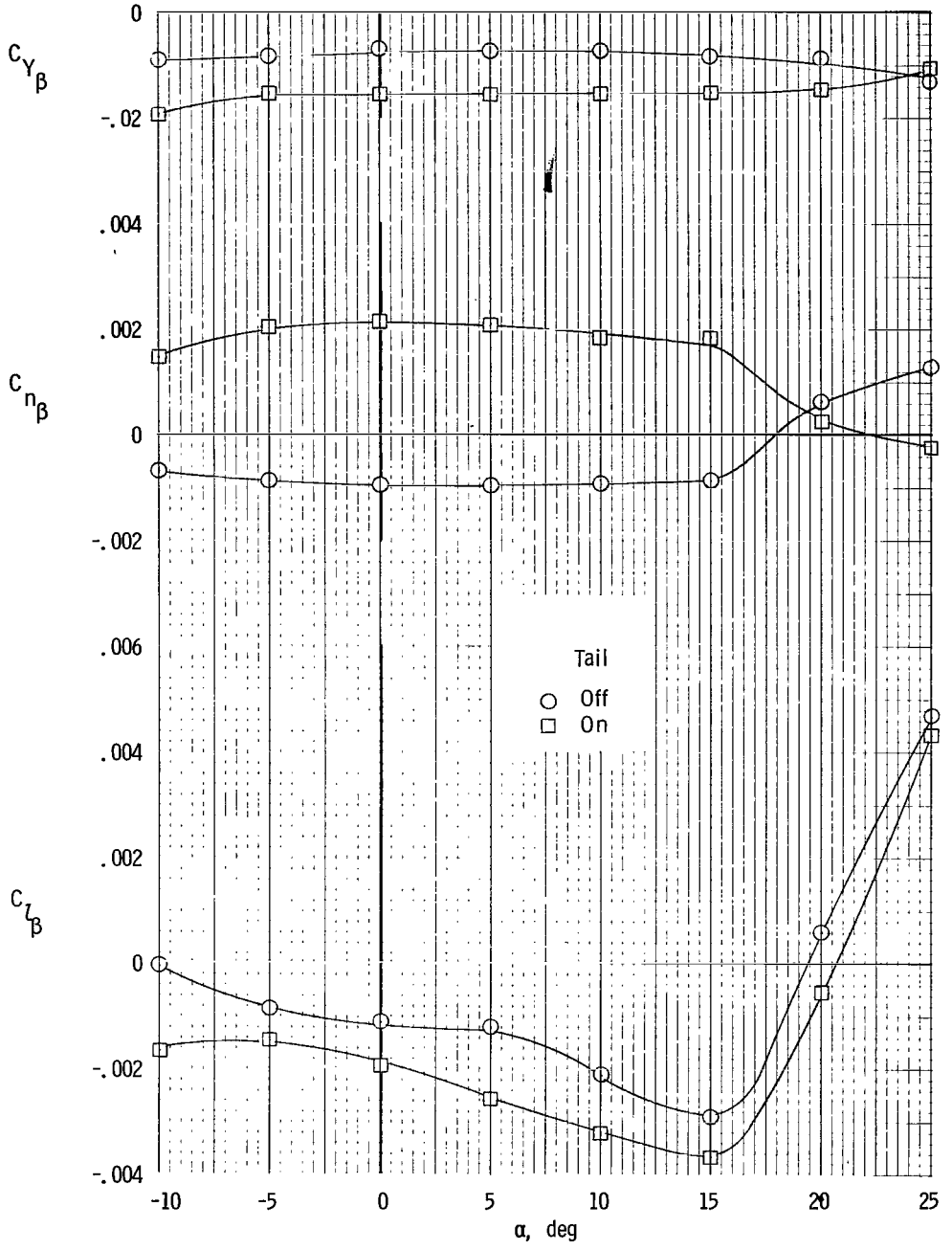

(a) $\delta_f = 0^0$.

Figure 9.- Effect of vertical tail on lateral-directional characteristics. Fans covered.

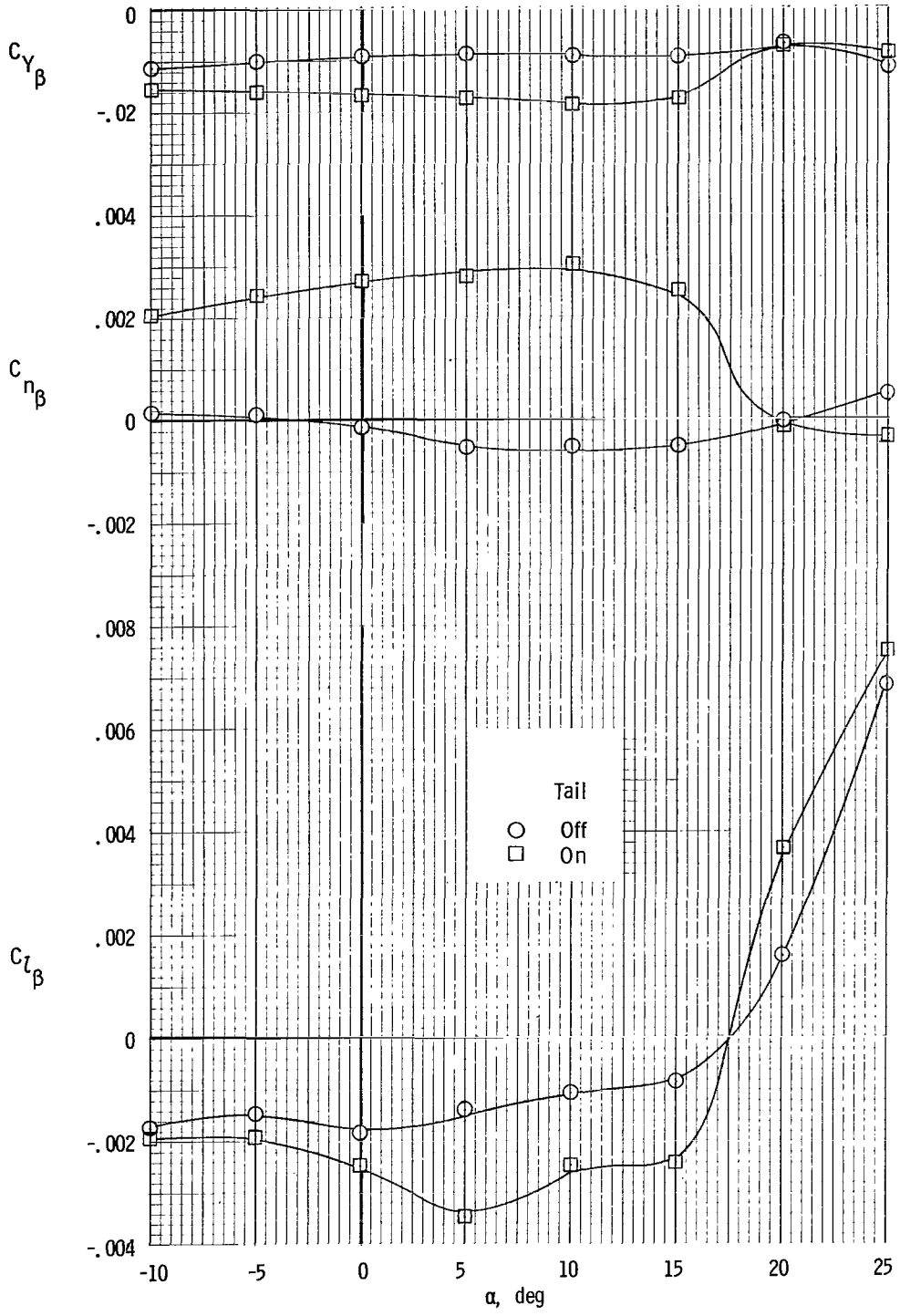

(b) $\delta_f = 40^o$.

Figure 9.- Concluded.

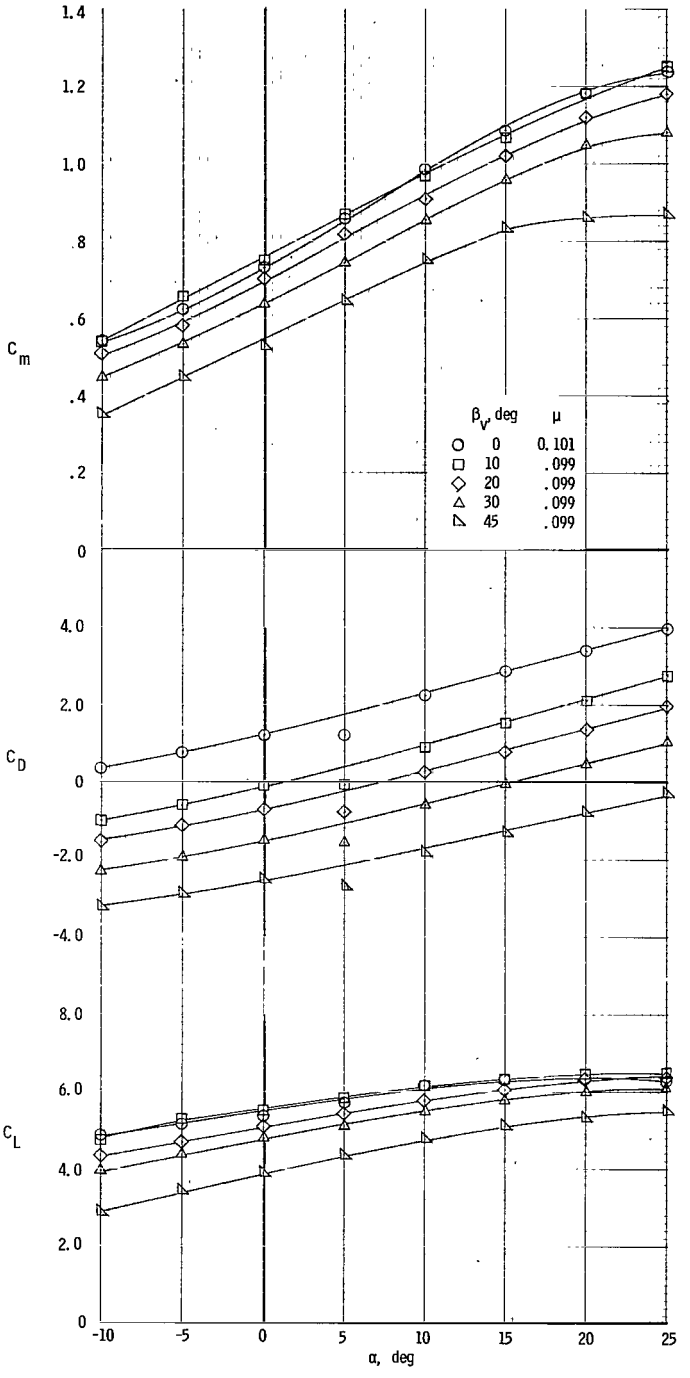

(a) Nominal $\mu = 0.10$.

Figure 10.- Effect of fan-exit-vane deflection on longitudinal aerodynamic characteristics for various tip-speed ratios and for $\delta_f = 0^o$. Horizontal tail off.

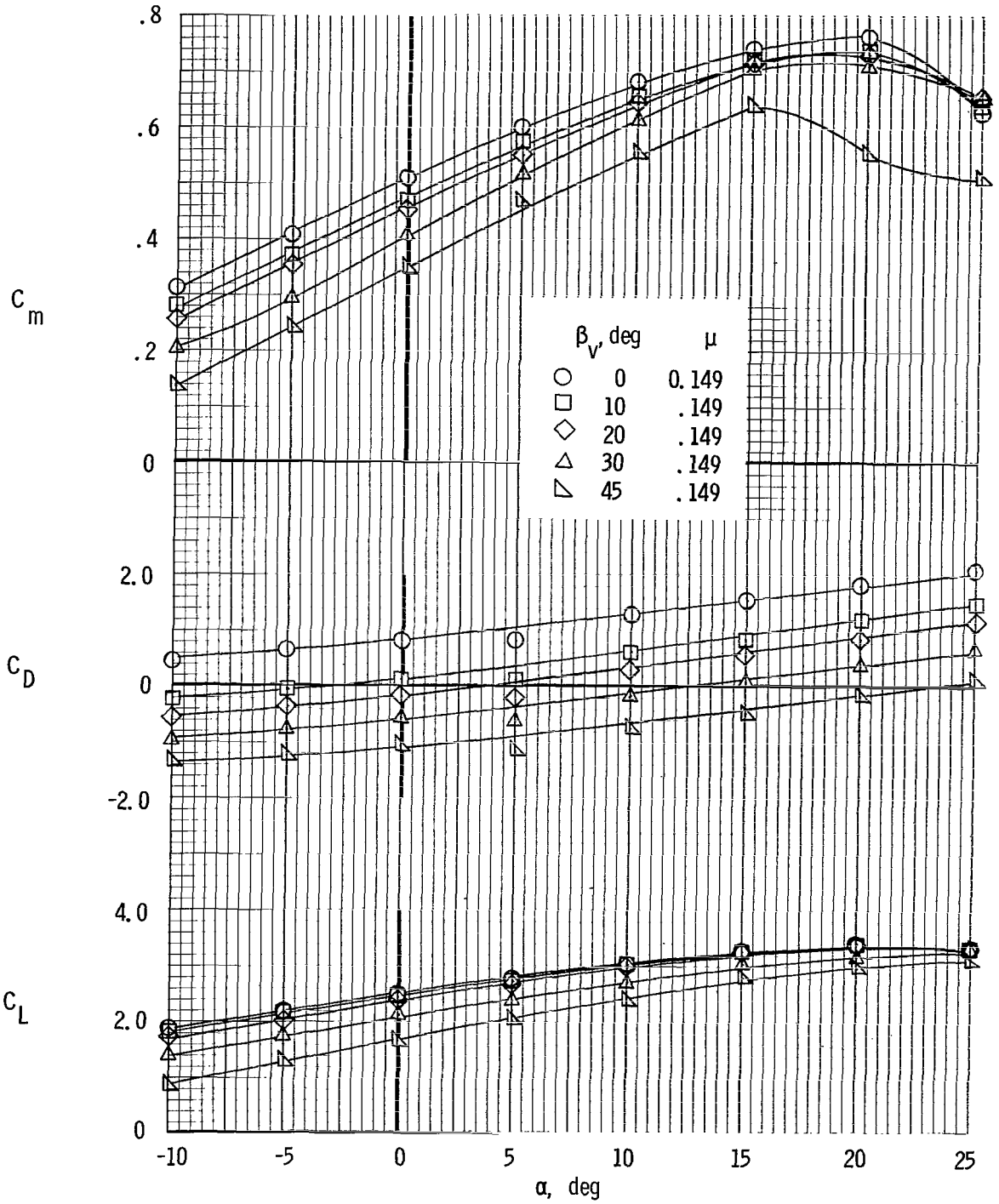

(b) Nominal $\mu = 0.15$.

Figure 10.- Continued.

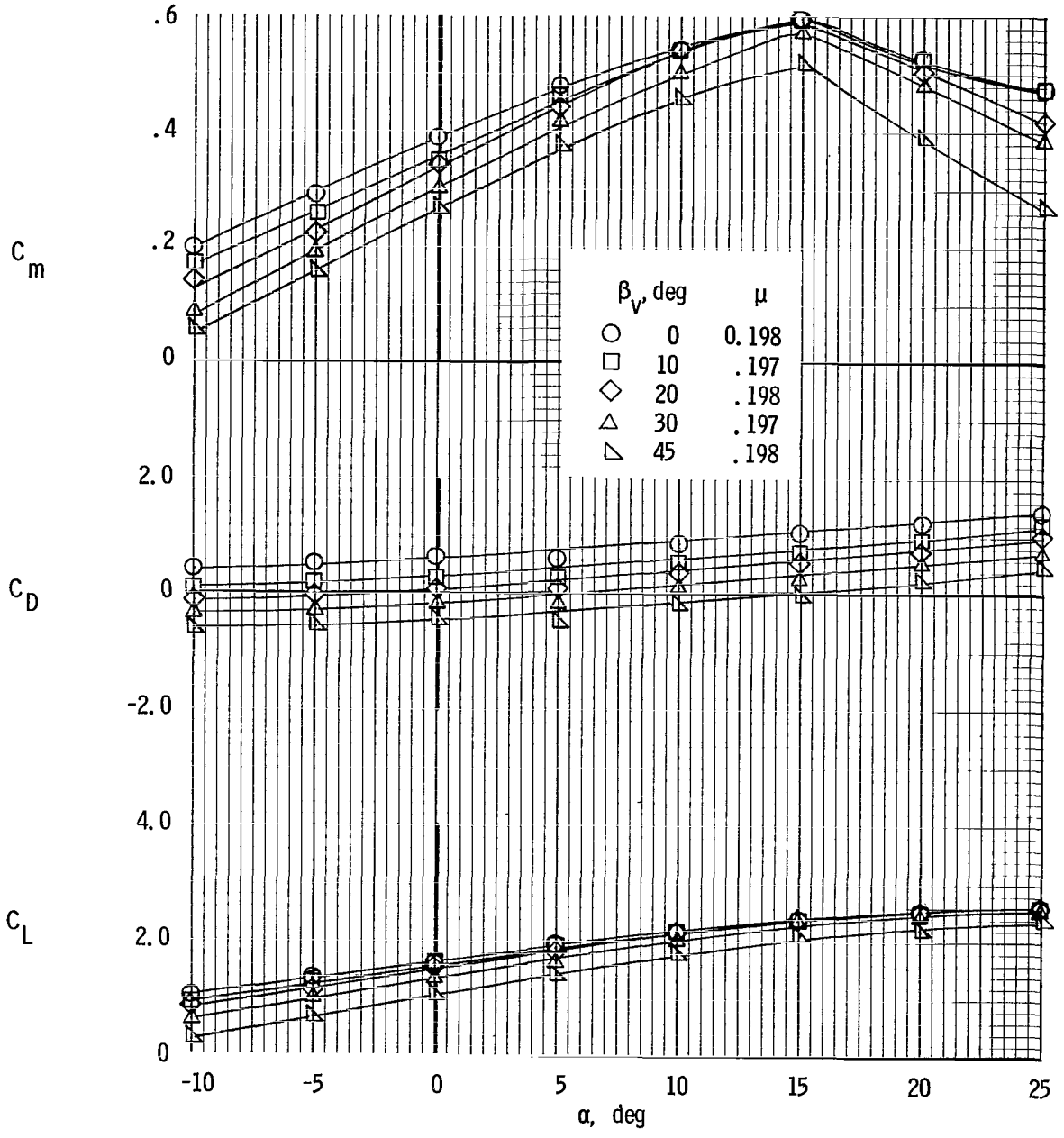

(c) Nominal $\mu = 0.20$.

Figure 10.- Continued.

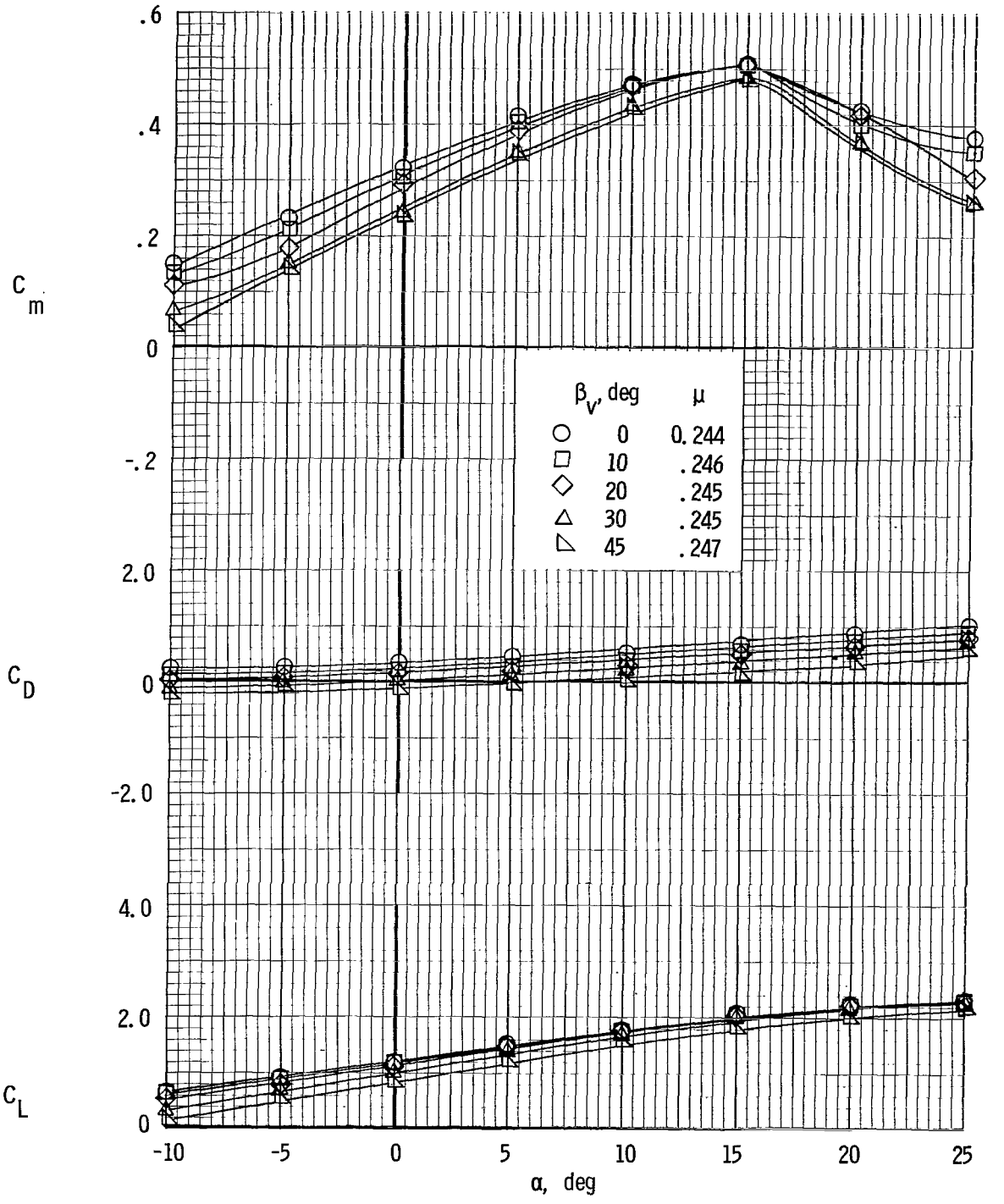

(d) Nominal $\mu = 0.25$.

Figure 10.- Continued.

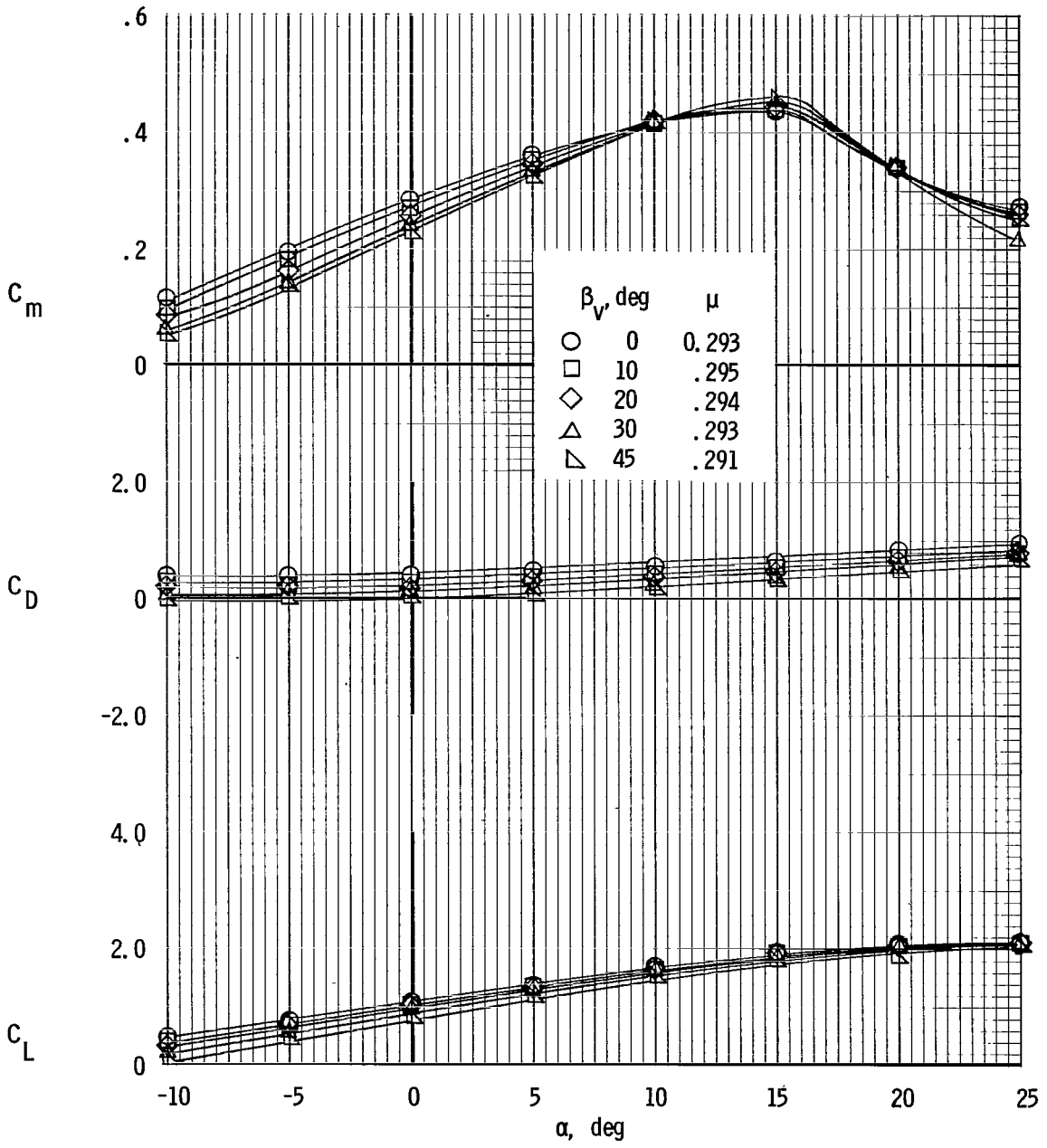

(e) Nominal $\mu = 0.30$.

Figure 10.- Concluded.

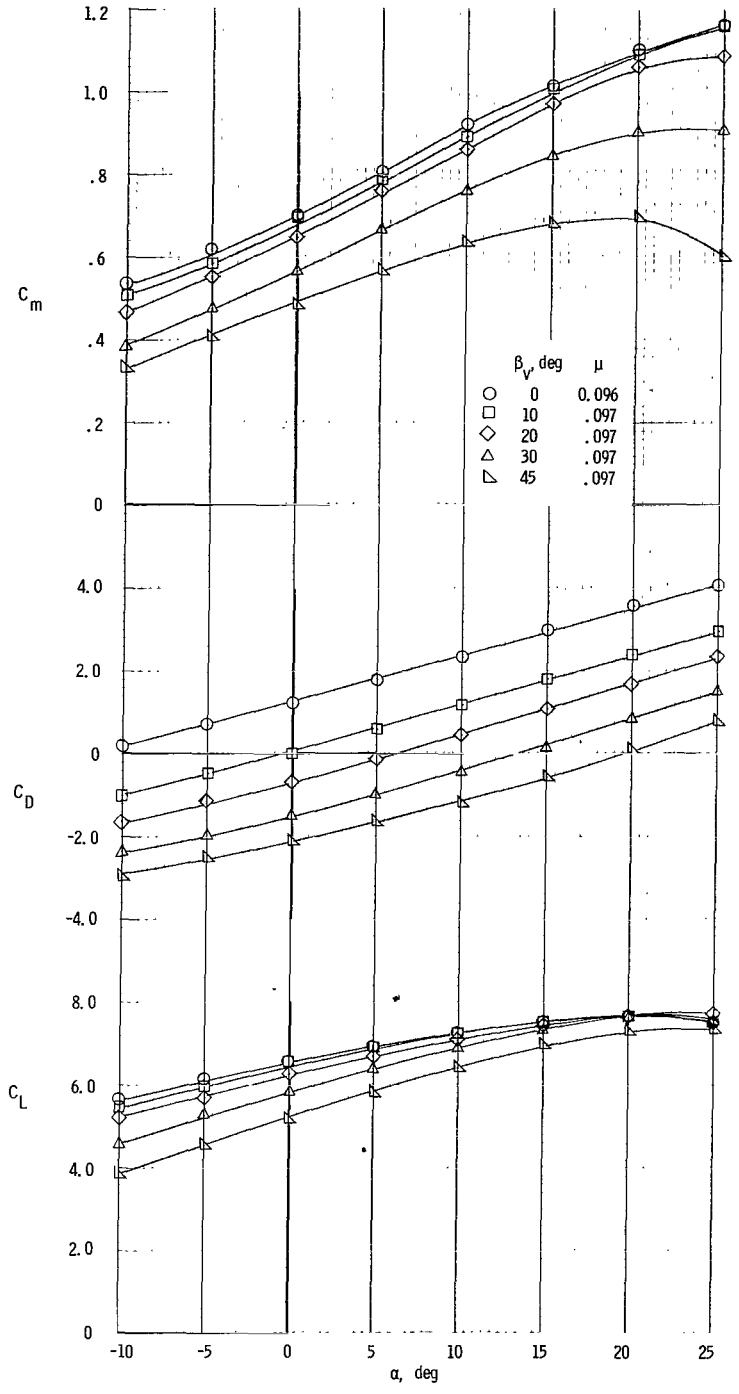

(a) Nominal $\mu = 0.10$.

Figure 11.- Effect of fan-exit-vane deflection on longitudinal aerodynamic characteristics for various tip-speed ratios and for $\delta_f = 40^0$. Horizontal tail off.

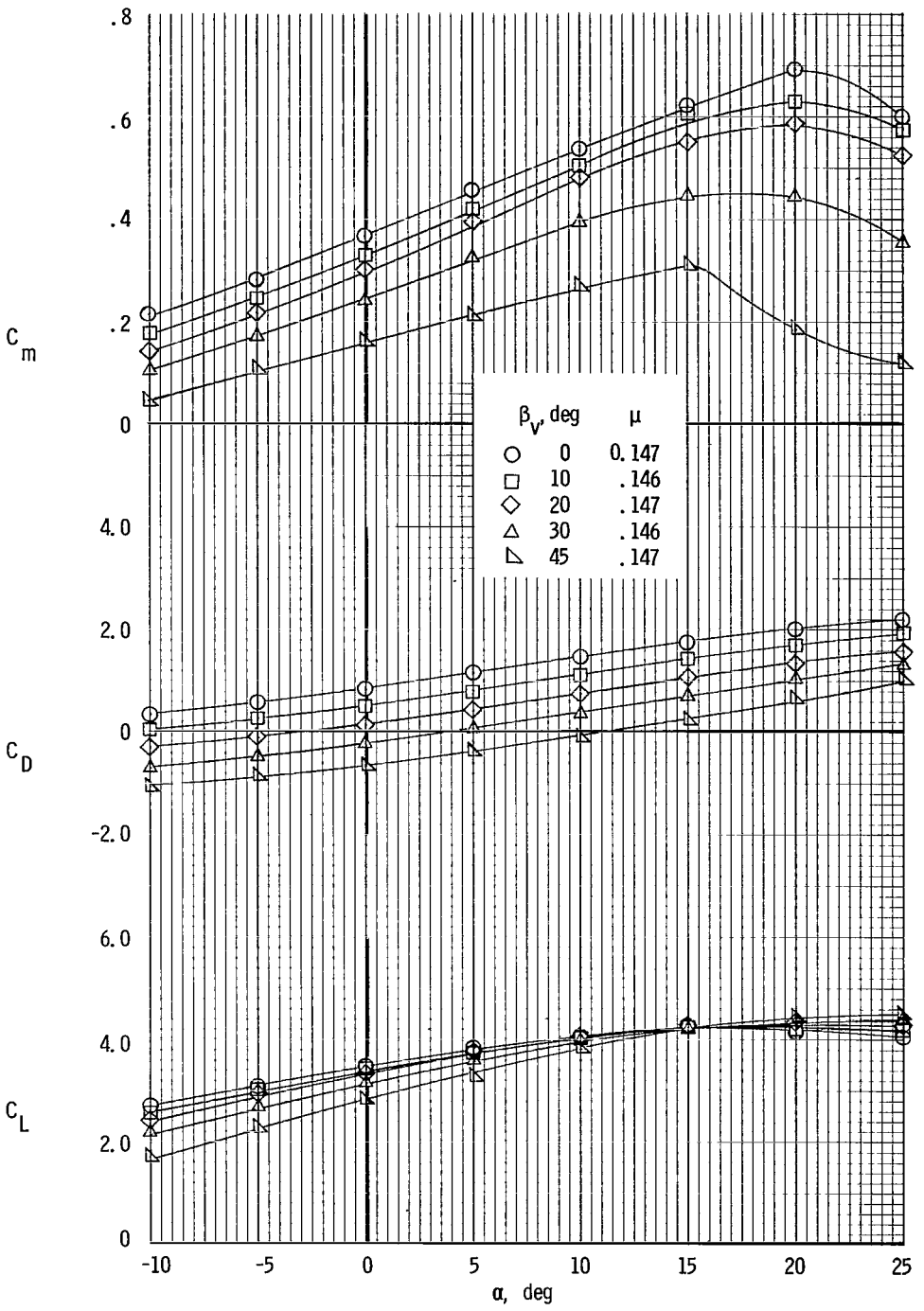

(b) Nominal $\mu = 0.15$.

Figure 11.- Continued.

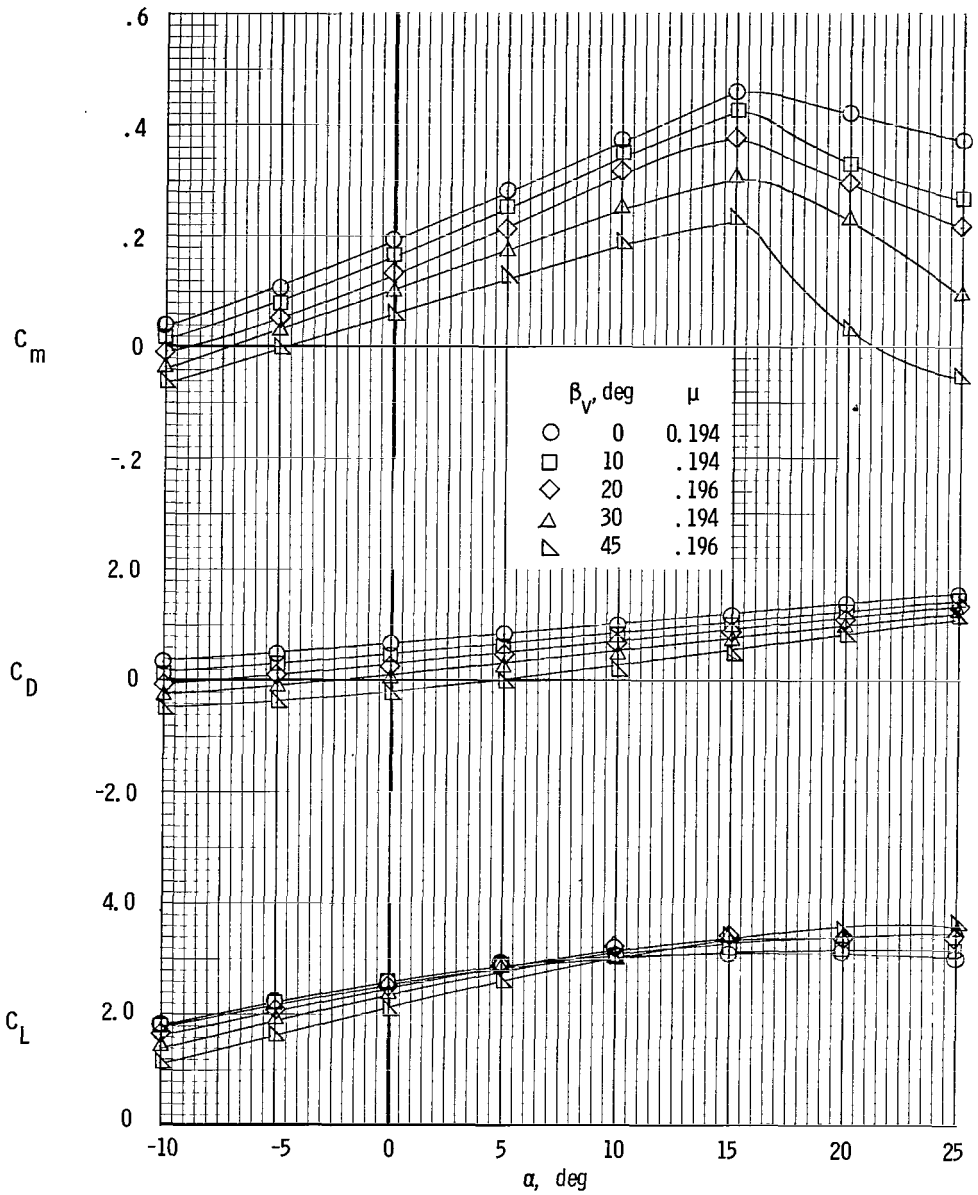

(c) Nominal $\mu = 0.20$.

Figure 11.- Continued.

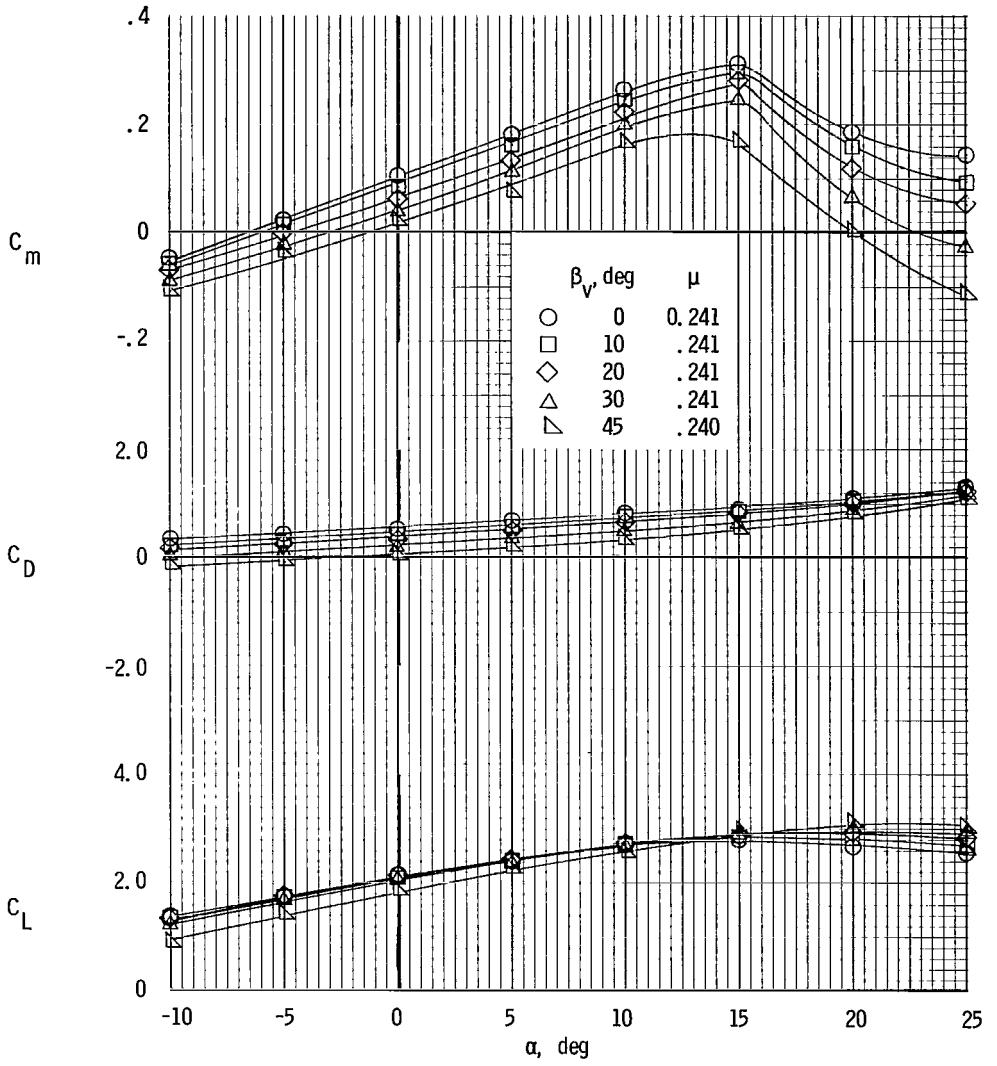

(d) Nominal $\mu = 0.25$.

Figure 11.- Continued.

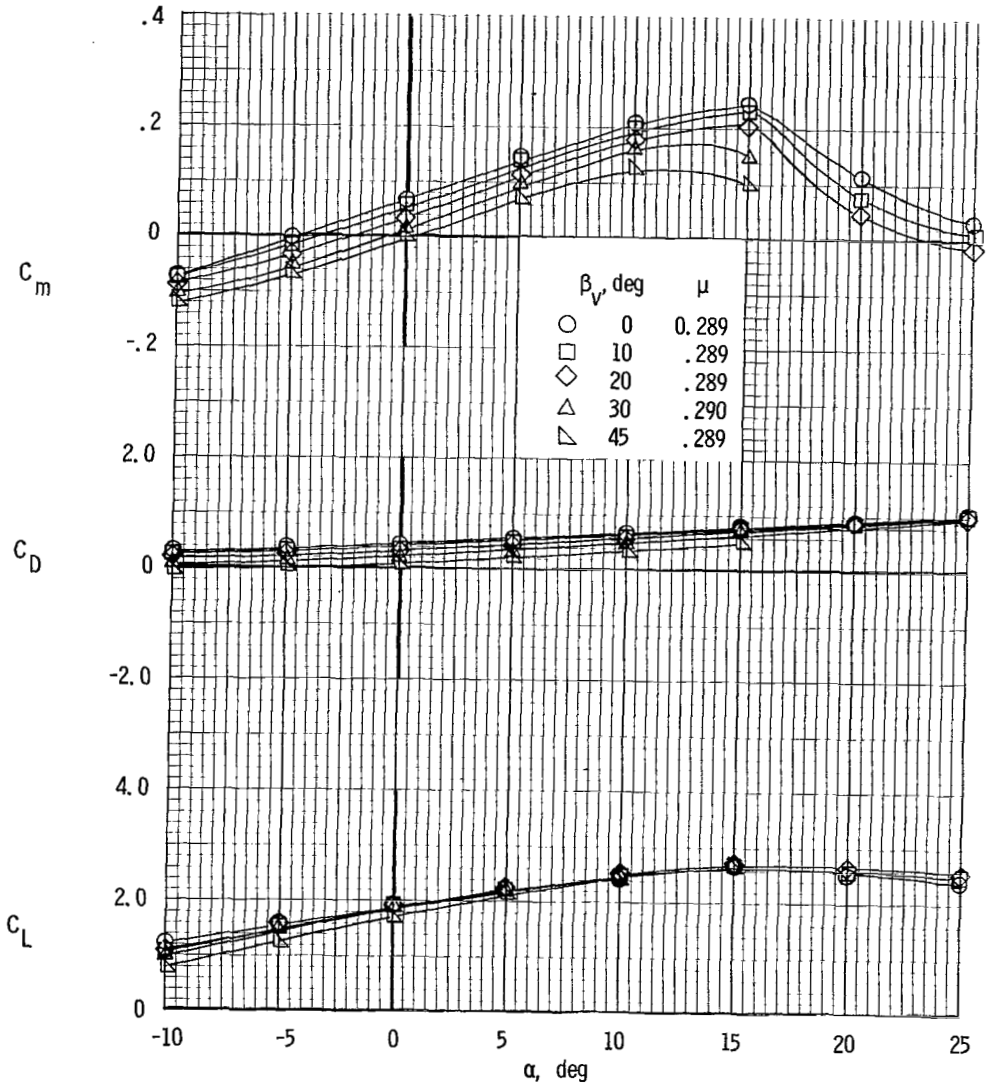

(e) Nominal $\mu = 0.30$.

Figure 11.- Concluded.

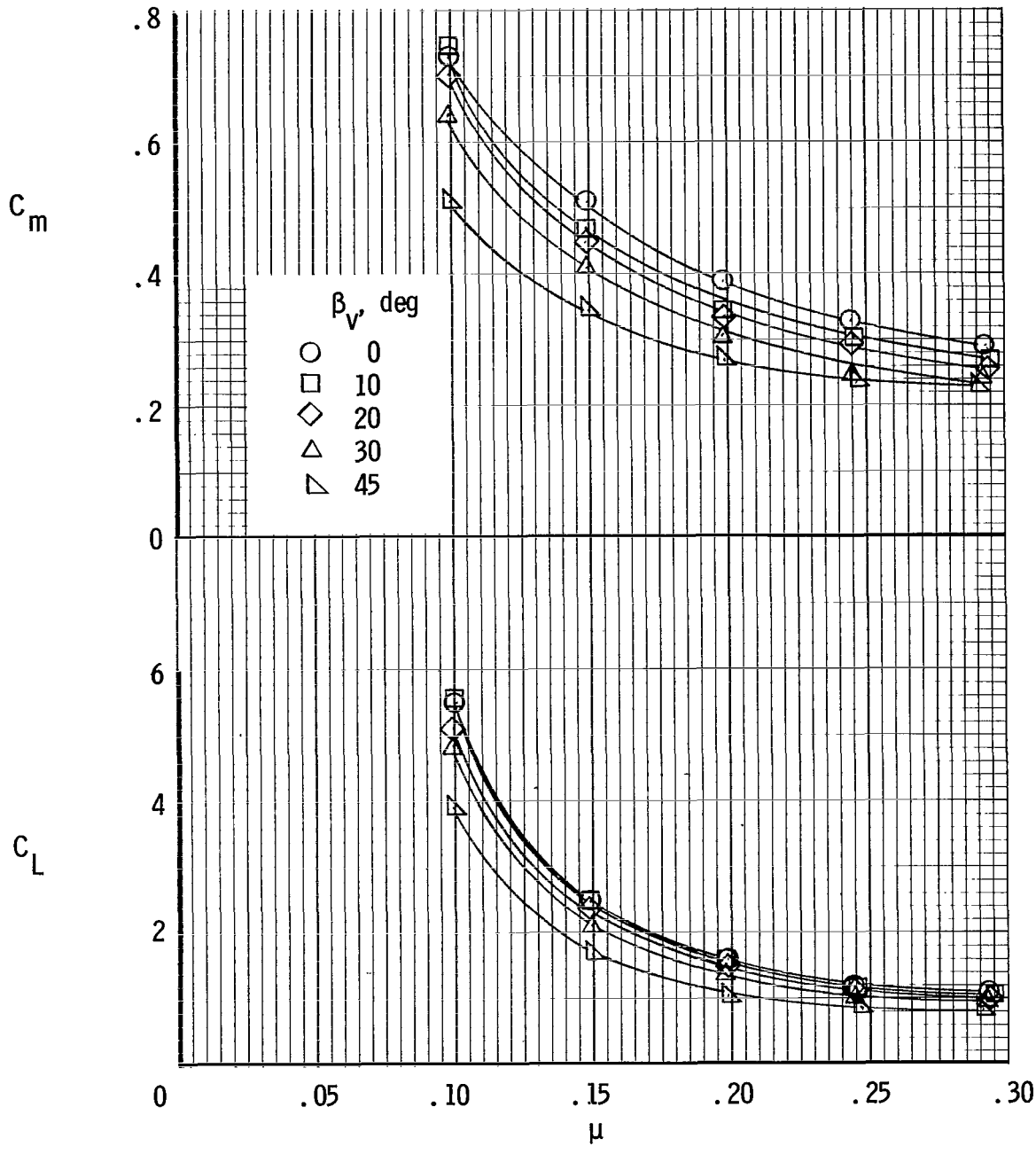

Figure 12.- Variation of longitudinal aerodynamic coefficients with tip-speed ratio for $\delta_f = 0^o$. $\alpha = 0^o$; horizontal tail off.

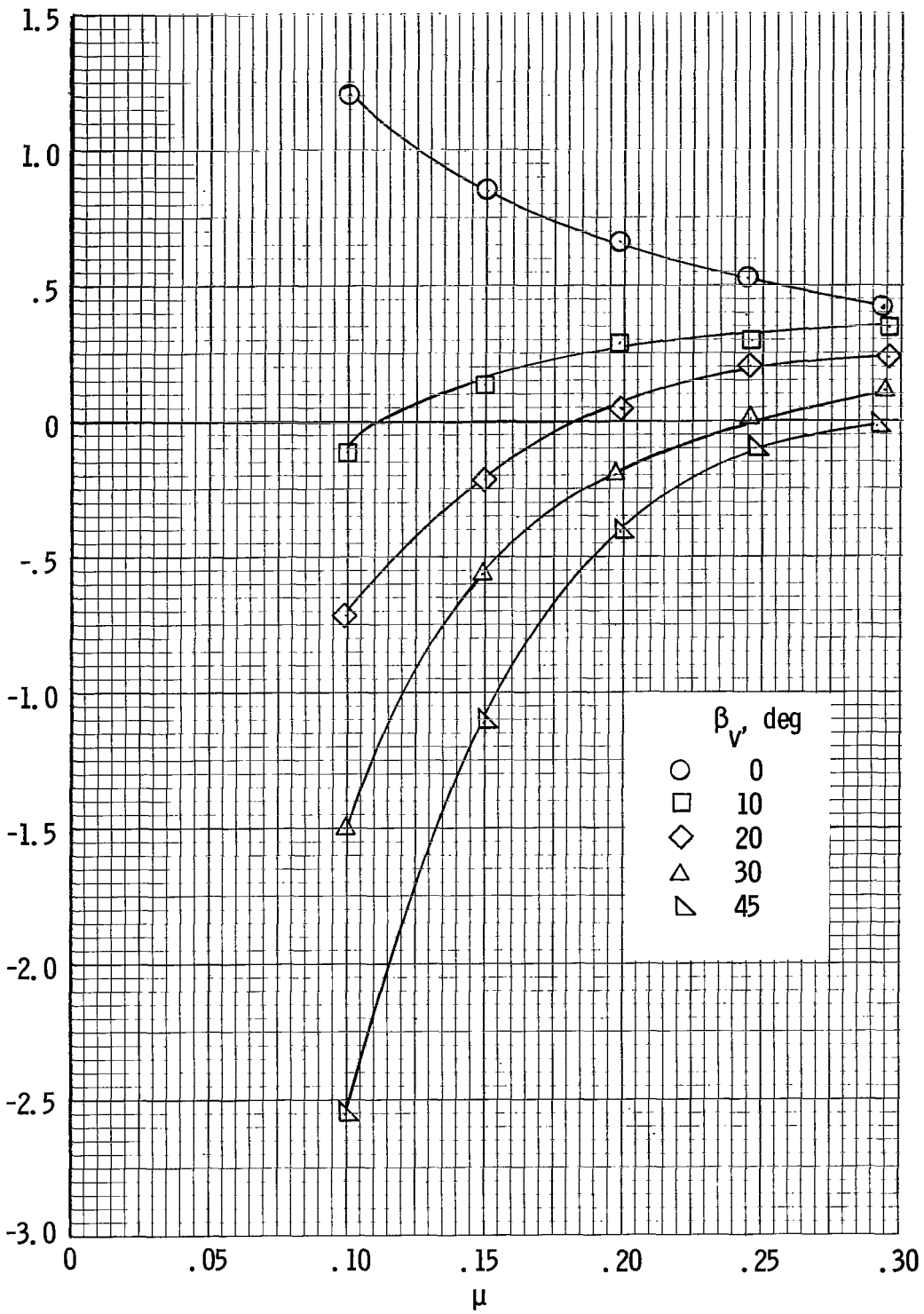

Figure 12.- Concluded.

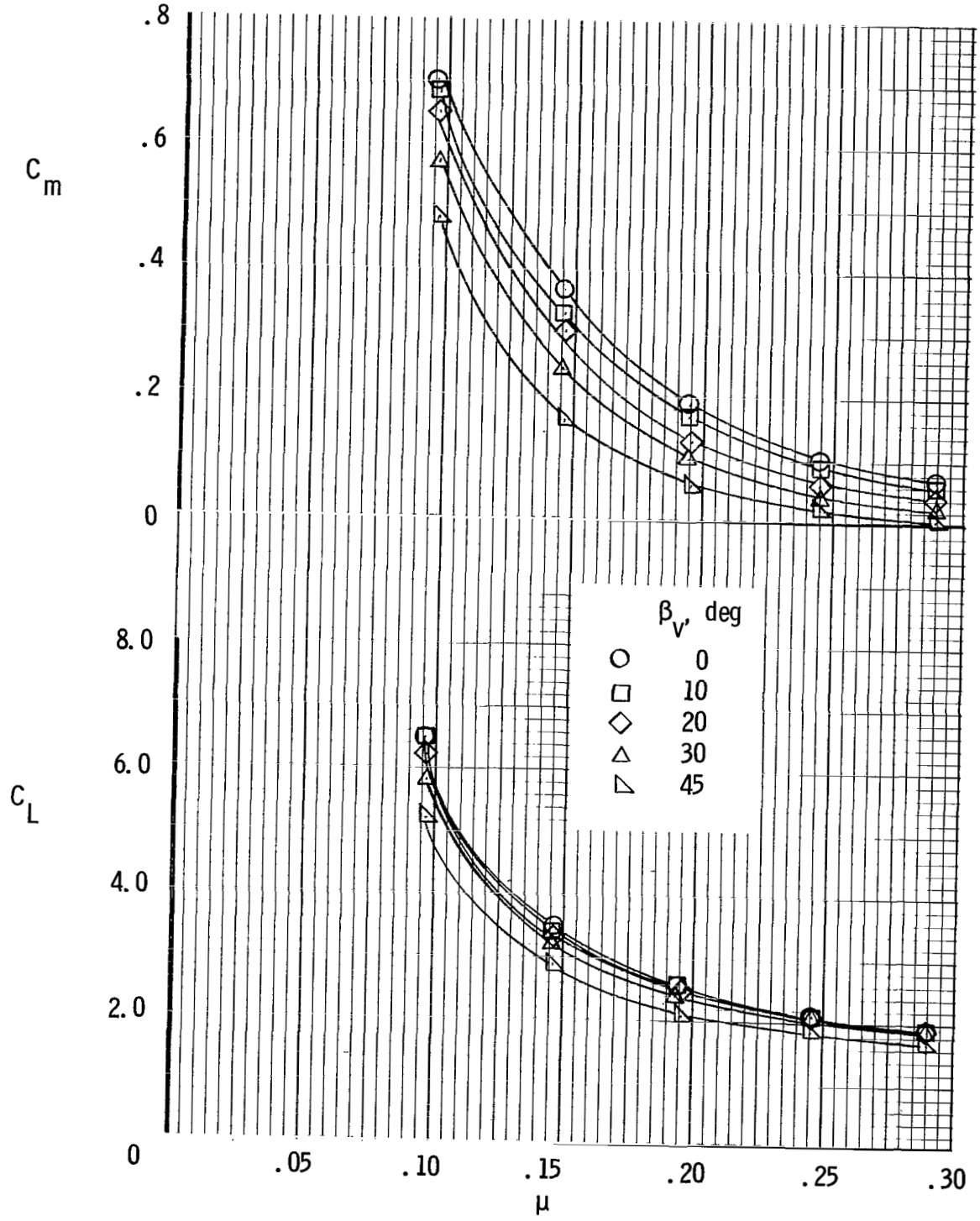

Figure 13.- Variation of longitudinal aerodynamic coefficients with tip-speed ratio for $\delta_f = 40^o$. $\alpha = 0^o$; horizontal tail off.

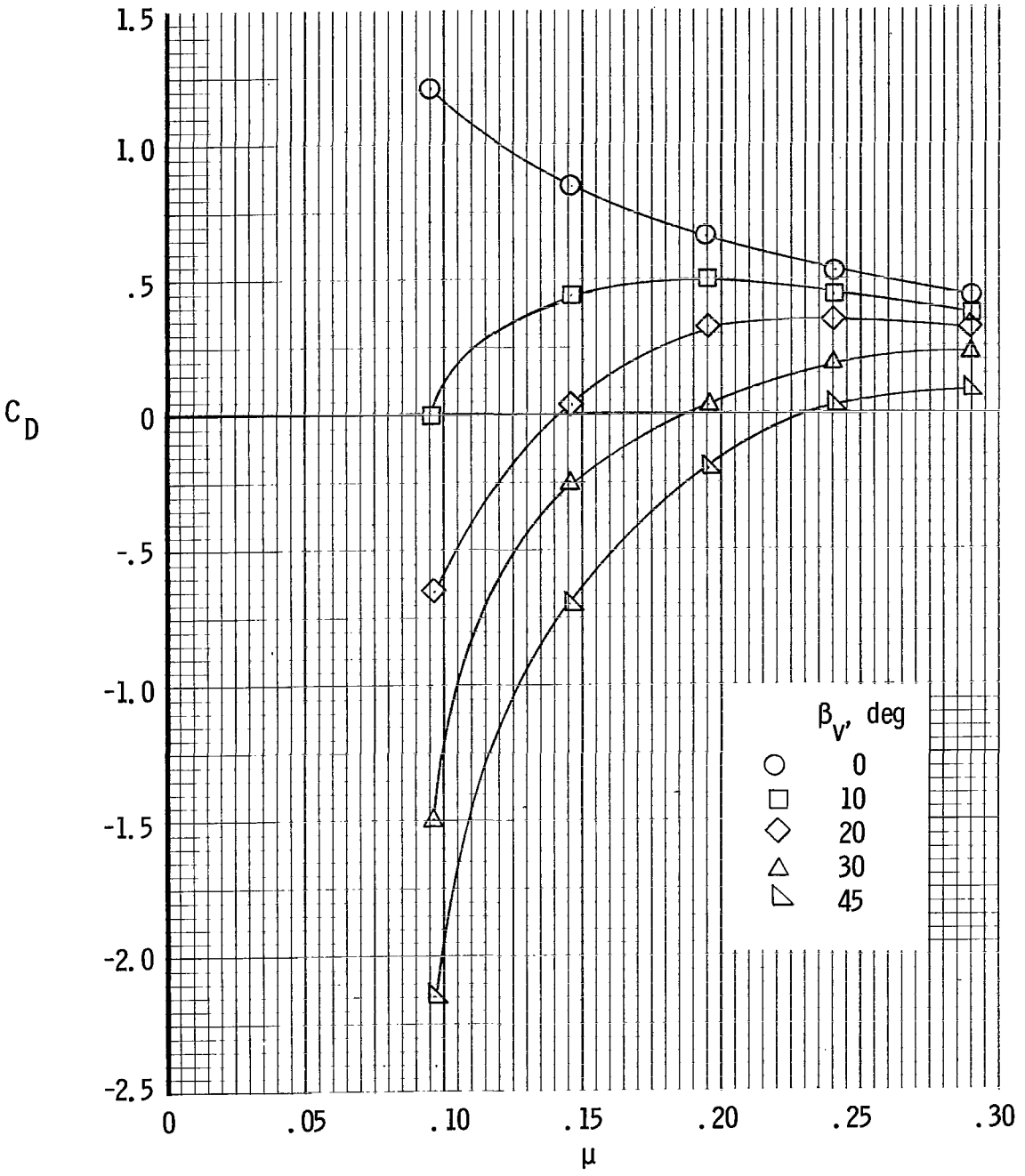

Figure 13.- Concluded.

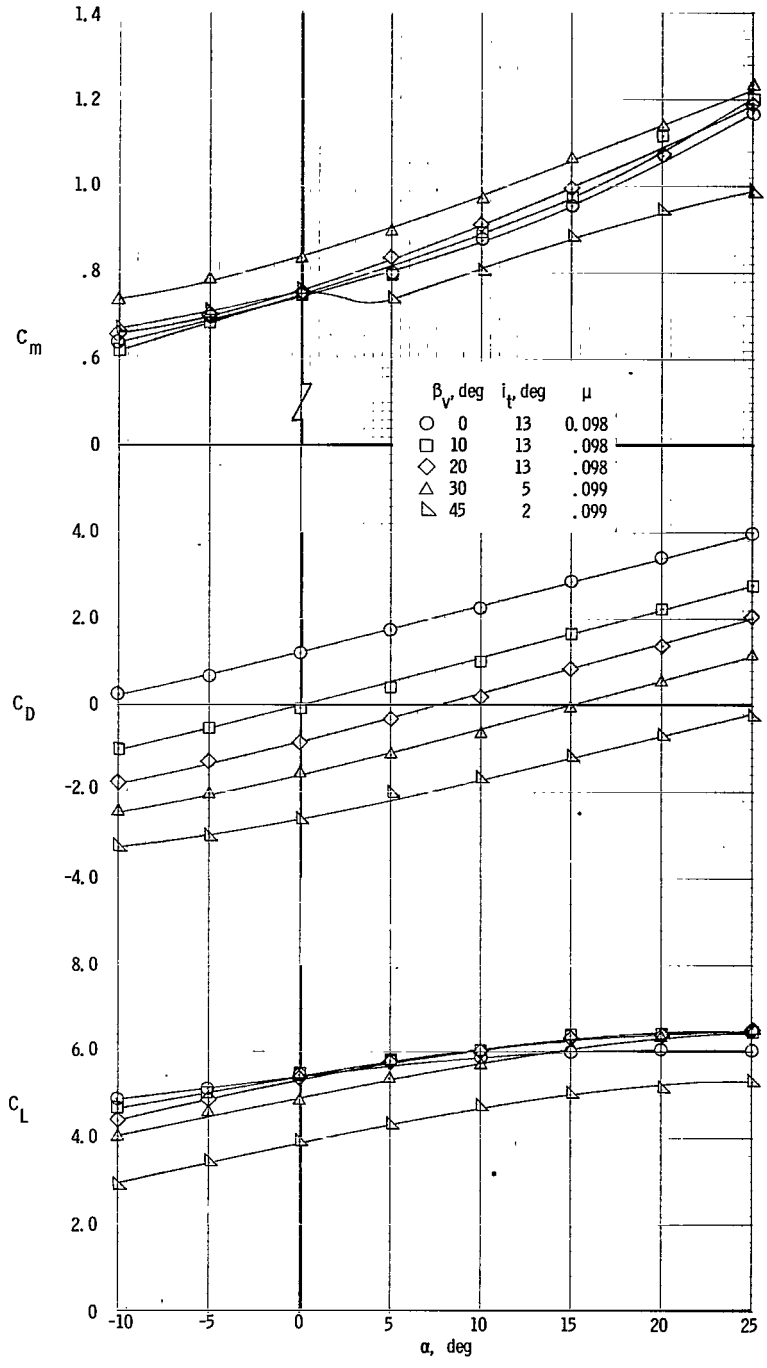

(a) Nominal $\mu = 0.10$.

Figure 14.- Effect of fan-exit-vane deflection on longitudinal aerodynamic characteristics for various tip-speed ratios and for $\delta_f = 0^0$. $S_h/S_w = 0.25$.

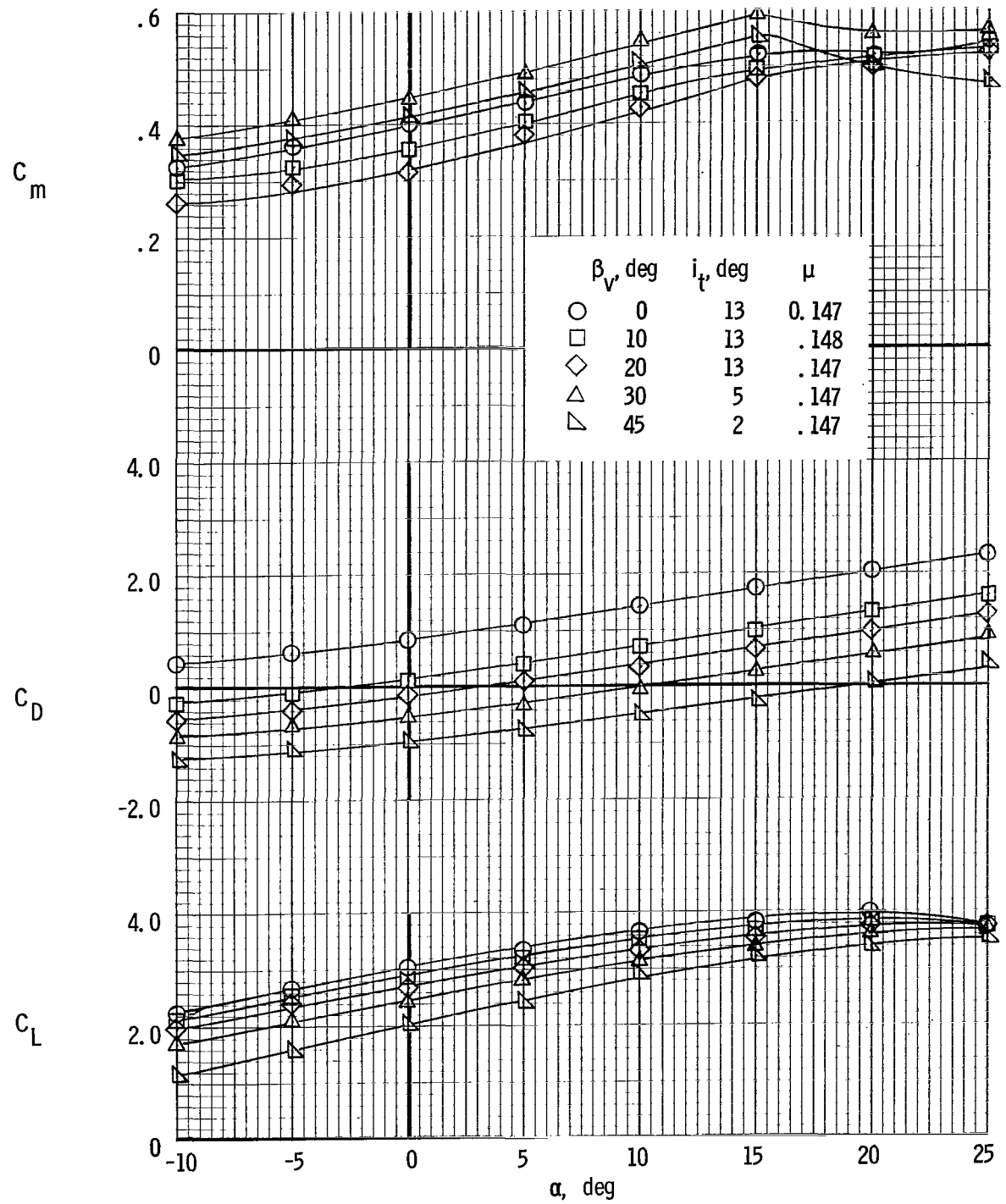

(b) Nominal μ = 0.15.

Figure 14.- Continued.

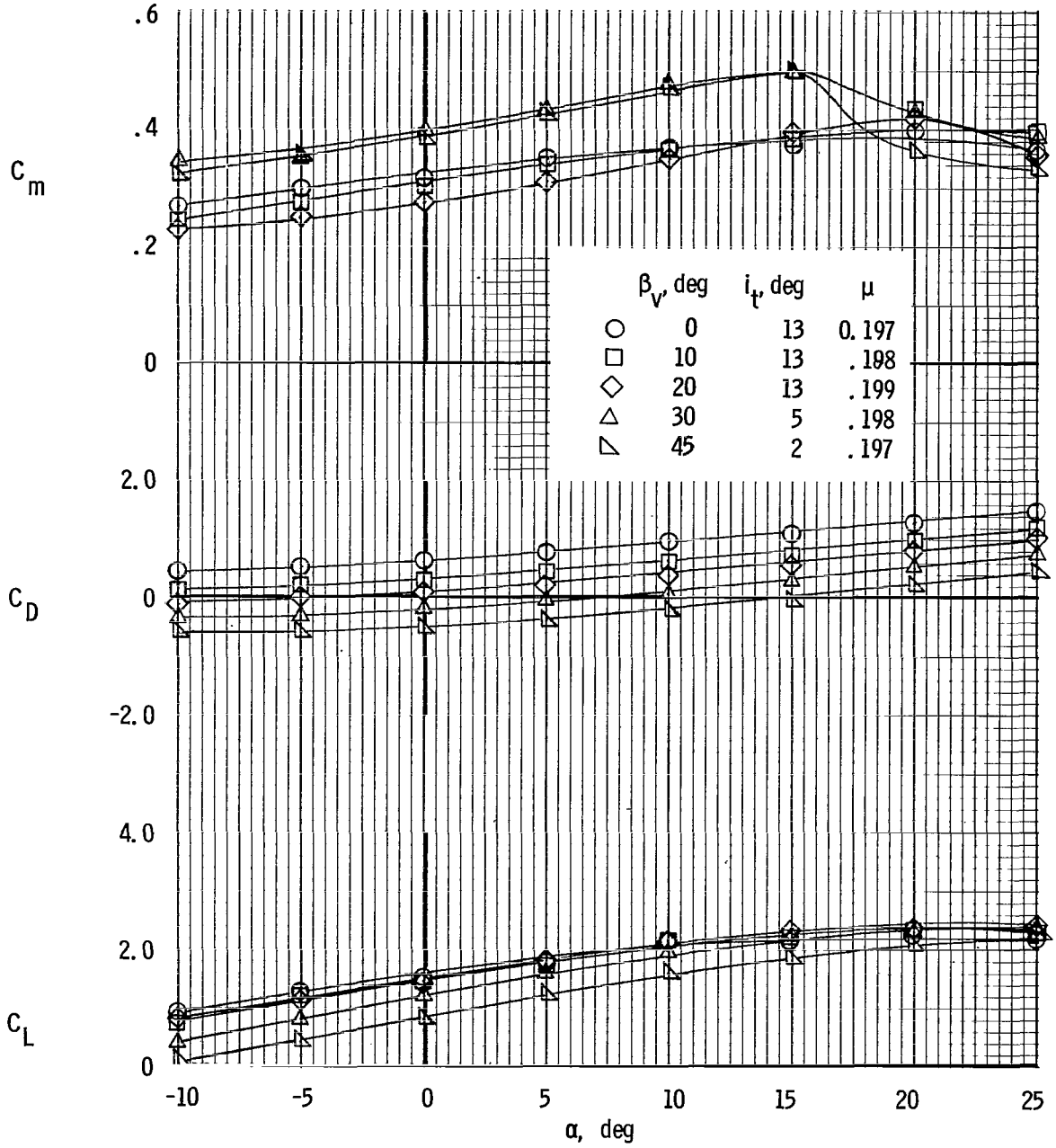

(c) Nominal $\mu = 0.20$.

Figure 14.- Continued.

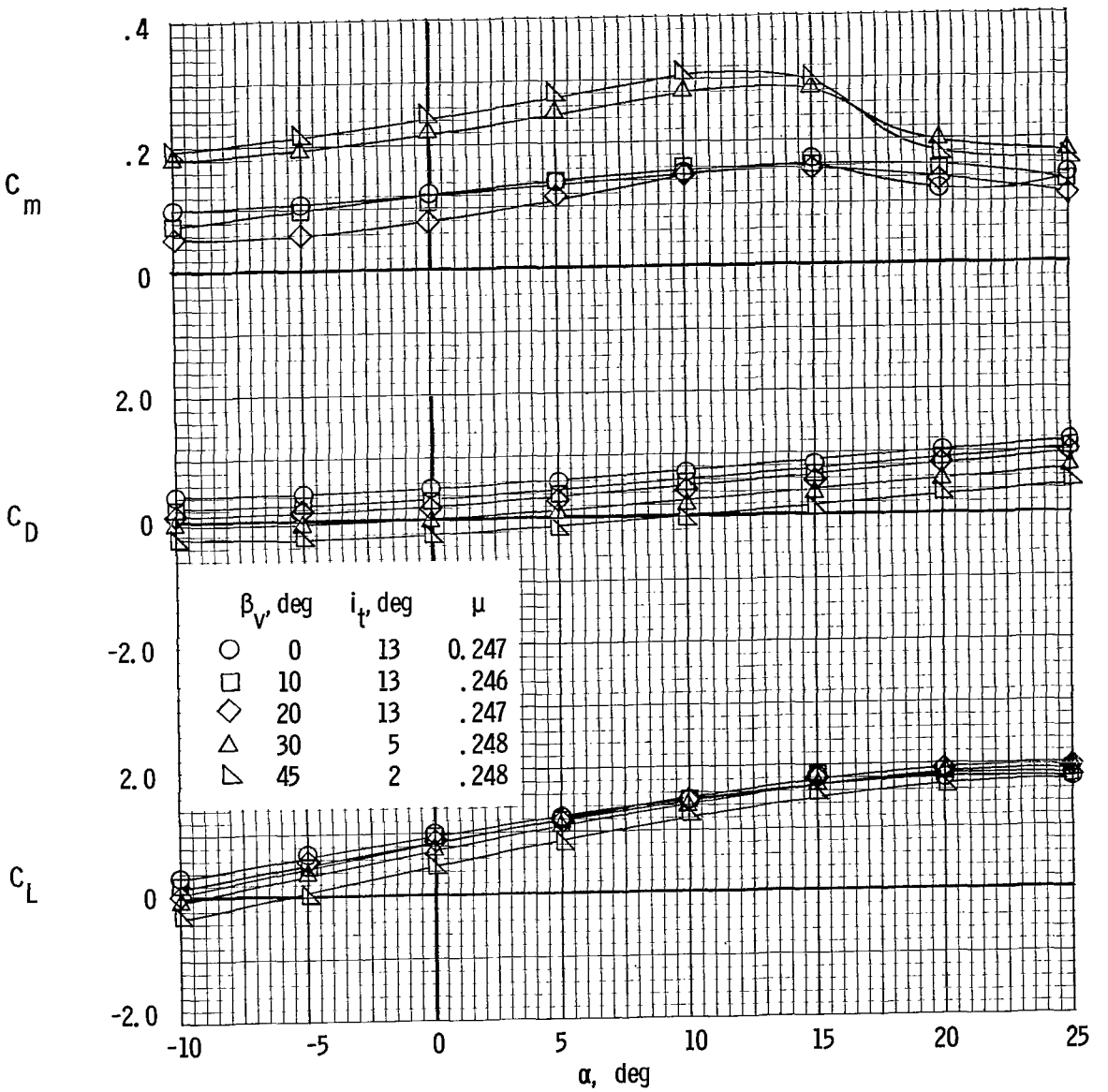

(d) Nominal $\mu = 0.25$.

Figure 14.- Continued.

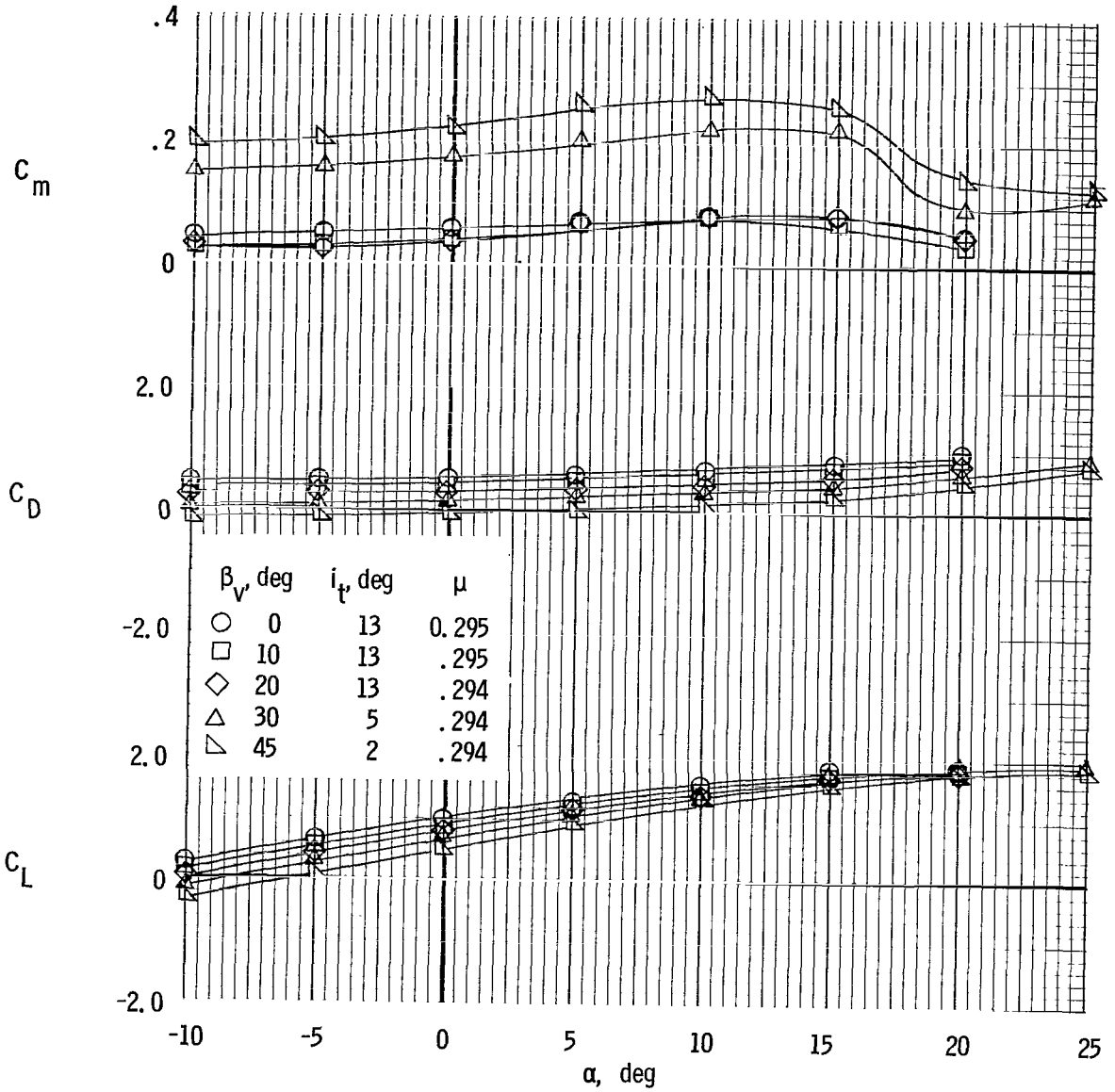

(e) Nominal μ = 0.30.

Figure 14.- Concluded.

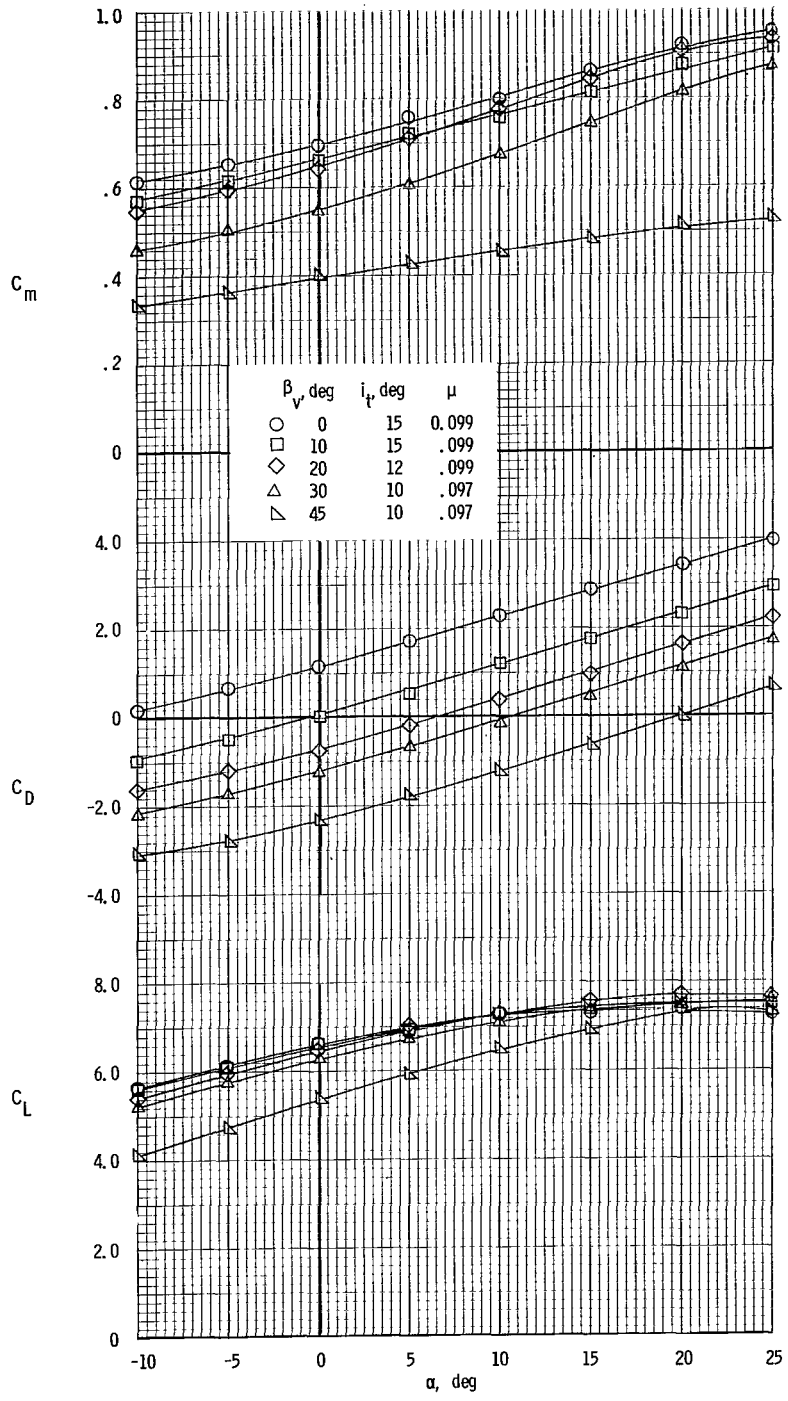

(a) Nominal $\mu = 0.10$.

Figure 15.- Effect of fan-exit-vane deflection on longitudinal aerodynamic characteristics for various tip-speed ratios and for $\delta_f = 40^o$. $S_h/S_w = 0.25$.

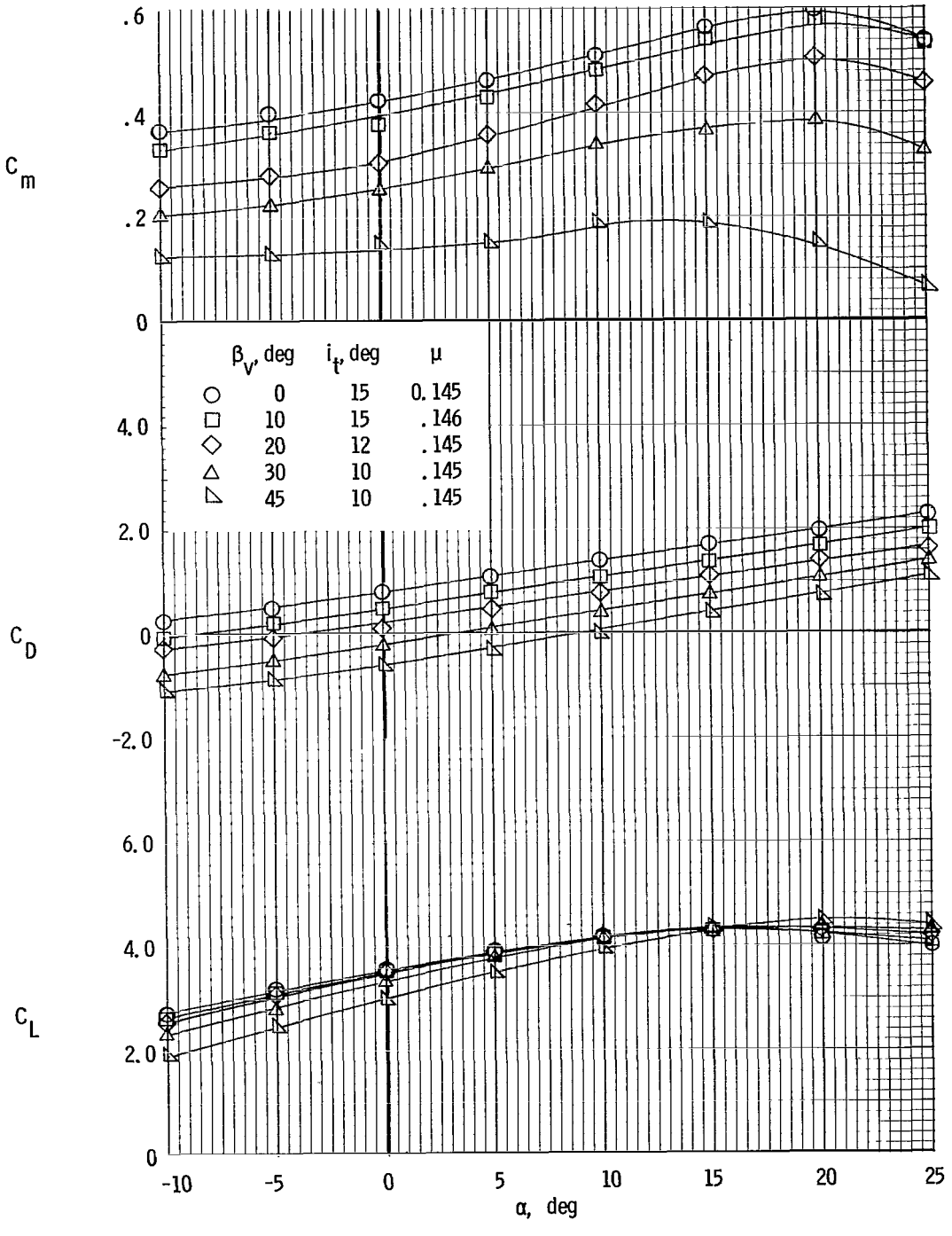

(b) Nominal $\mu = 0.15$.

Figure 15.- Continued.

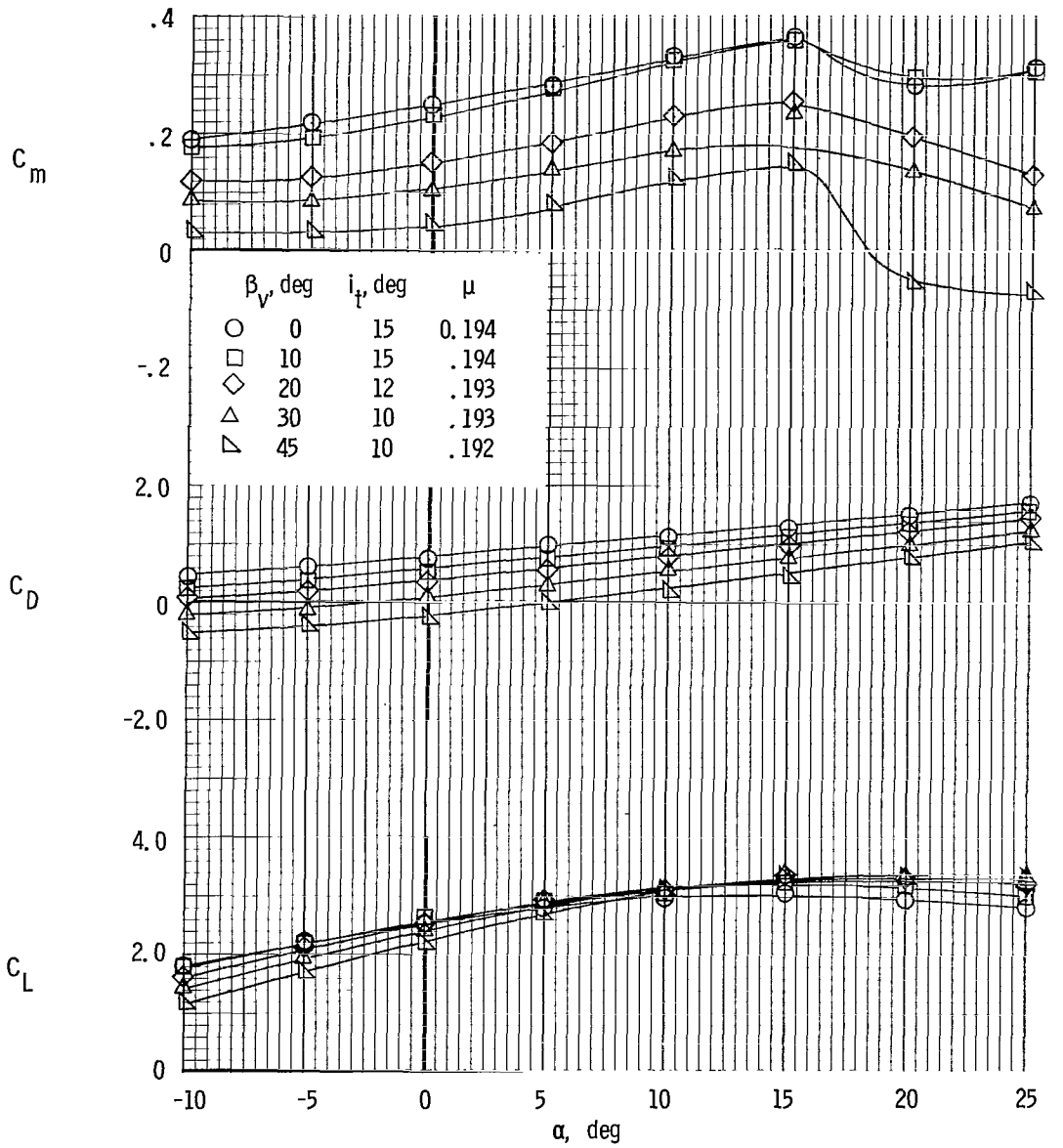

(c) Nominal $\mu = 0.20$.

Figure 15.- Continued.

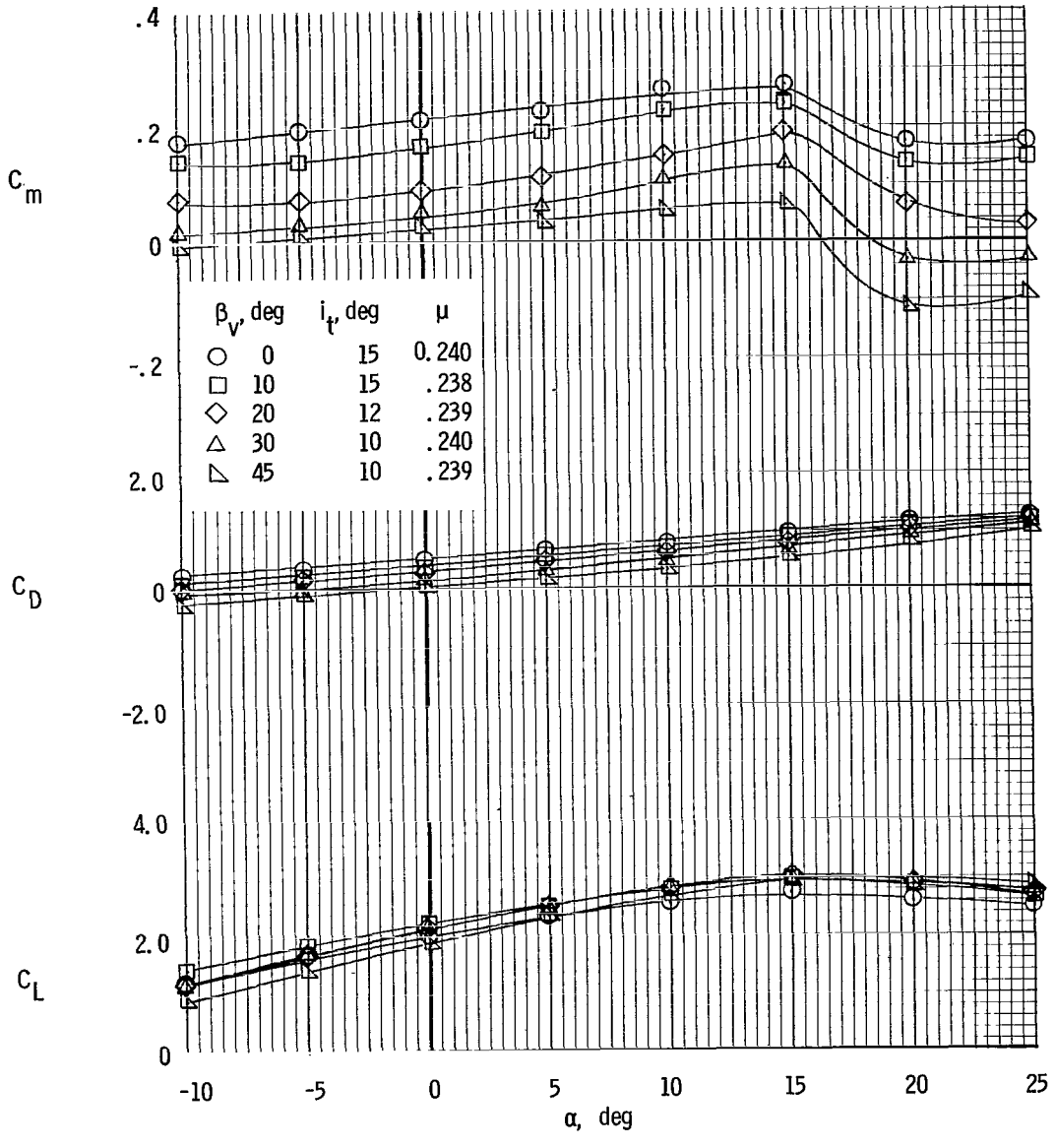

(d) Nominal μ = 0.25.

Figure 15.- Continued.

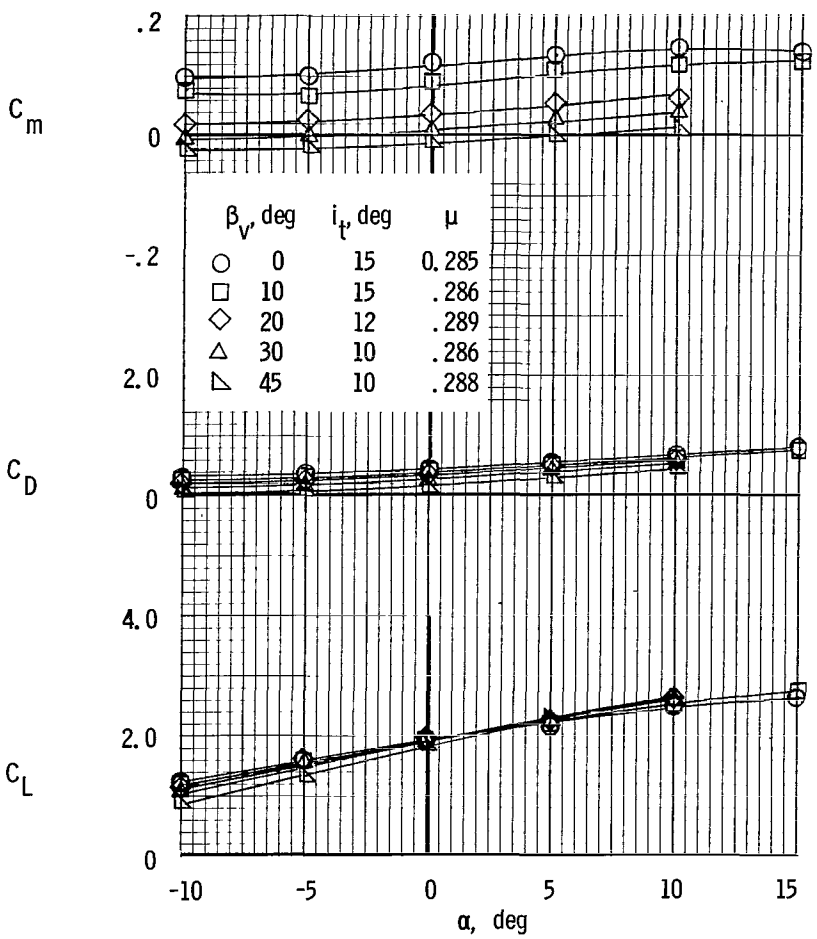

(e) Nominal $\mu = 0.30$.

Figure 15.- Concluded.

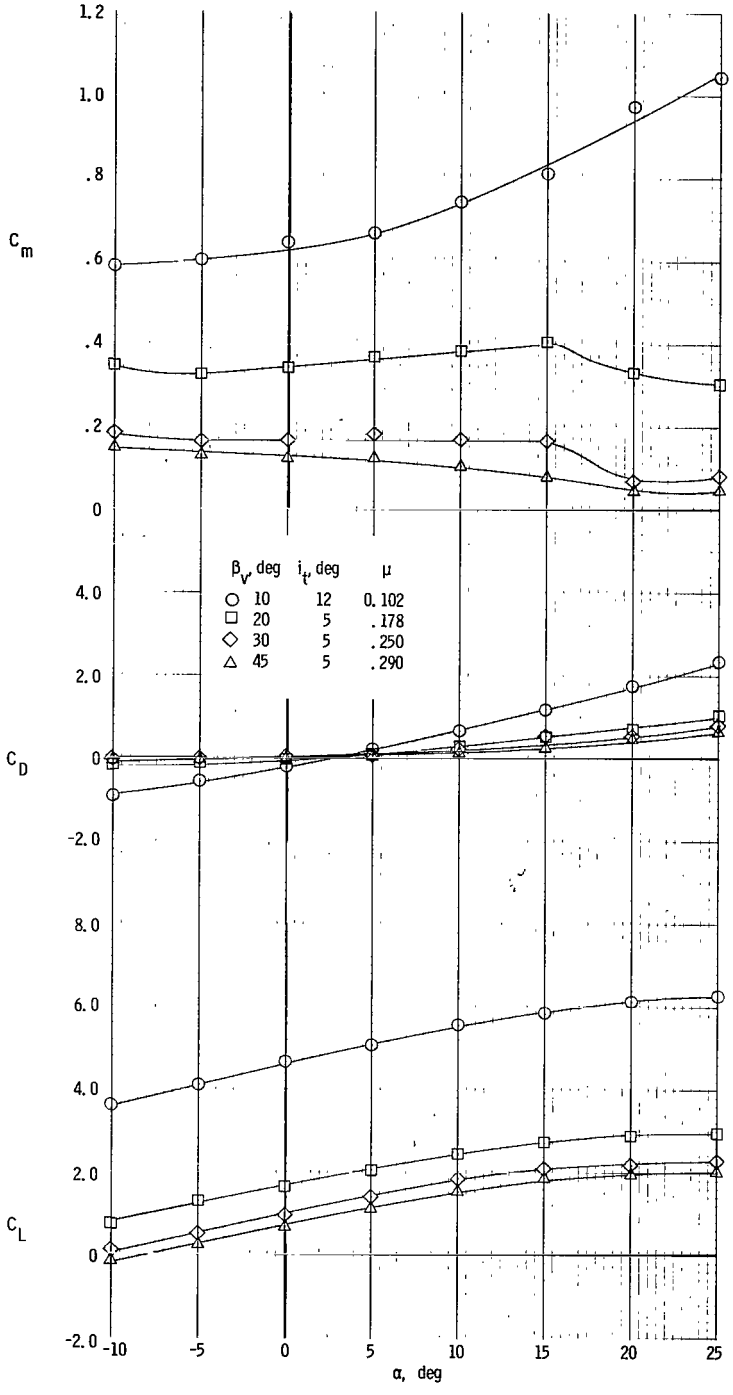

(a) $\delta_f = 0^0$.

Figure 16.- Longitudinal aerodynamic characteristics through transition speed range with $S_h/S_W = 0.30$. Drag trimmed at $\alpha = 0^0$.

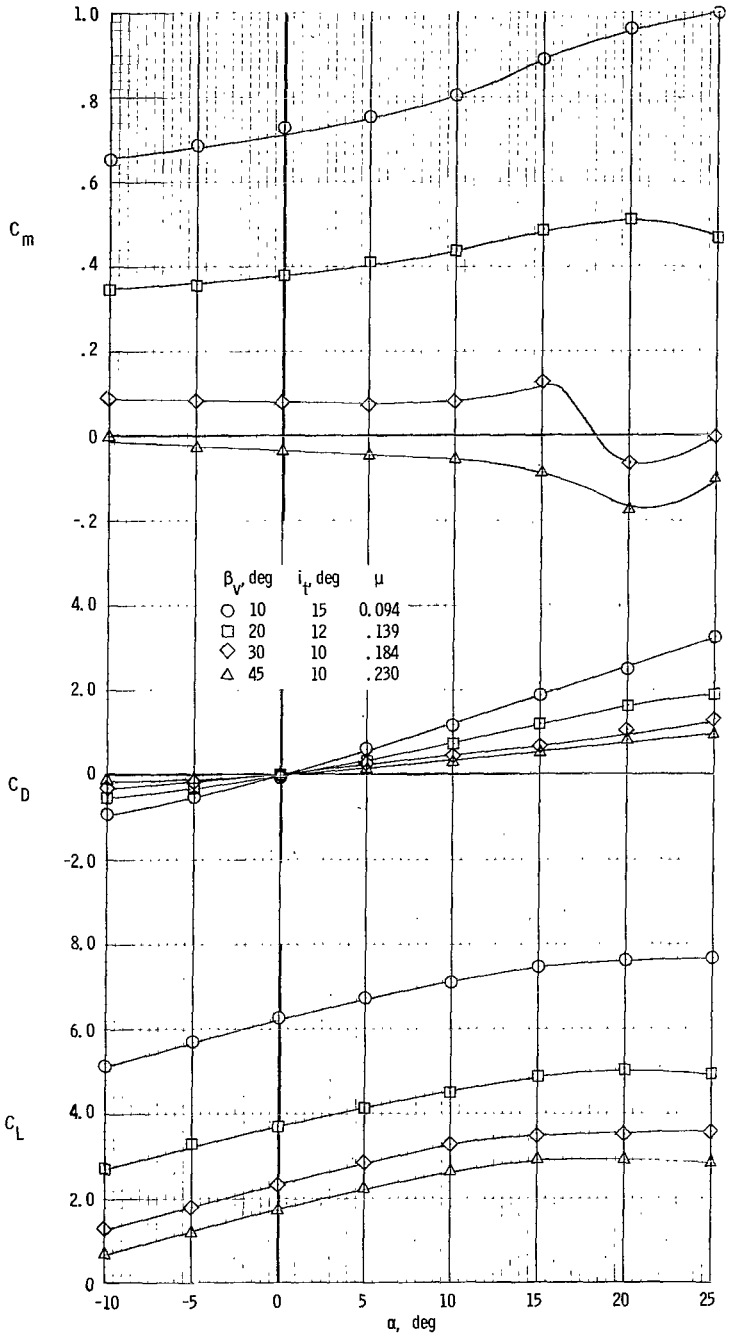

(b) $\delta_f = 40^o$.

Figure 16.- Concluded.

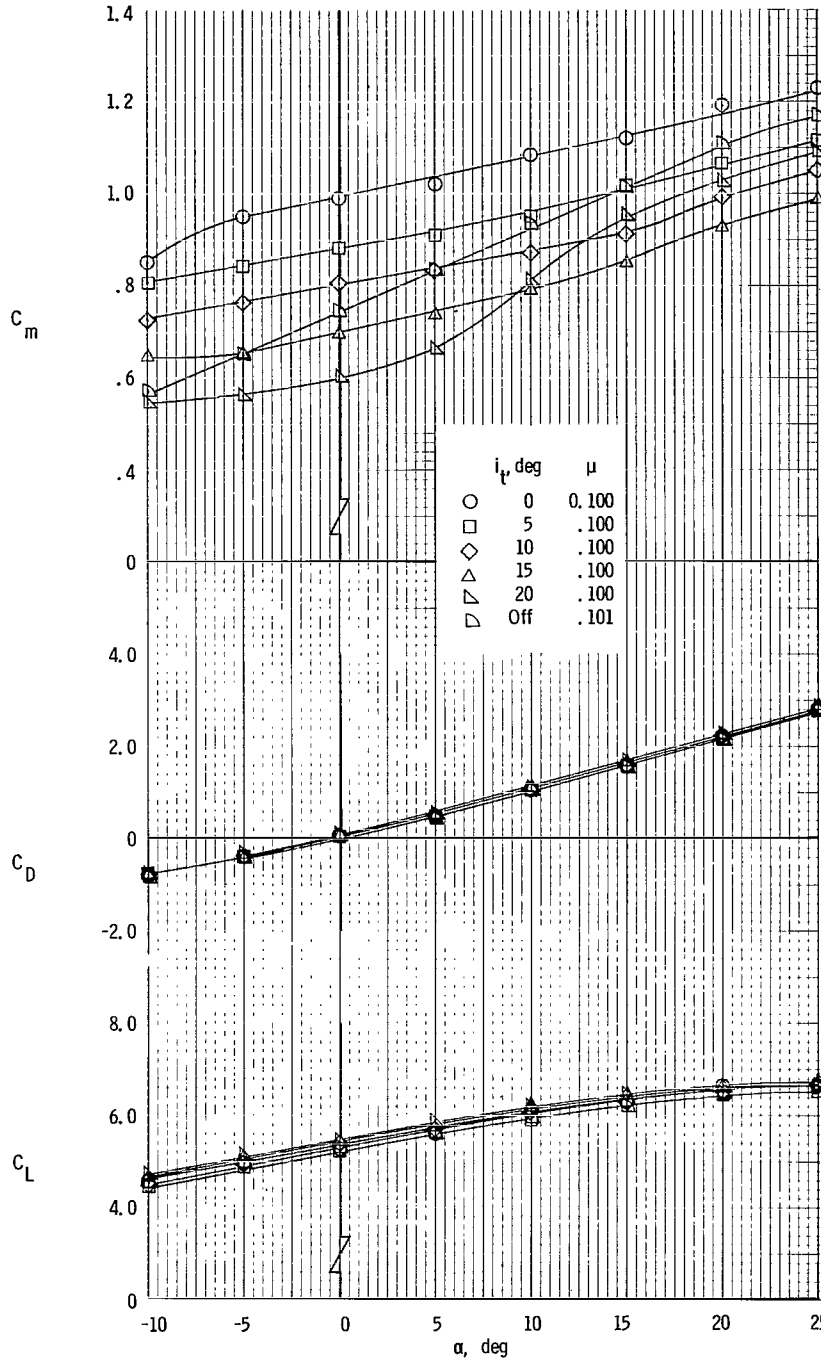

(a) $\beta_V = 10^0$.

Figure 17.- Effect of horizontal-tail incidence on longitudinal aerodynamic characteristics of model with $\delta_f = 0^0$. Drag trimmed at $\alpha = 0^0$; $S_h/S_W = 0.25$.

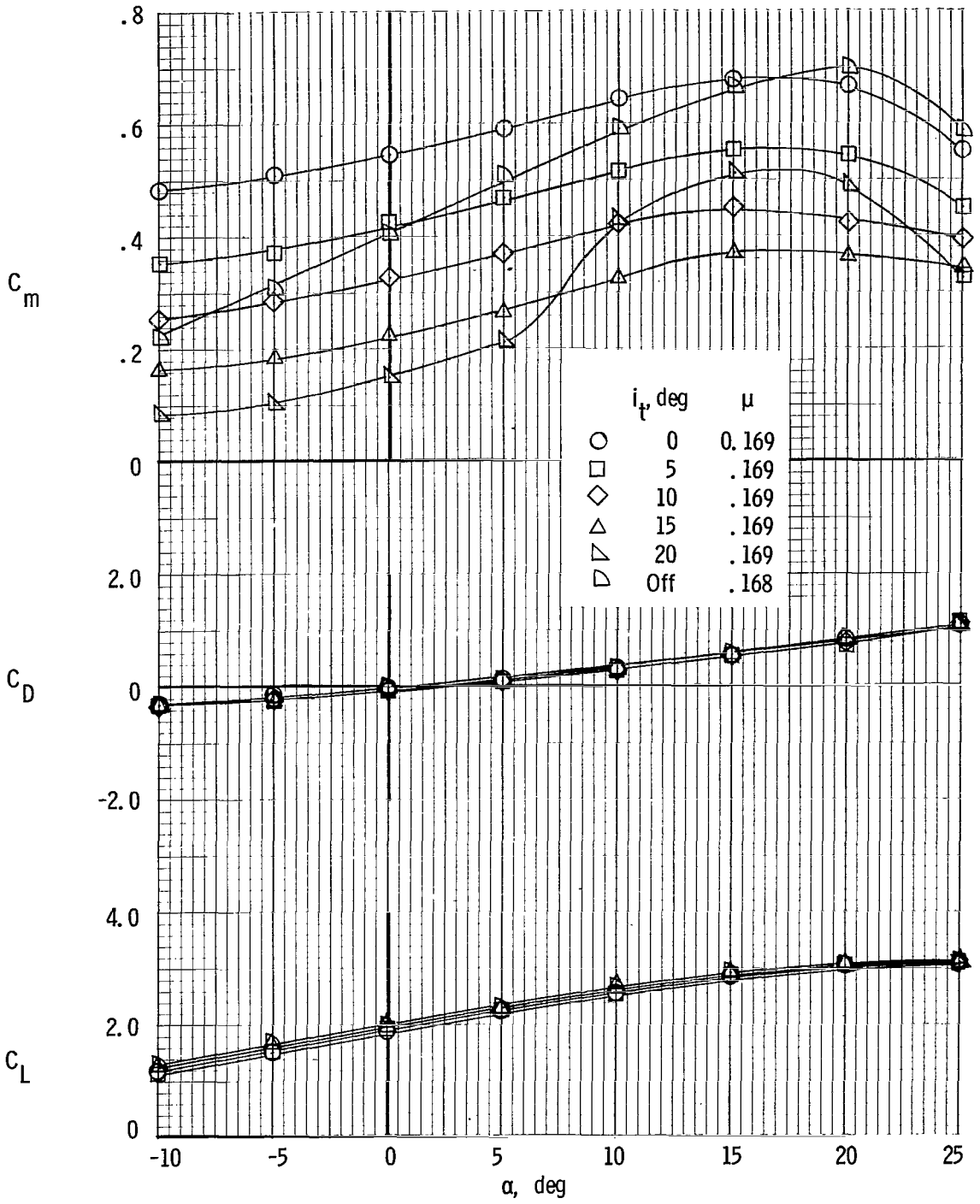

(b) $\beta_v = 20^0$.

Figure 17.- Continued.

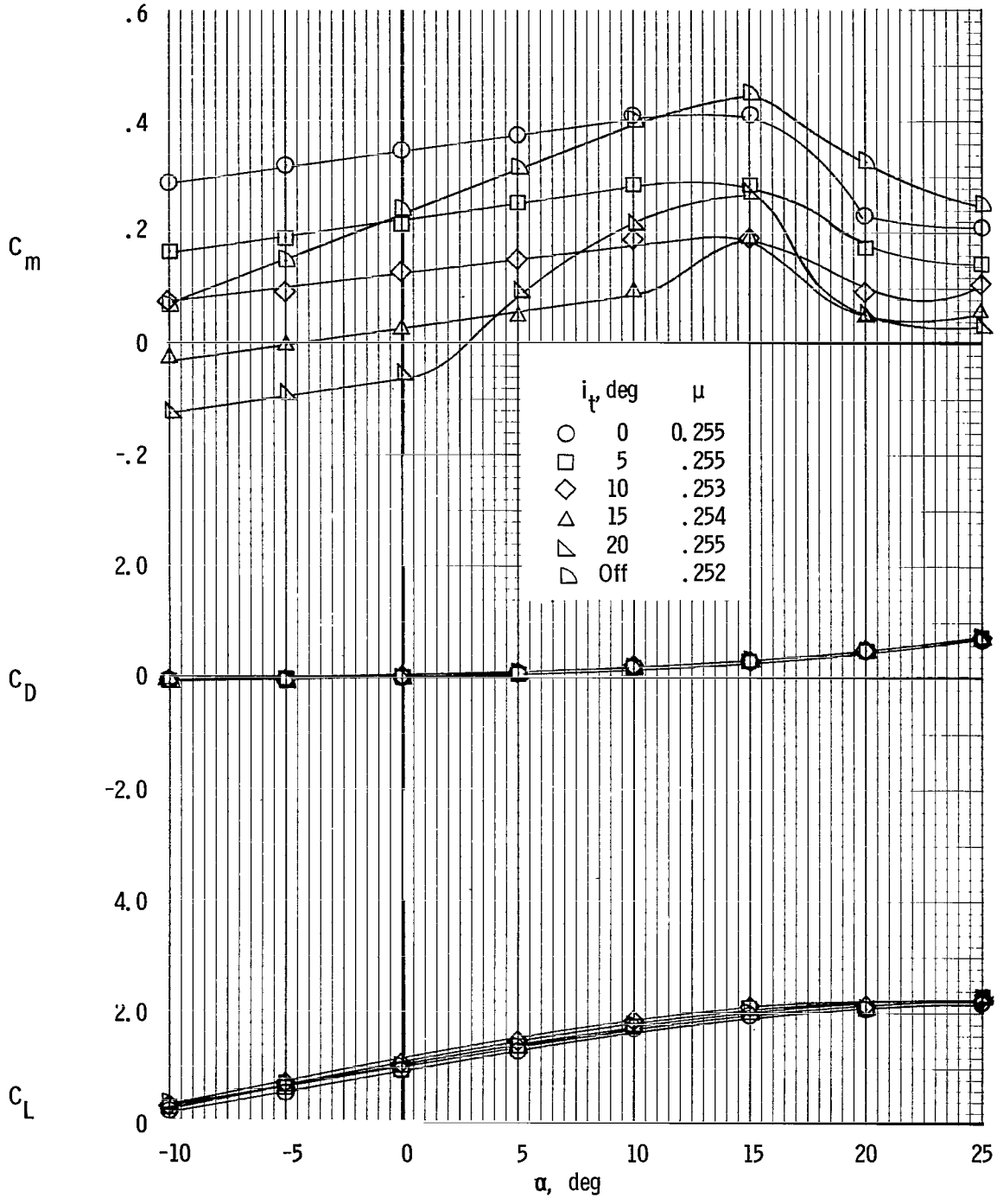

(c) $\beta_v = 30^0$.

Figure 17.- Continued.

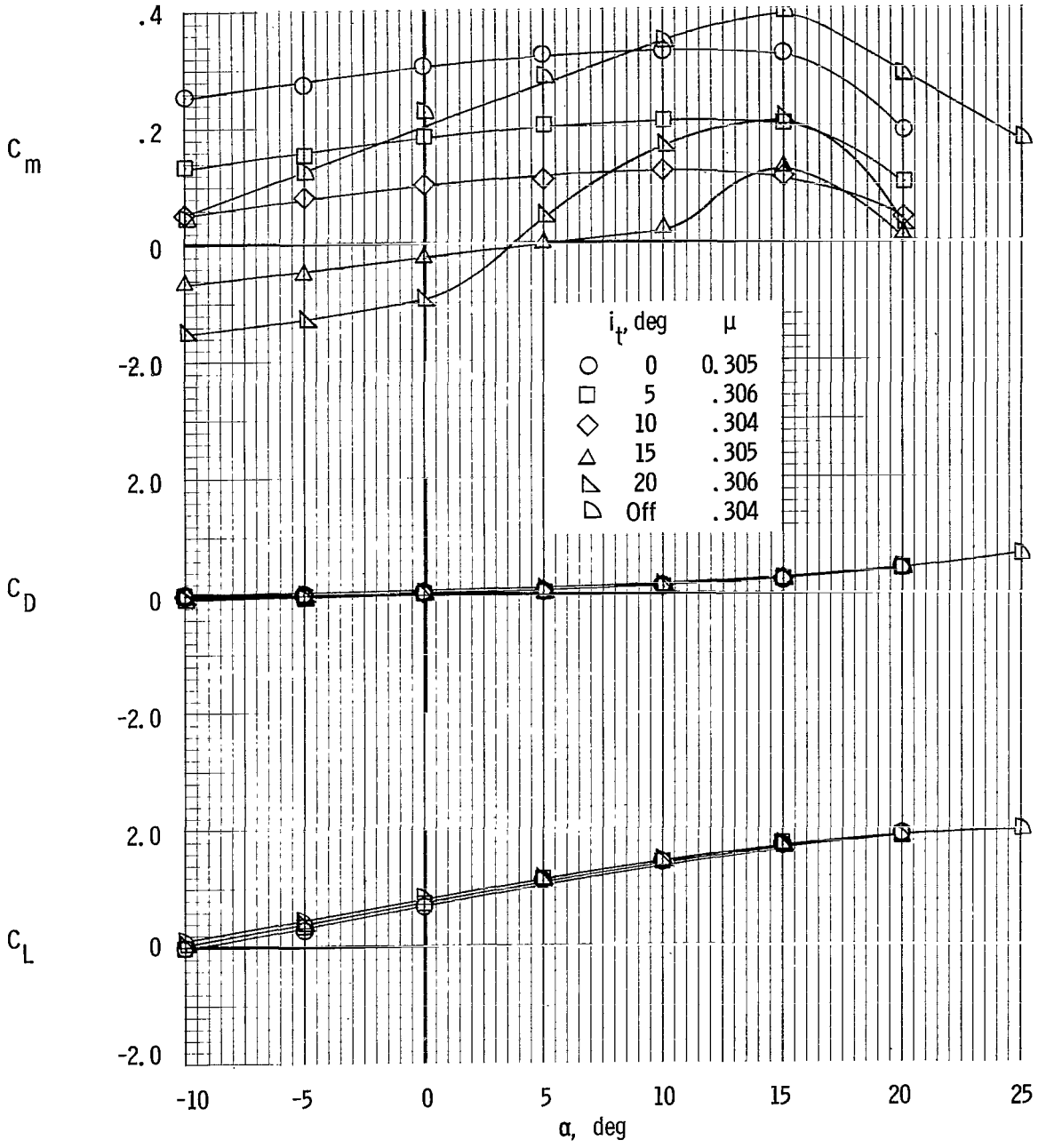

(d) $\beta_V = 45^o$.

Figure 17.- Concluded.

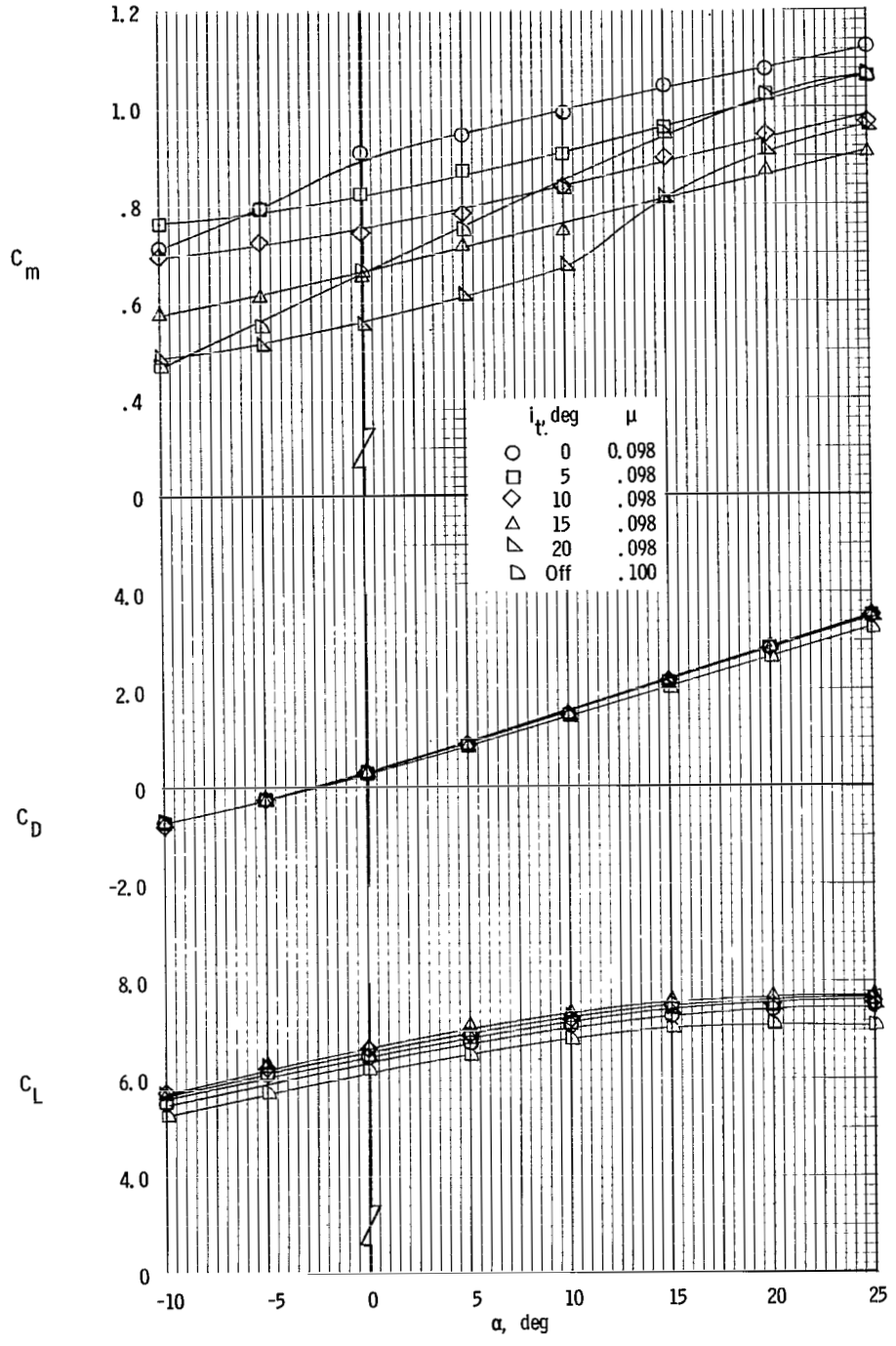

(a) $\beta_V = 10^0$.

Figure 18.- Effect of horizontal-tail incidence on longitudinal aerodynamic characteristics of model with $\delta_f = 40^0$. Drag trimmed at $\alpha = 0^0$; $S_h/S_w = 0.25$.

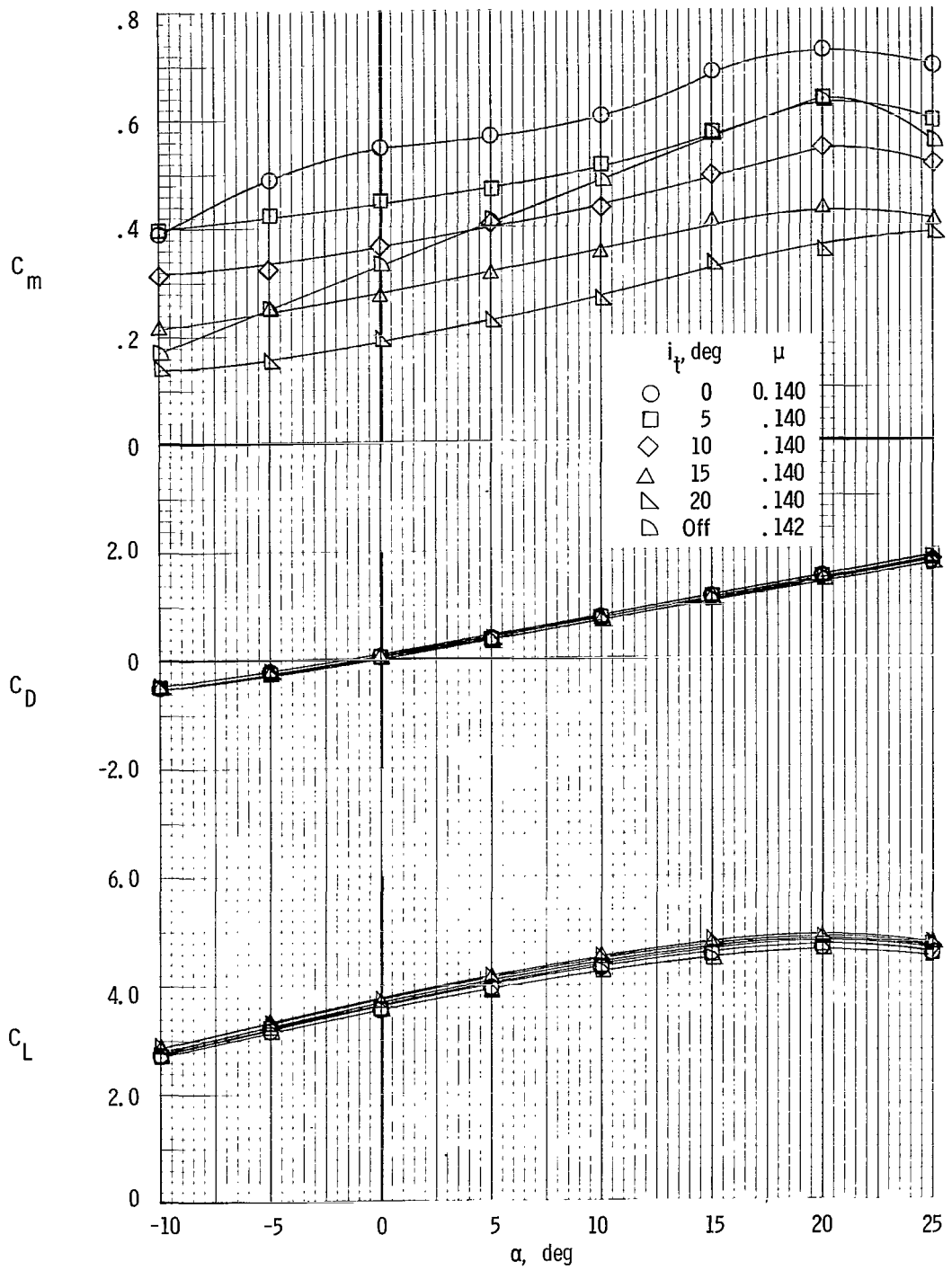

(b) $\beta_V = 20^\circ$.

Figure 18.- Continued.

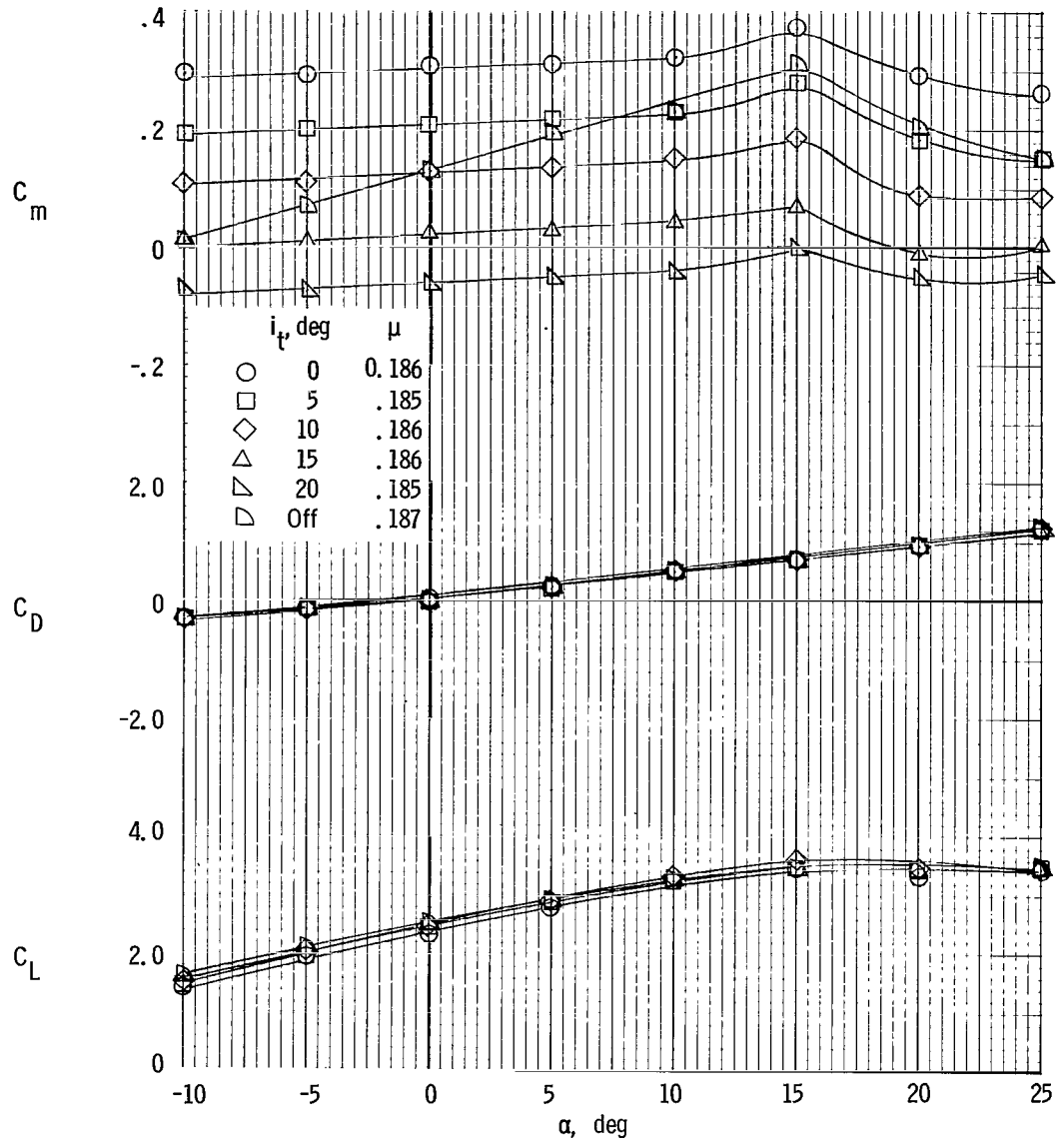

(c) $\beta_V = 30^0$.

Figure 18.- Continued.

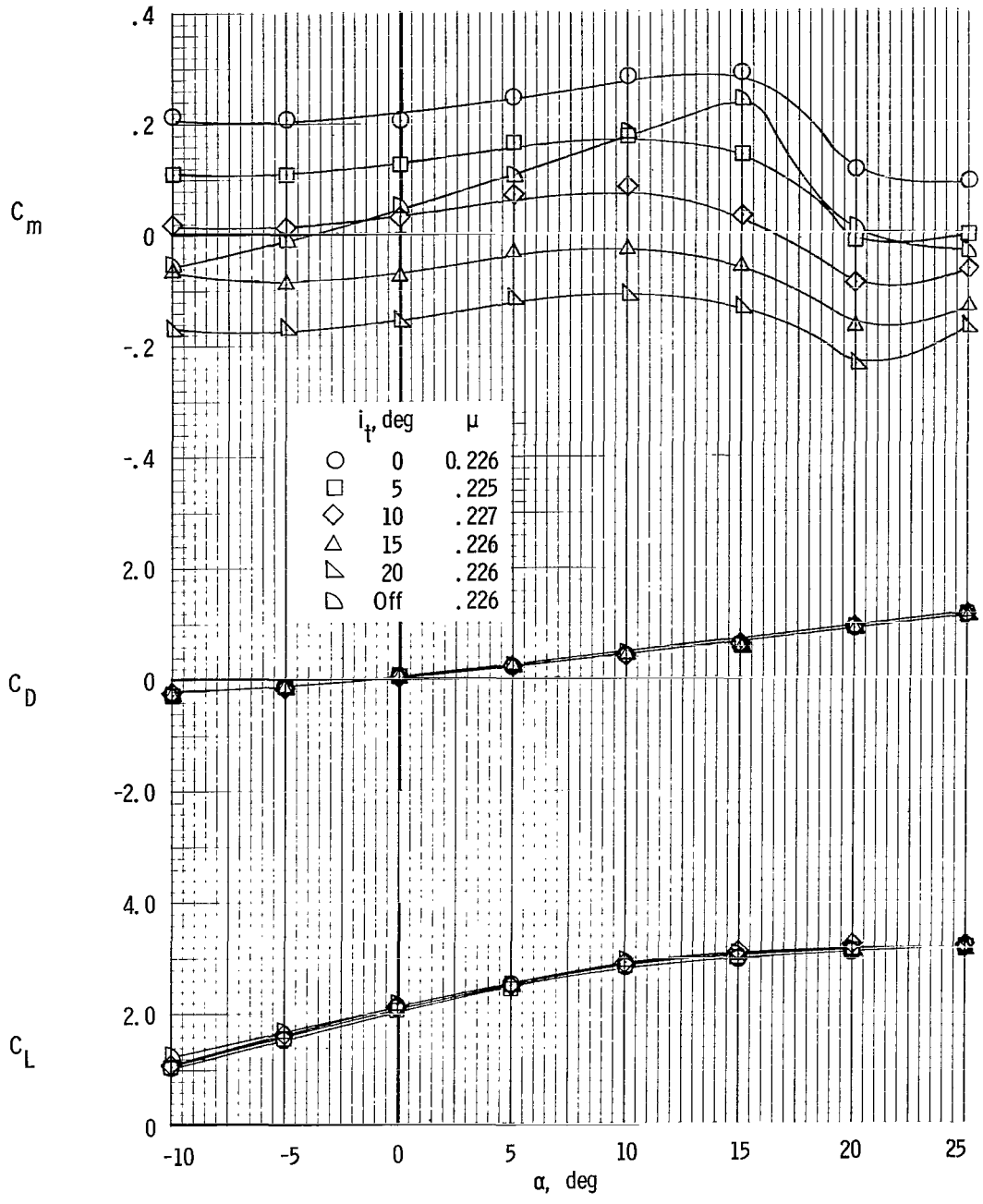

(d) $\beta_V = 45^o$.

Figure 18.- Concluded.

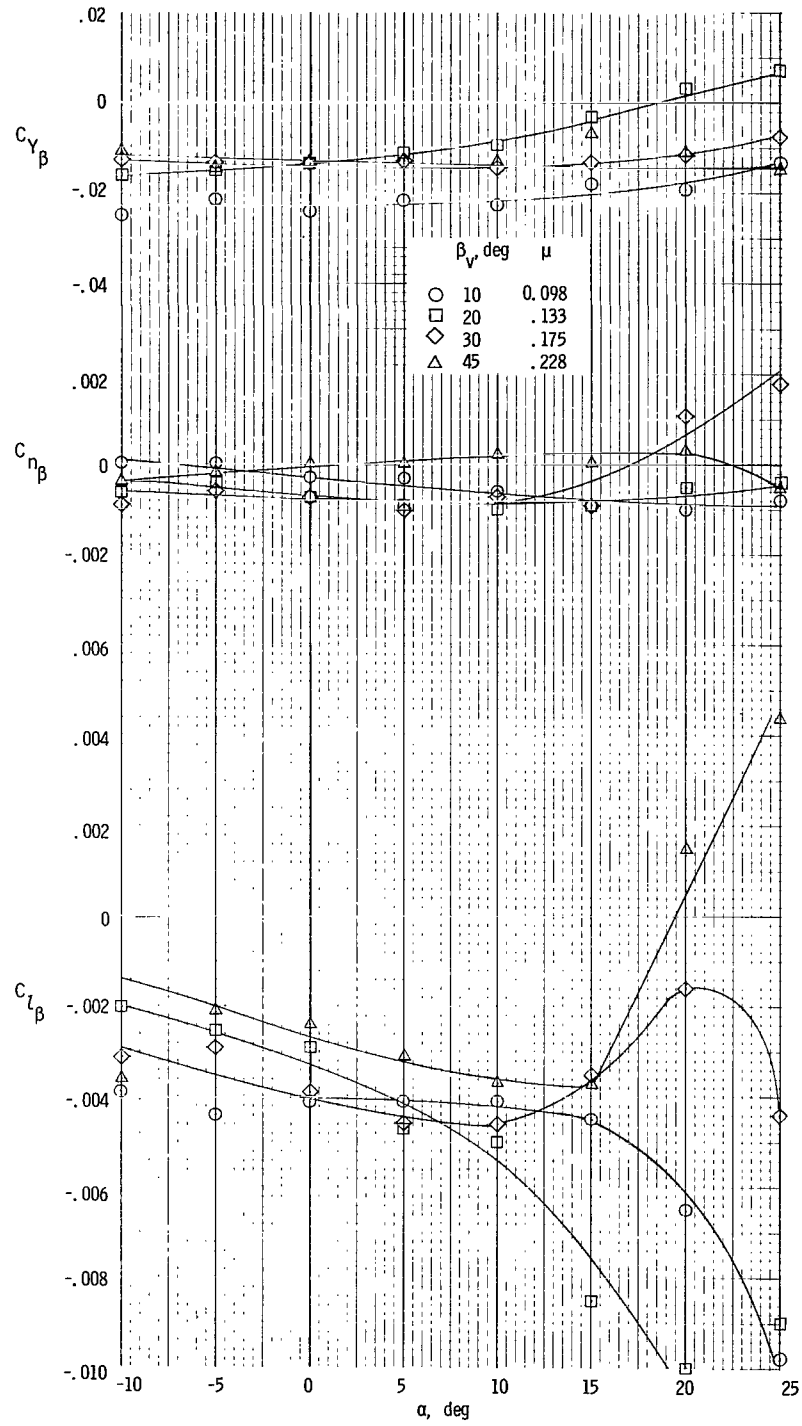

Figure 19.- Variation of static lateral-directional stability characteristics with angle of attack through transition speed range for $\delta_f = 40^0$. Tails off; drag trimmed at $\alpha = 0^0$.

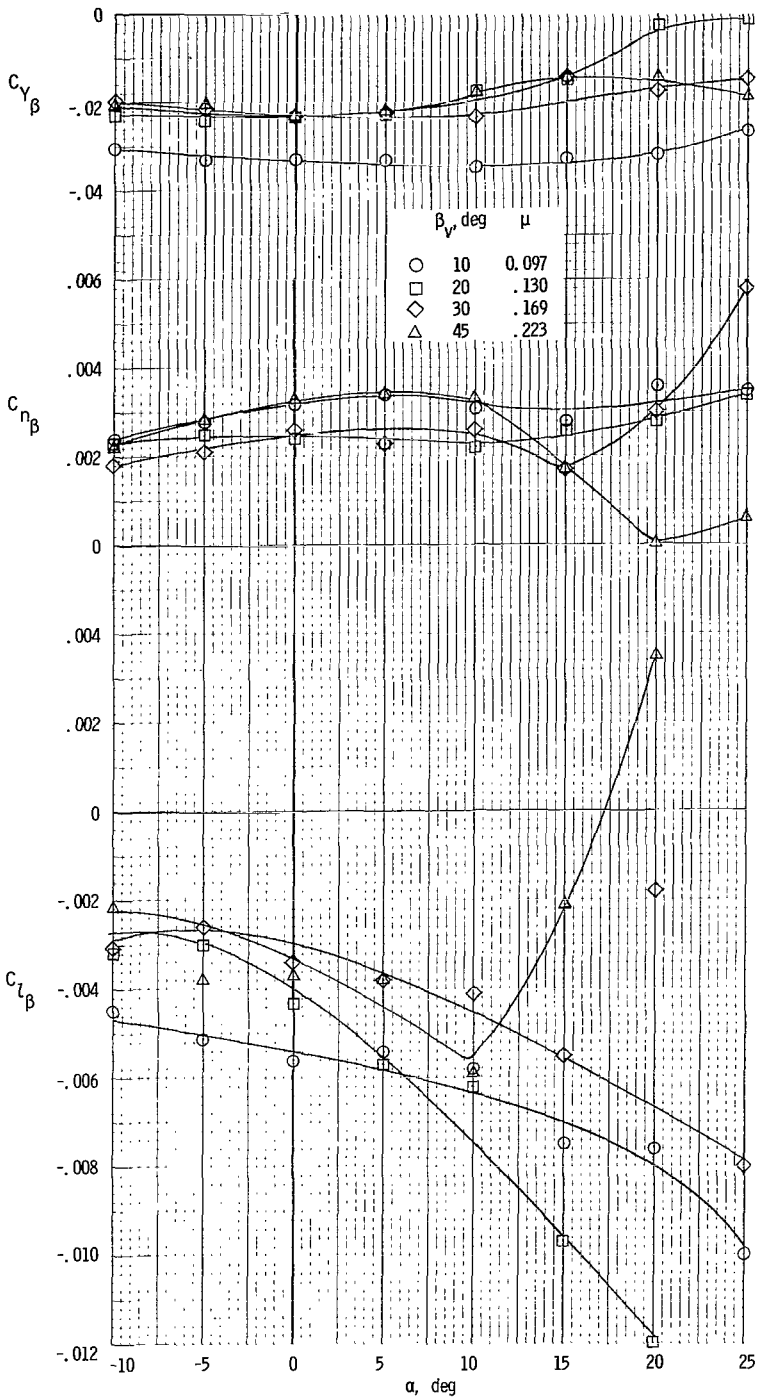

(a) Drag trimmed at $\alpha = 0^0$.

Figure 20.- Variation of static lateral-directional stability characteristics with angle of attack through transition speed range for $\delta_f = 40^0$. $S_h/S_w = 0.25$.

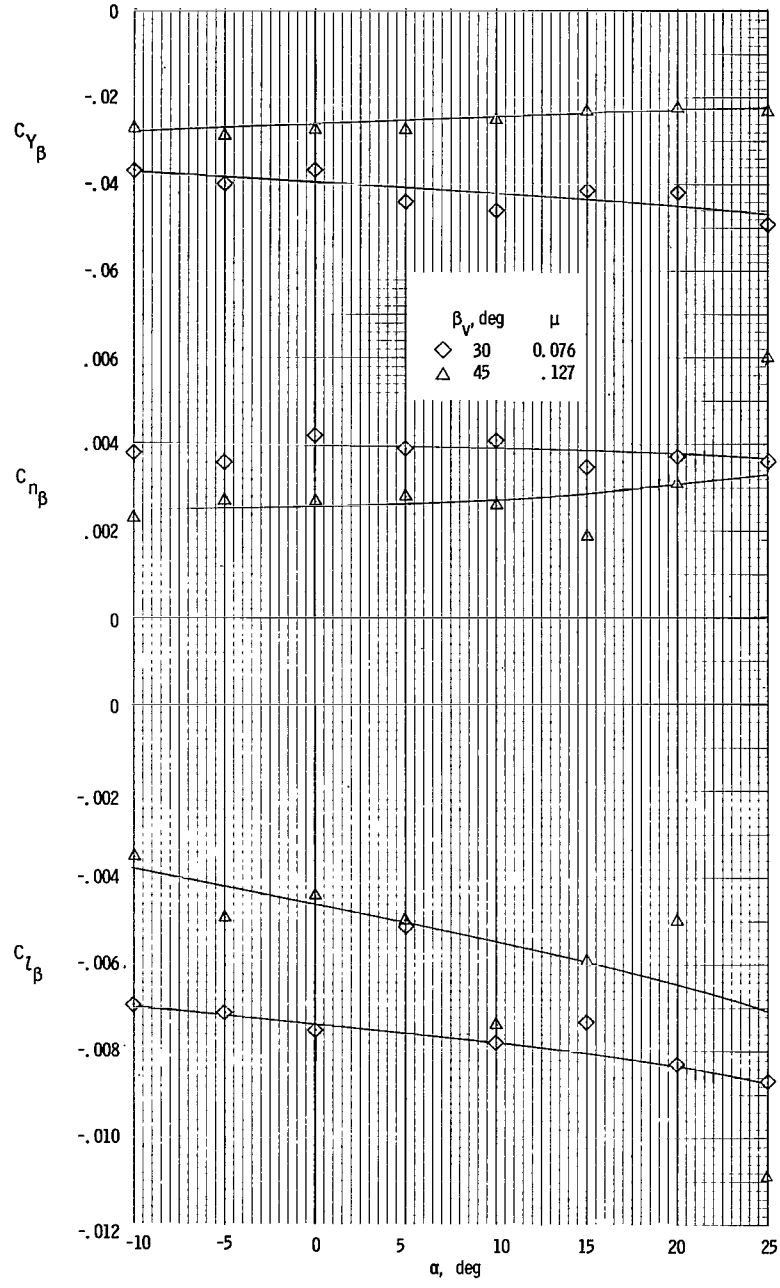

(b) $F_D/F_L = -0.15$ at $\alpha = 0^o$.

Figure 20.- Continued.

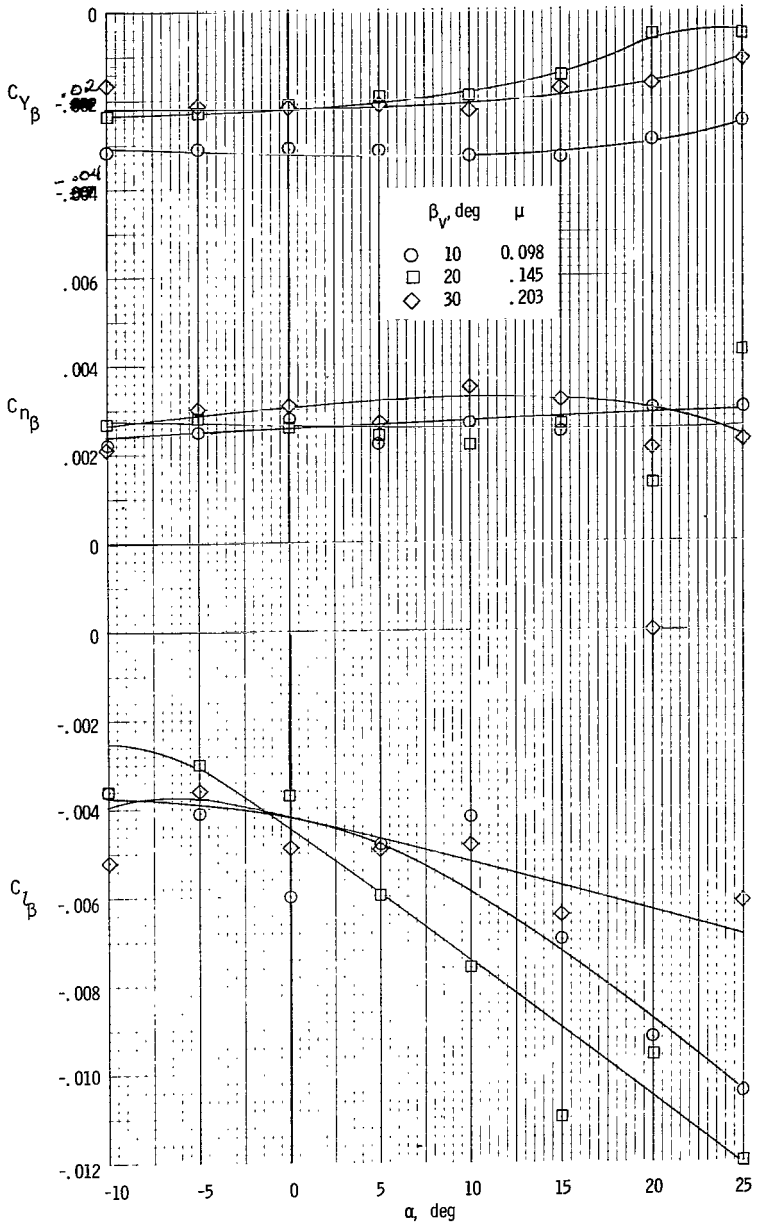

(c) $F_D/F_L = 0.15$ at $\alpha = 0^o$.

Figure 20.- Concluded.

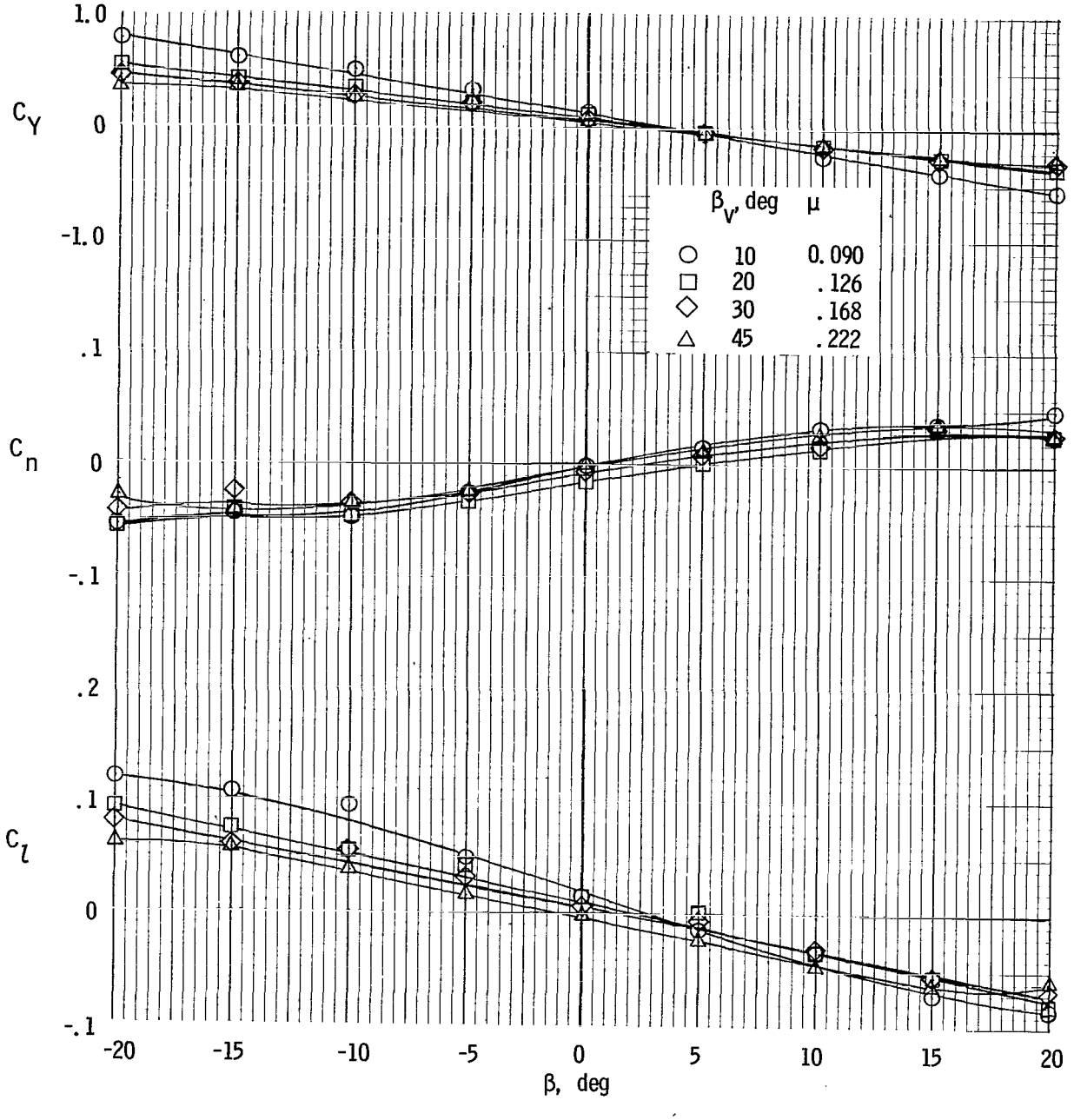

(a) $\alpha = 0^o$, drag trimmed.

Figure 21.- Variation of lateral aerodynamic coefficients with sideslip angle. $\delta_f = 40^o$; $S_h/S_w = 0.25$.

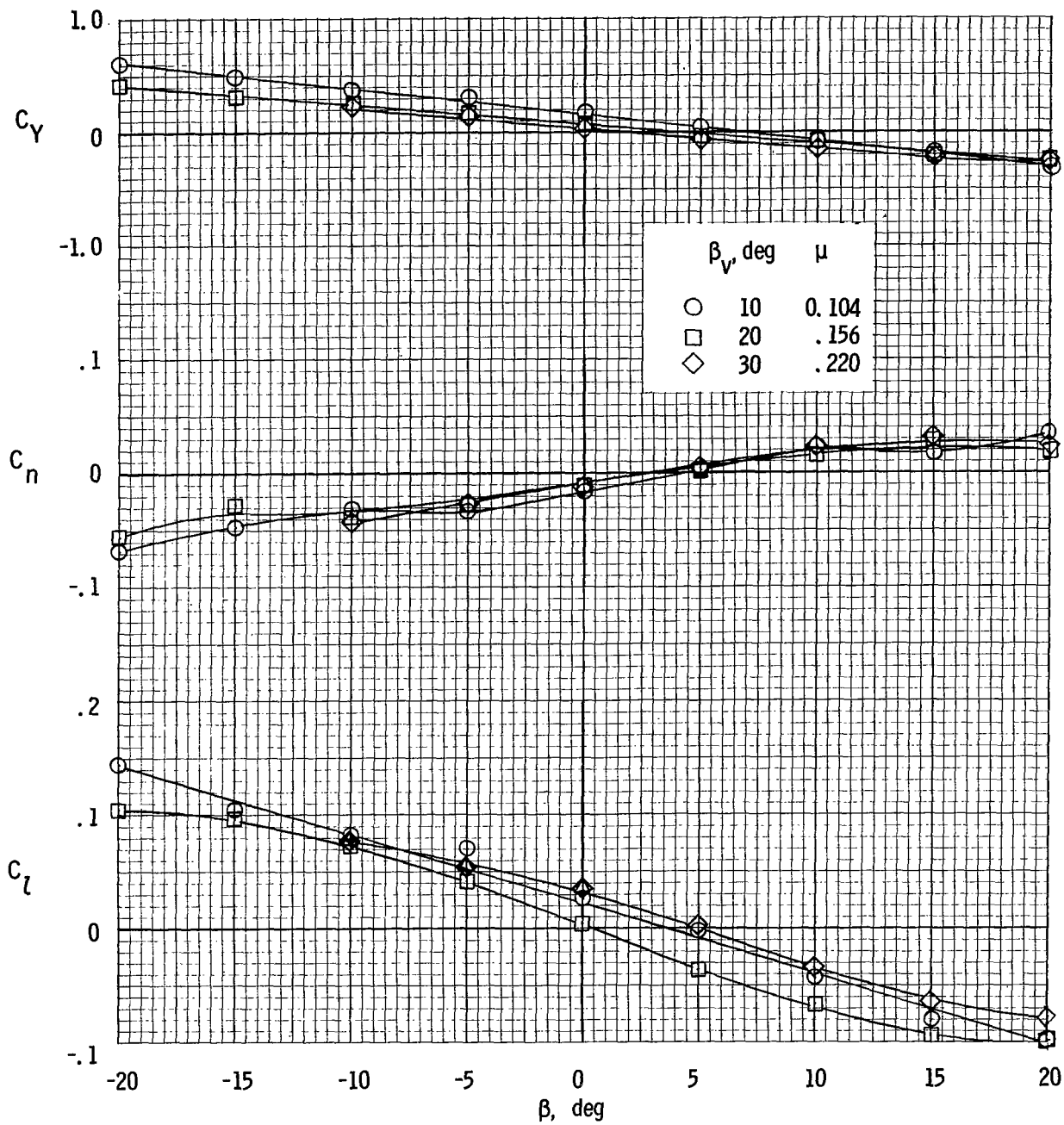

(b) $\alpha = 10^{\circ}$, drag trimmed.

Figure 21.- Concluded.

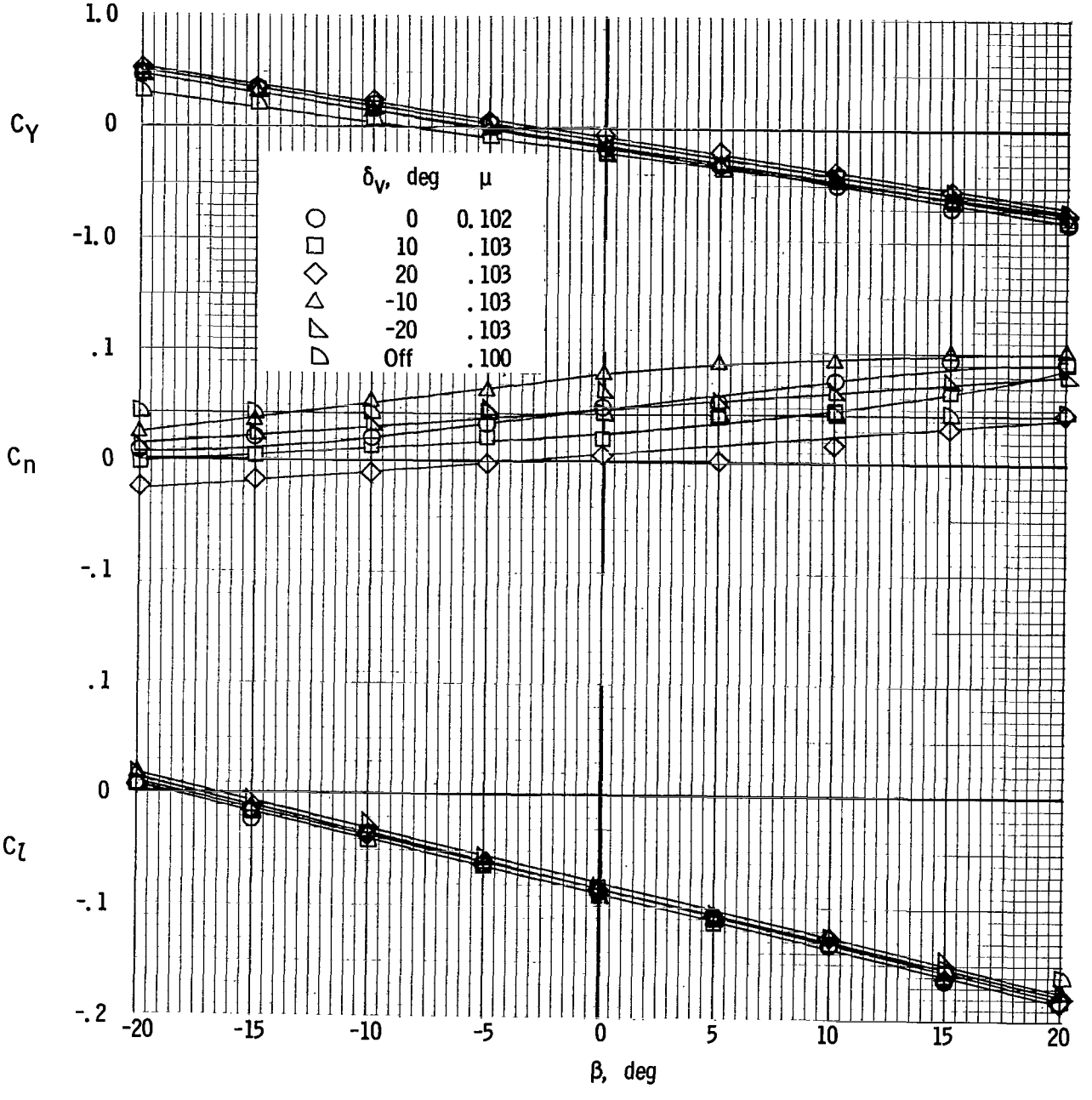

(a) $\beta_V = 10^0$.

Figure 22.- Effect of vertical-tail deflection on lateral-directional characteristics of model with $\delta_f = 0^0$. Drag trimmed at $\alpha = 0^0$.

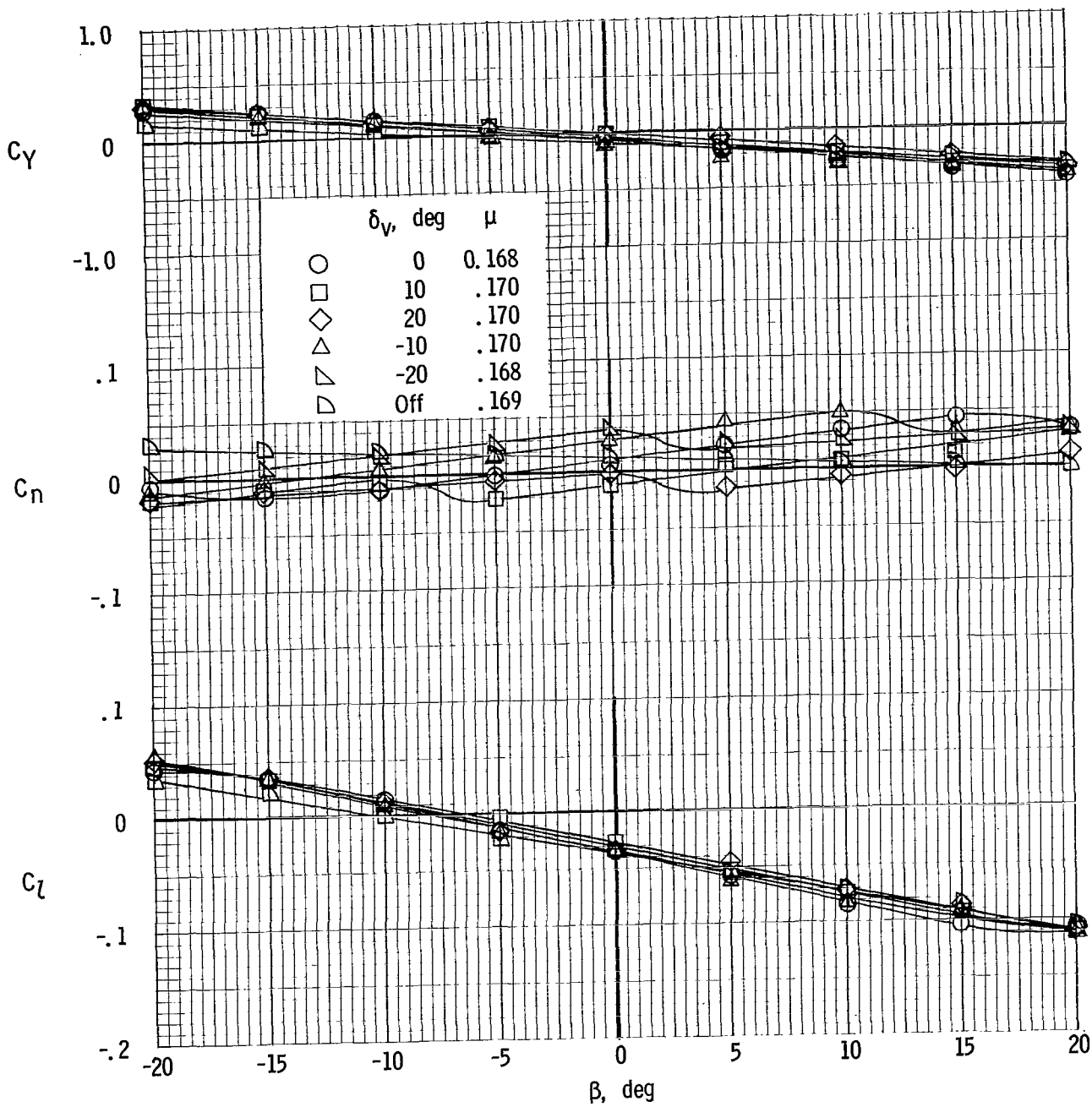

(b) $\beta_V = 20^0$.

Figure 22.- Continued.

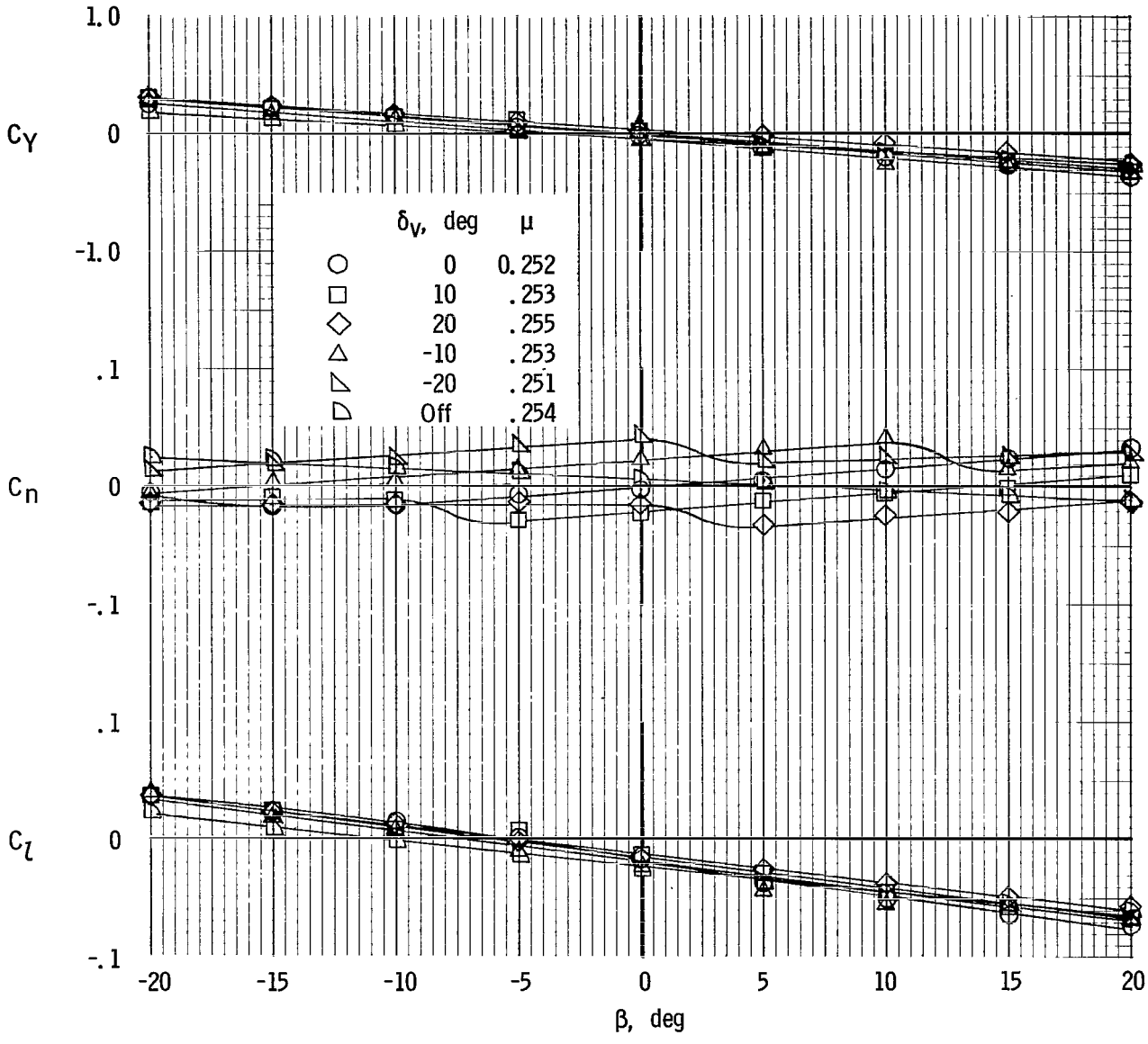

(c) $\beta_V = 30^o$.

Figure 22.- Continued.

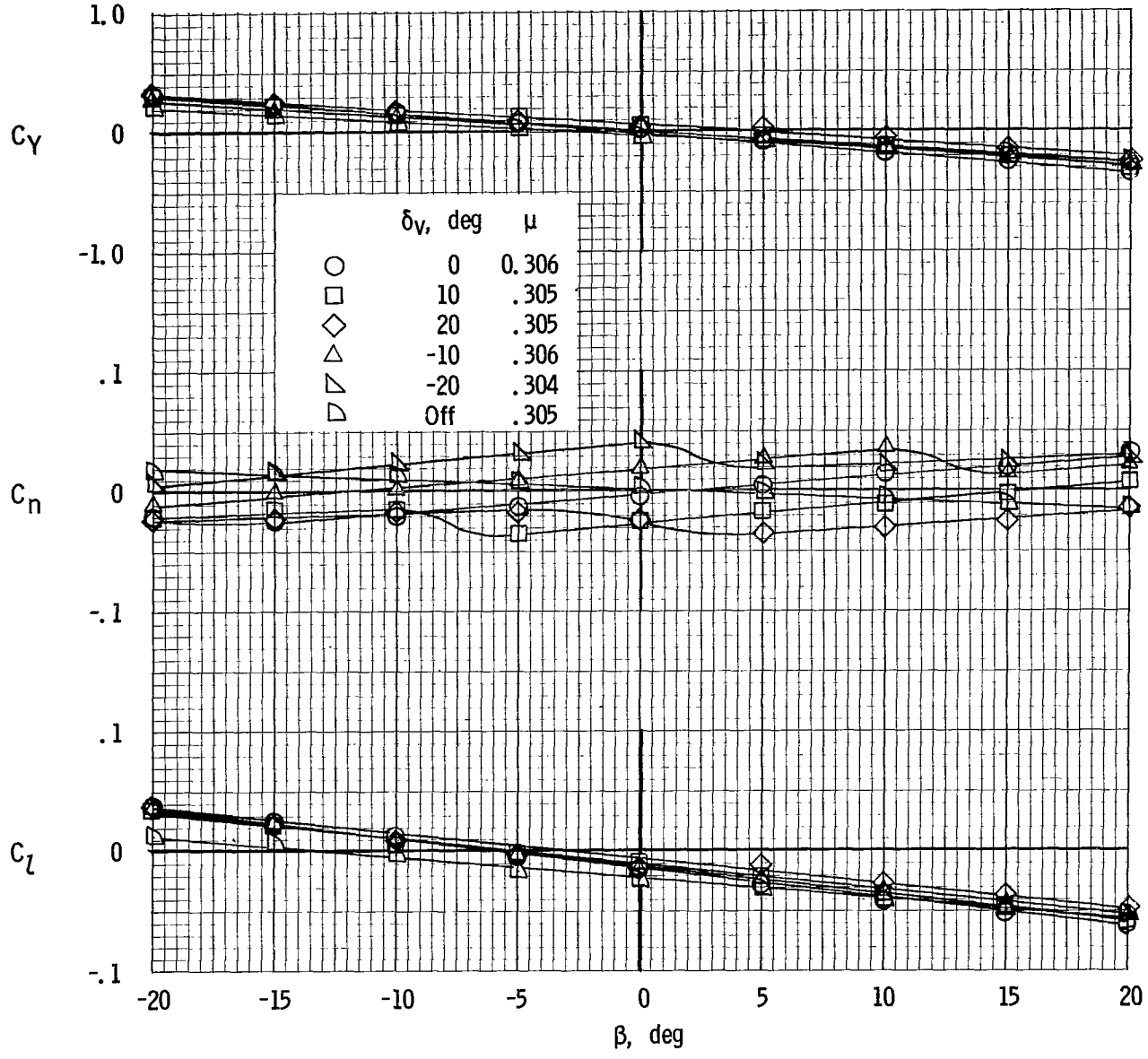

(d) $\beta_V = 45^o$.

Figure 22.- Concluded.

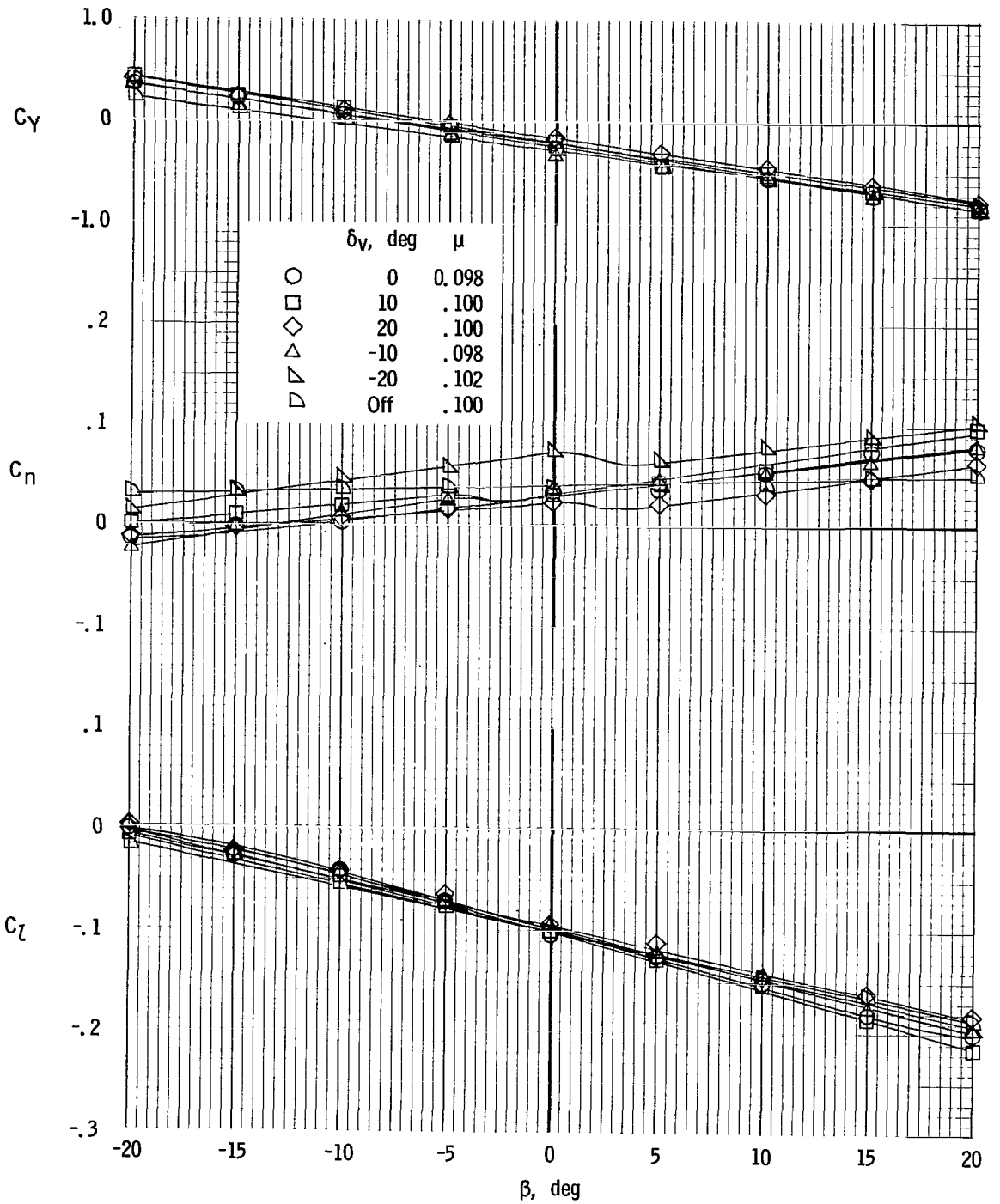

(a) $\beta_V = 10^0$.

Figure 23.- Effect of vertical-tail deflection on lateral-directional characteristics of model with $\delta_f = 40^0$. Drag trimmed at $\alpha = 0^0$.

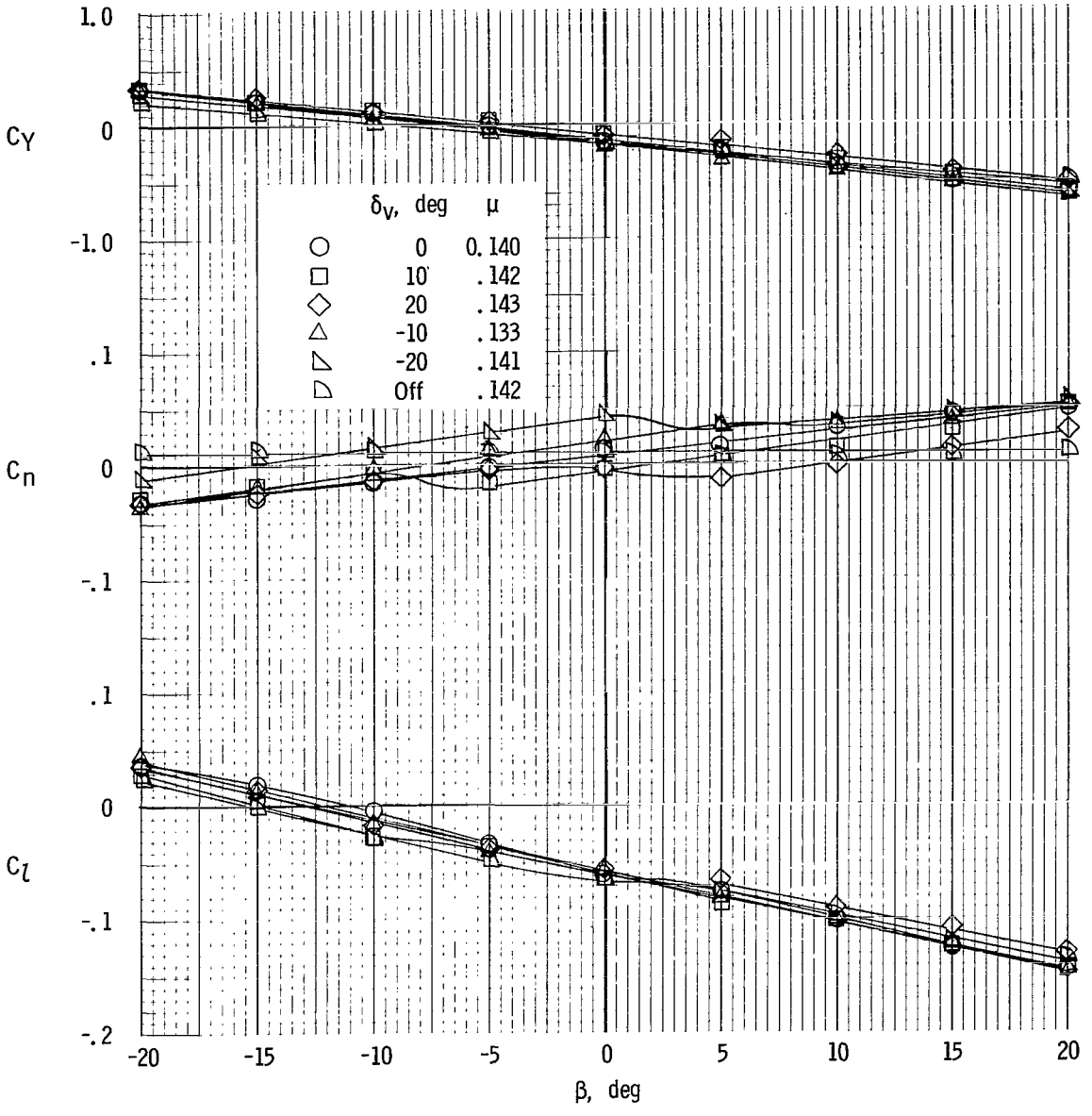

(b) $\beta_V = 20^0$.

Figure 23.- Continued.

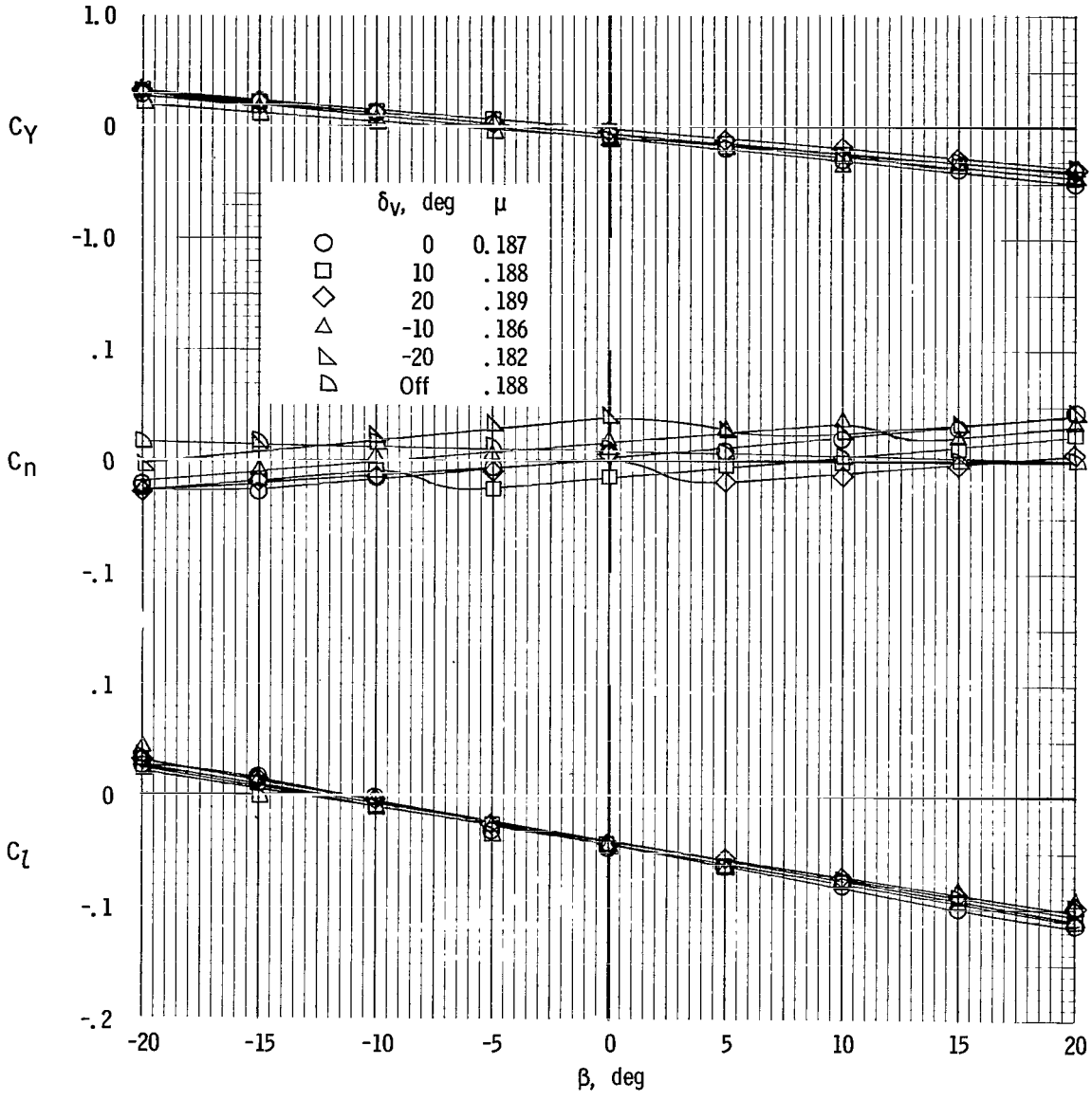

(c) $\beta_V = 30^0$.

Figure 23.- Continued.

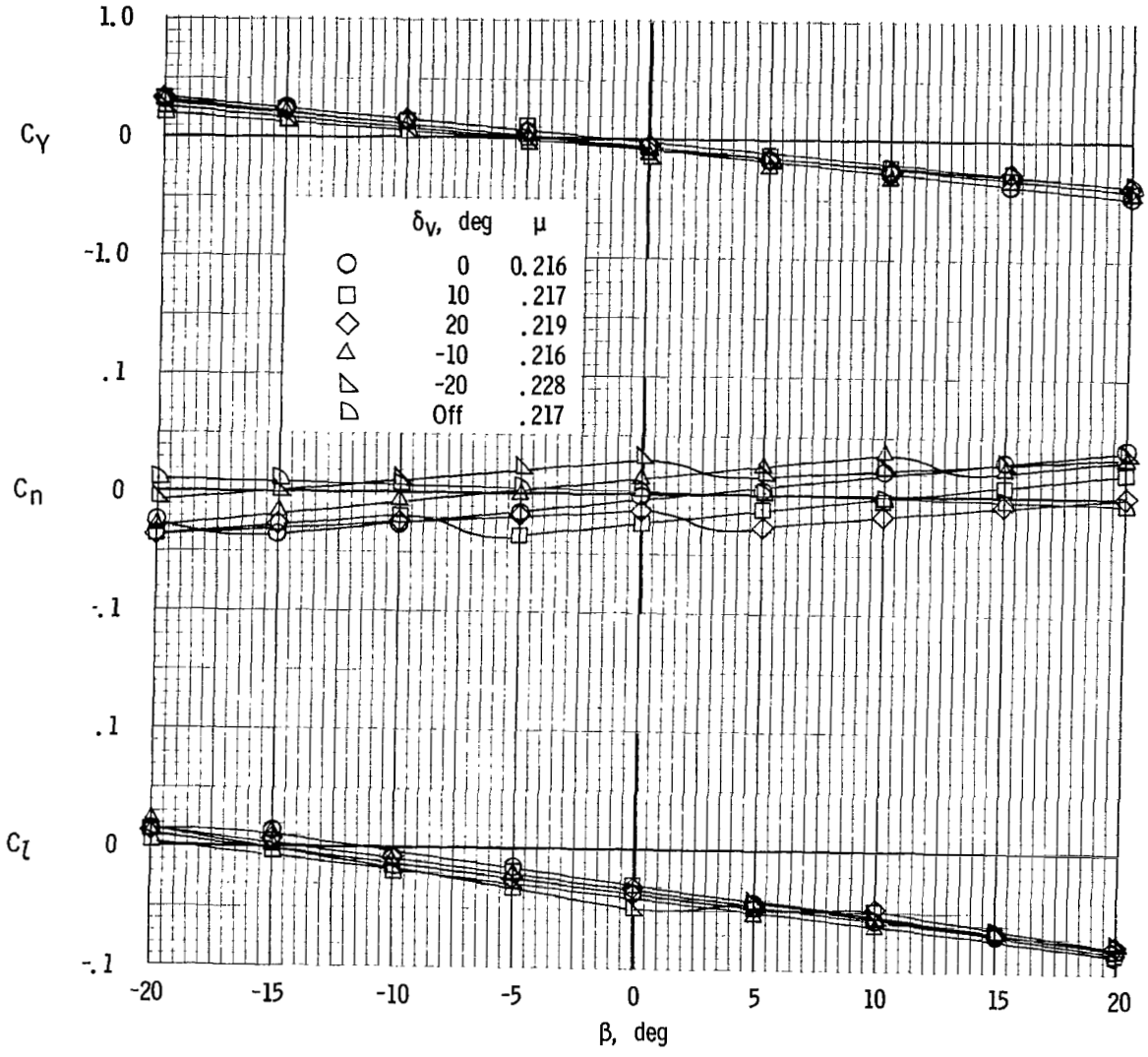

(d) $\beta_V = 45^0$.

Figure 23.- Concluded.

WING

Area	229.5 ft^2 (21.32 m^2)
Span	36.46 ft (11.11 m)
Mean aerodynamic chord	6.91 ft (2.11 m)
Aspect ratio	5.8
Taper ratio	0.3
Airfoil section	NACA 65-412

HORIZONTAL TAIL

Area	61.4 ft^2 (5.70 m^2)
Span	13.98 ft (4.26 m)
Mean aerodynamic chord	4.67 ft (1.42 m)
Aspect ratio	3.2
Taper ratio	0.4
Airfoil section	NACA 64-009

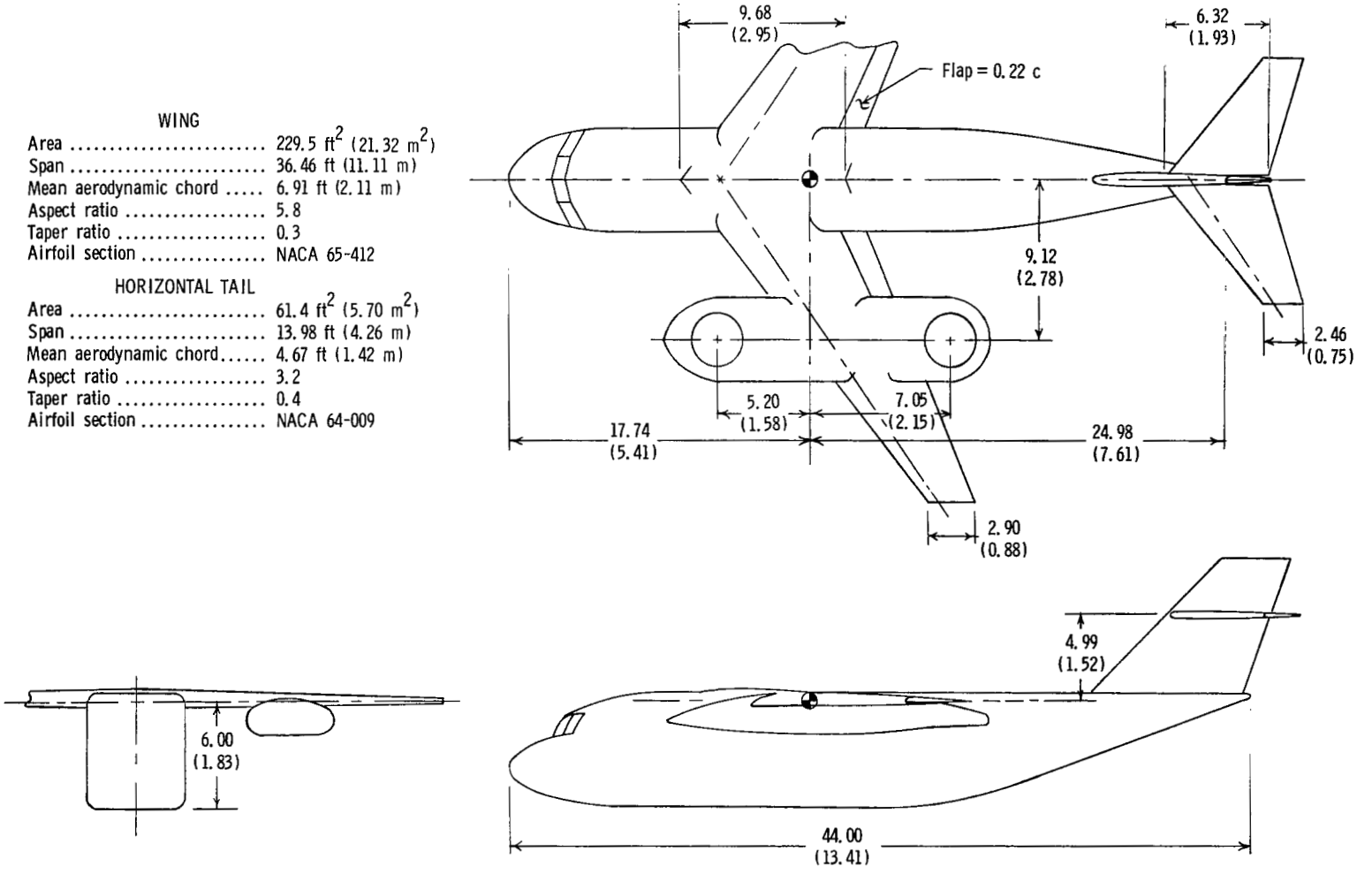

Figure 24.- Sketch of large-scale Ames model. (Dimensions are given first in feet and parenthetically in meters.)

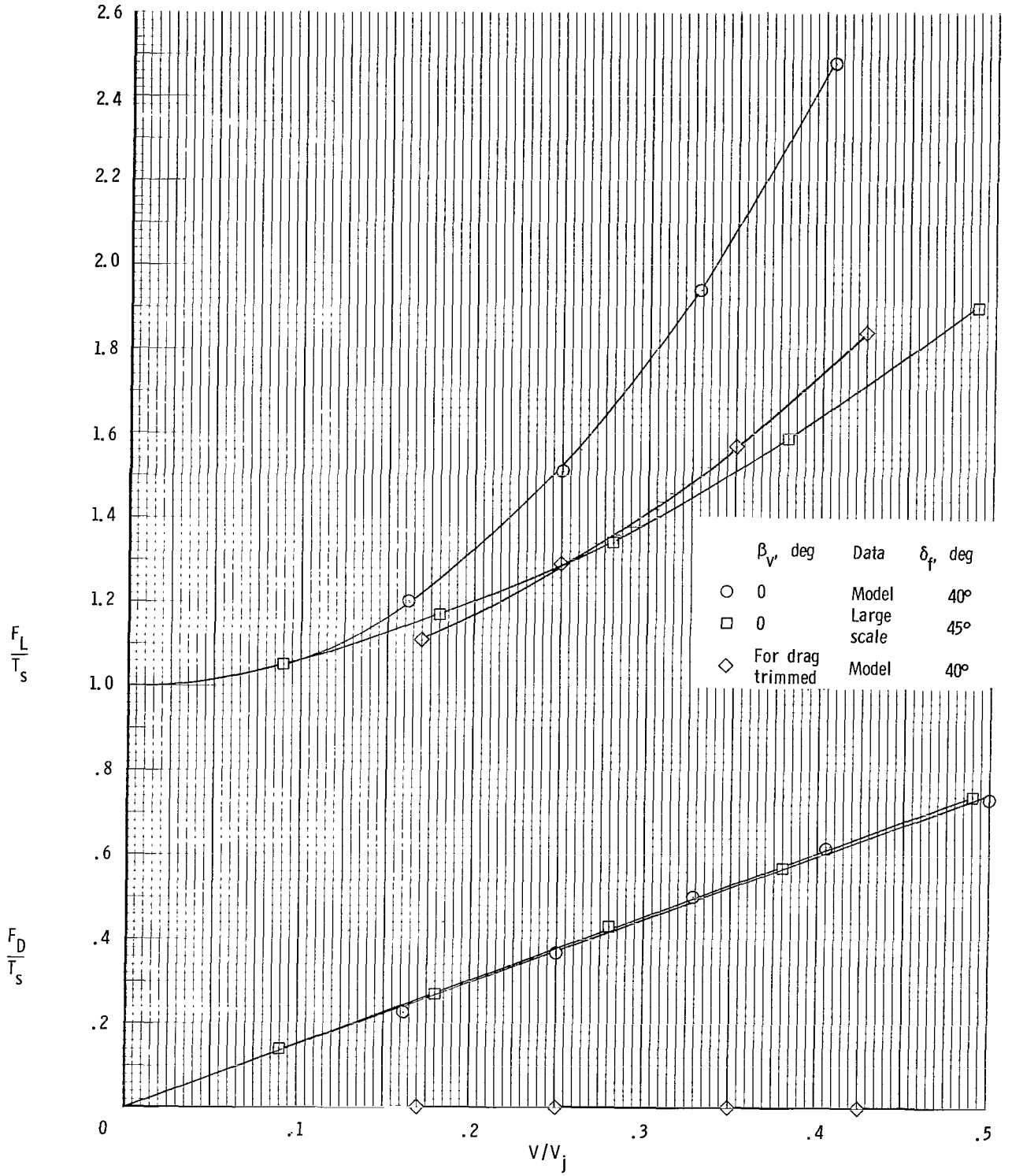

Figure 25.- Variation of lift and drag through transition speed range for constant fan speed. $\alpha = 0^0$.

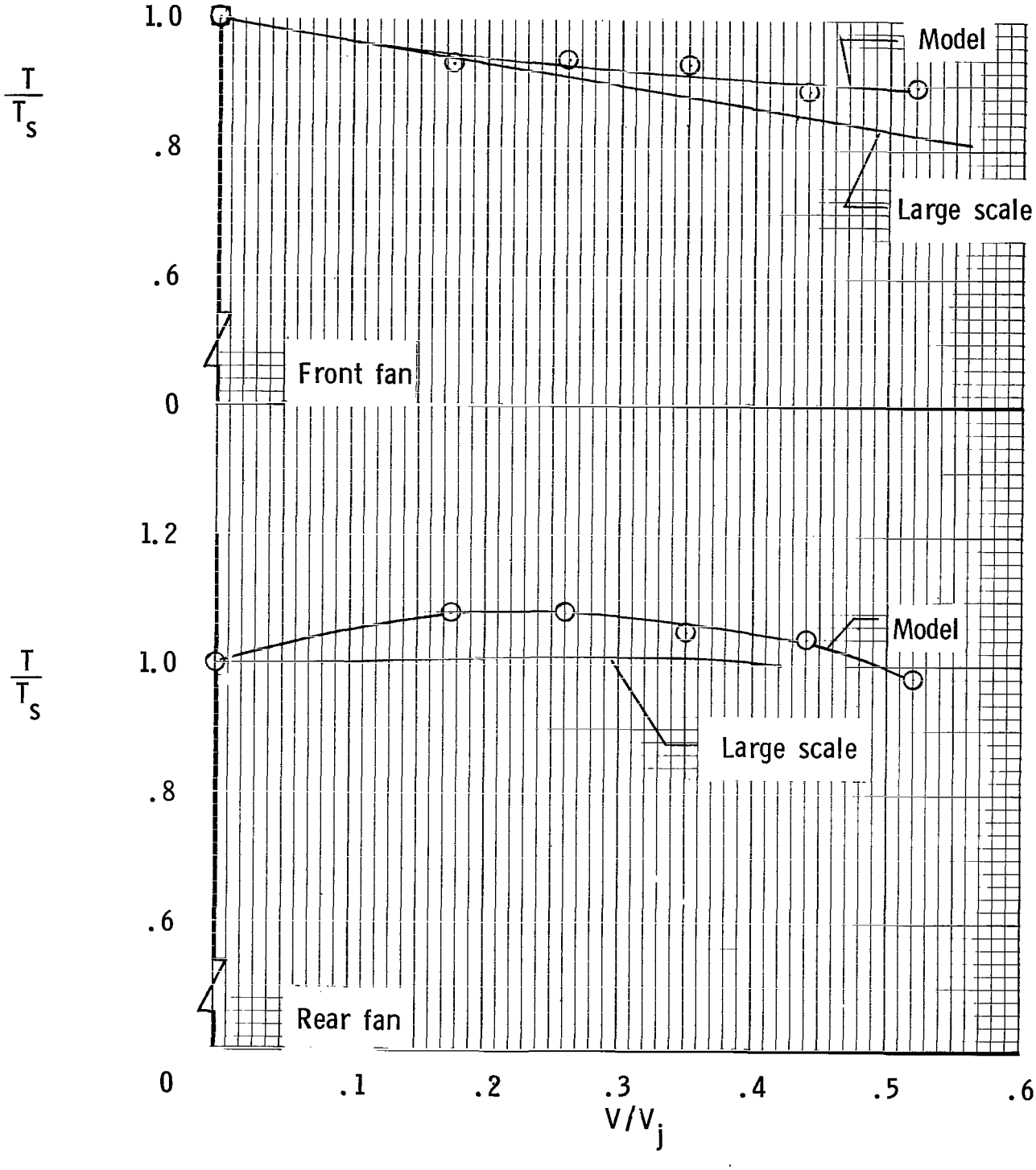

Figure 26.- Comparison of fan thrust characteristics for present model with those for large-scale Ames model. $\beta_v = 0^0$; $\alpha = 0^0$; $\delta_f = 0^0$.

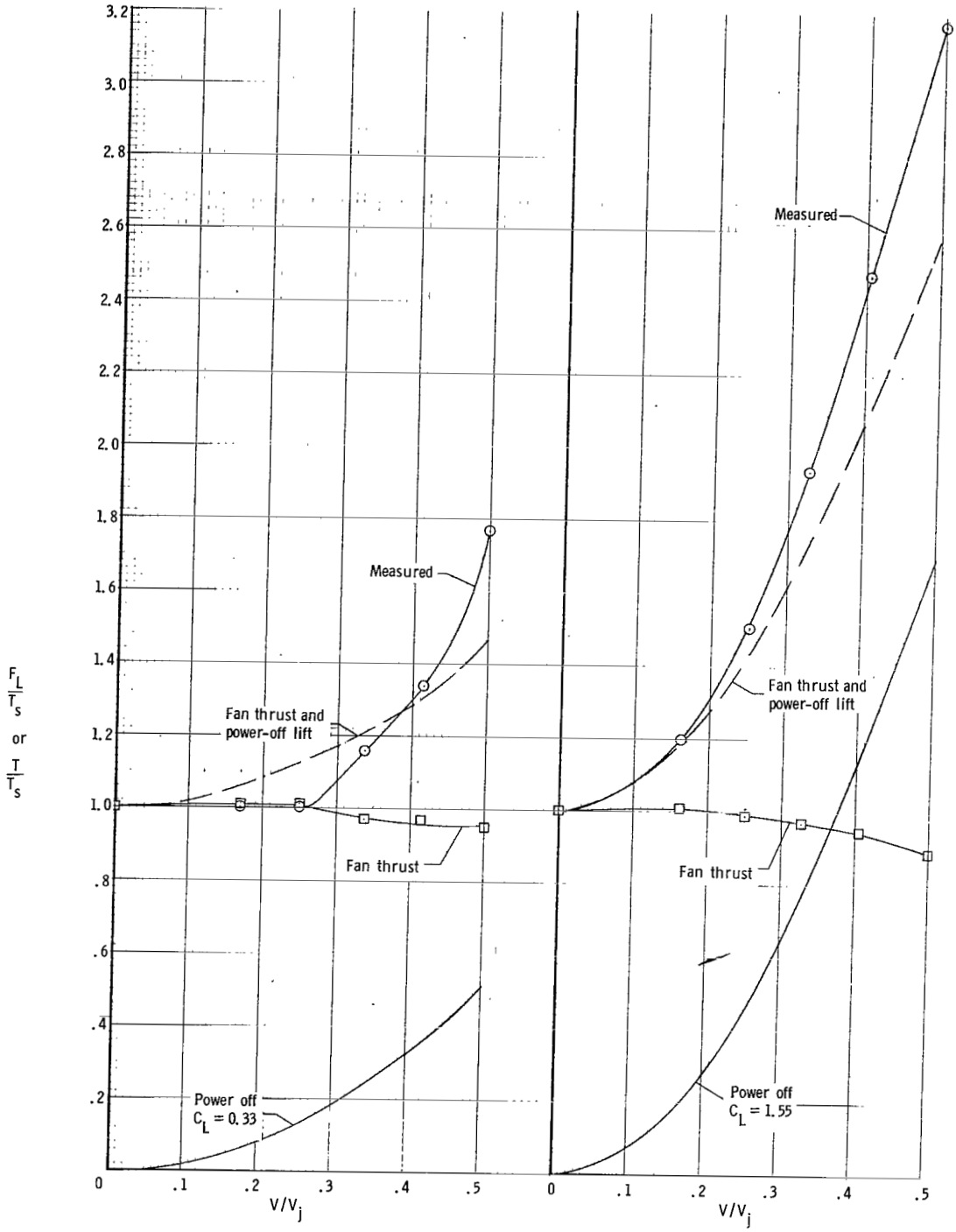

(a) $\delta_f = 0^0$.

(b) $\delta_f = 40^0$.

Figure 27.- Effect of fan operation and forward speed on lift at constant fan speed. $\beta_V = 0^0$; horizontal tail off; $\alpha = 0^0$.

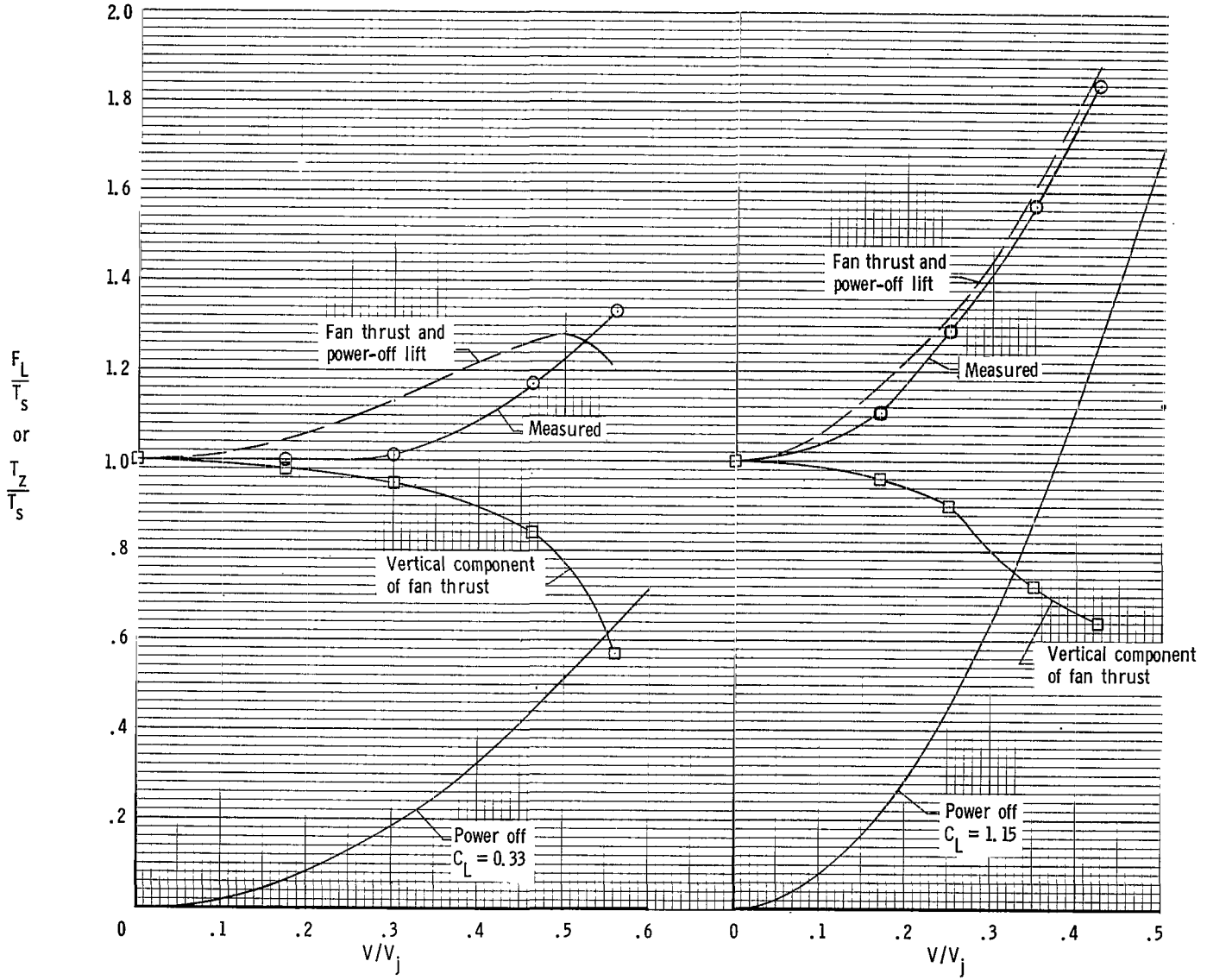

(a) $\delta_f = 0^o$.

(b) $\delta_f = 40^o$.

Figure 28.- Effect of fan operation and forward speed on lift through transition speed range. β_V set to give drag trimmed at $\alpha = 0^o$.

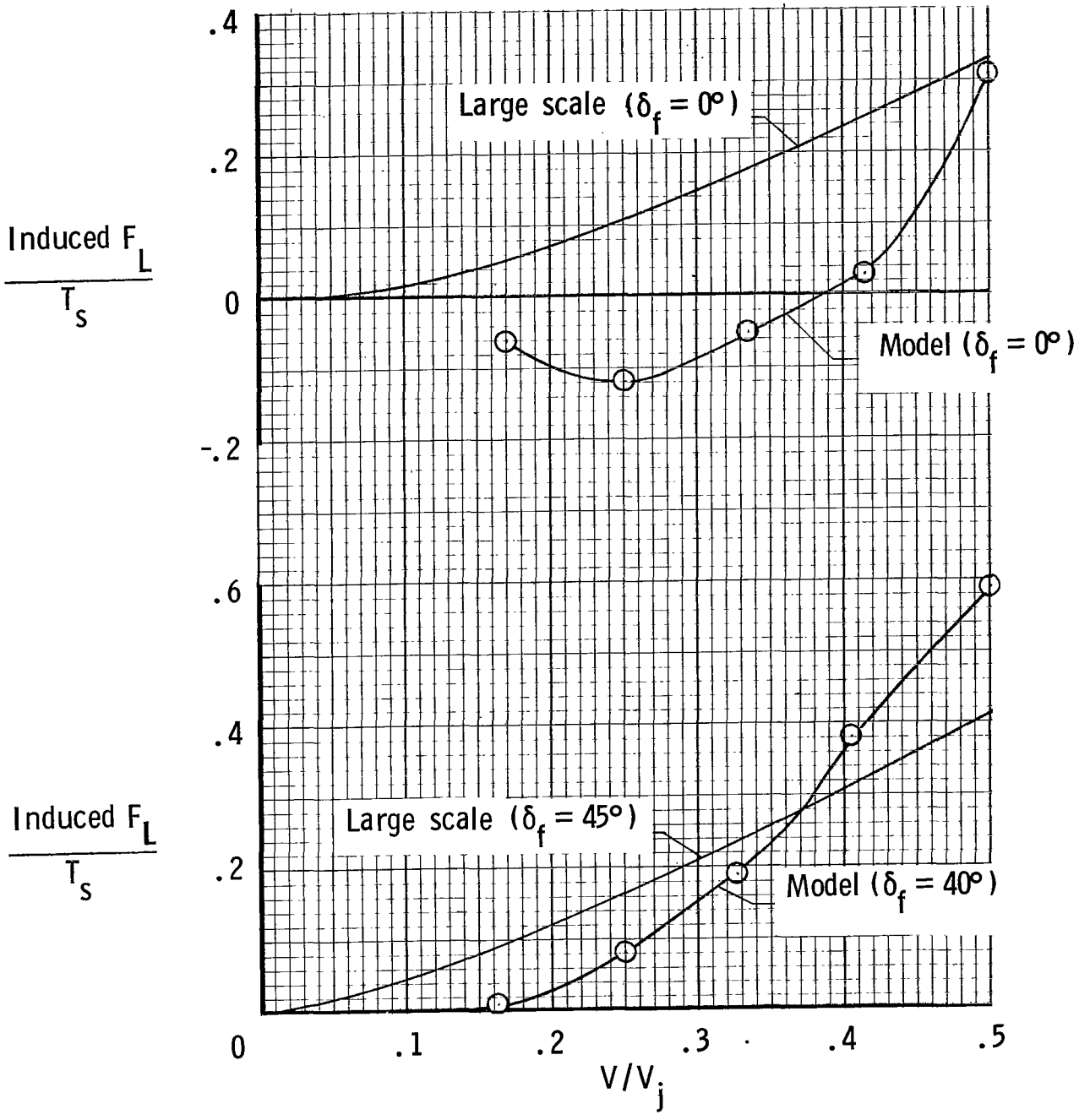

Figure 29.- Comparison of induced lift for present model with that for large-scale Ames model. $\alpha = 0^o$; $\beta_v = 0^o$.

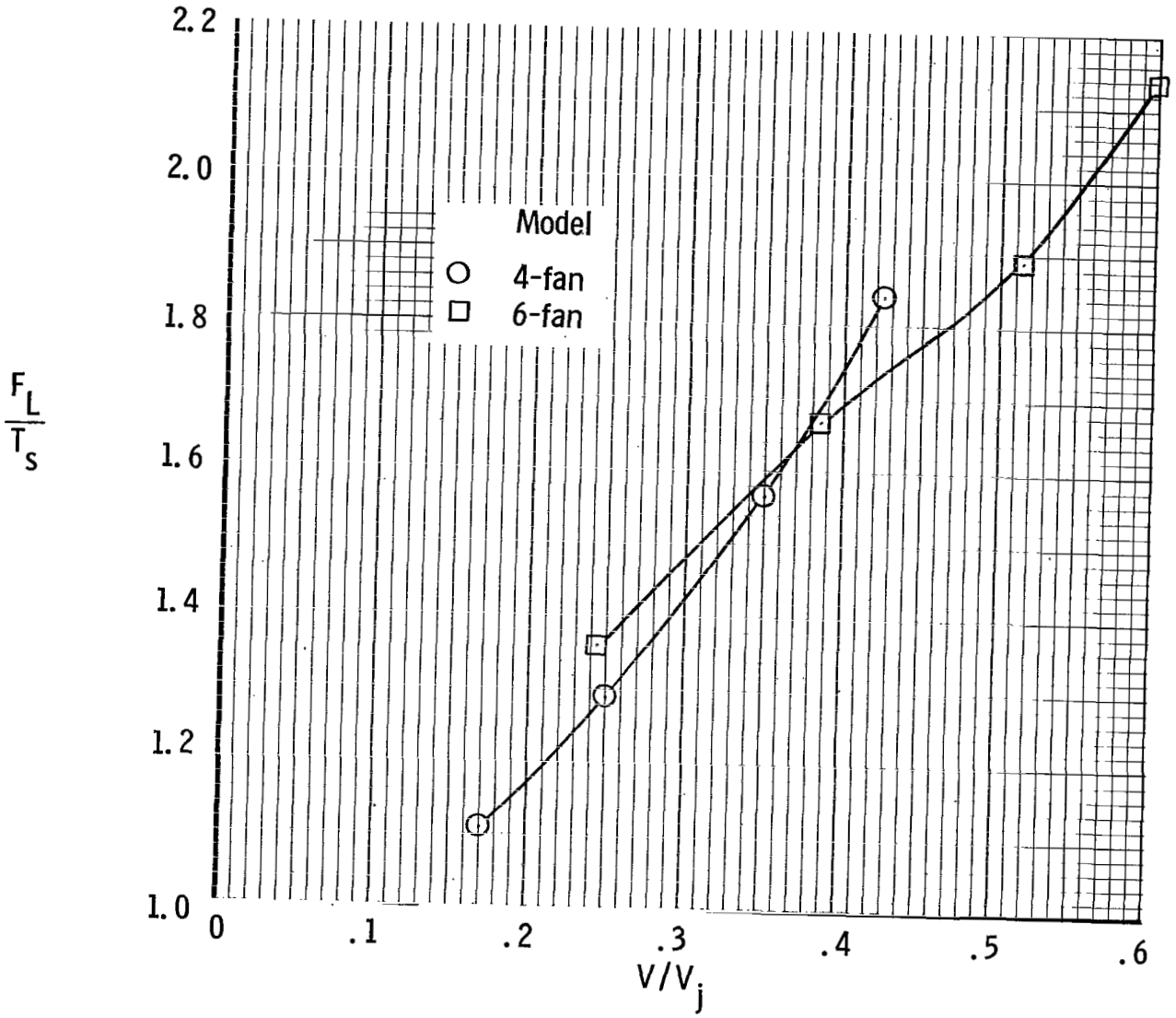

Figure 30.- Comparison of lift characteristics of present model with those of six-fan model of reference 3. $\delta_f = 40^0$; drag trimmed at $\alpha = 0^0$.

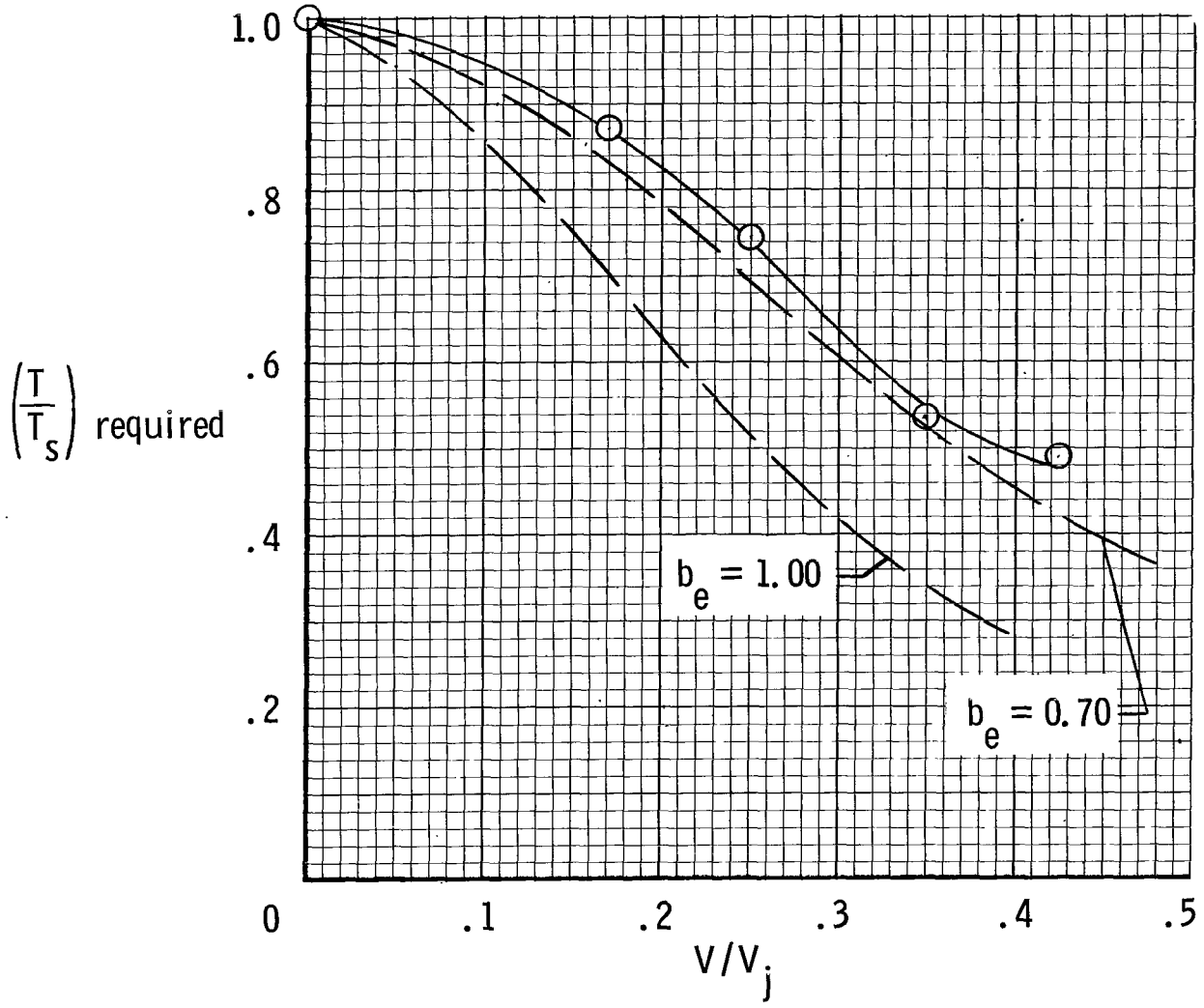

Figure 31.- Variation of thrust required with forward speed compared with theory (ref. 4). $\delta_f = 40^0$; drag trimmed at $\alpha = 0^0$.

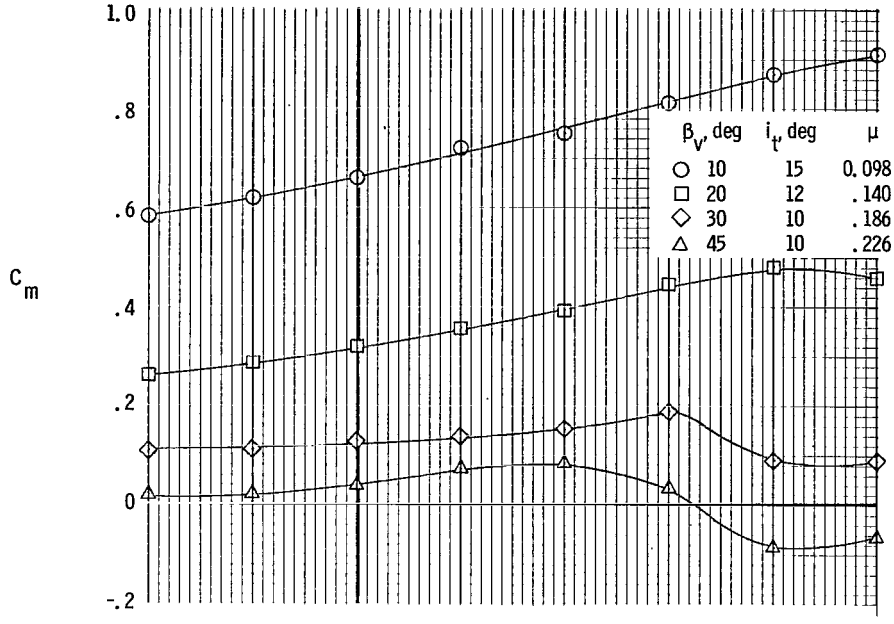

(a) $S_h/S_w = 0.25$.

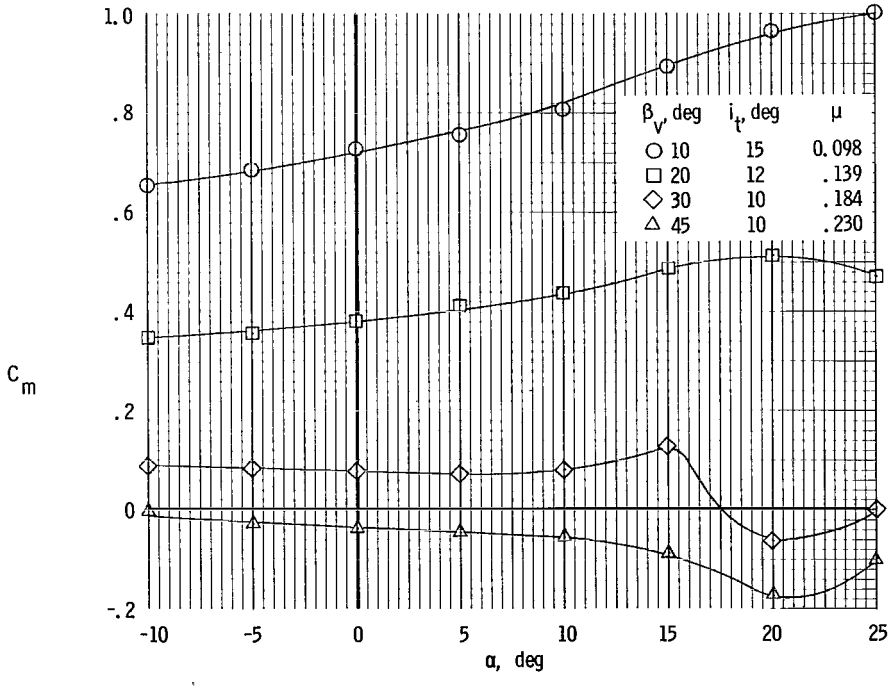

(b) $S_h/S_w = 0.30$.

Figure 32.- Variation of pitching-moment coefficient with angle of attack through transition speed range. $\delta_f = 40^0$; drag trimmed at $\alpha = 0^0$.

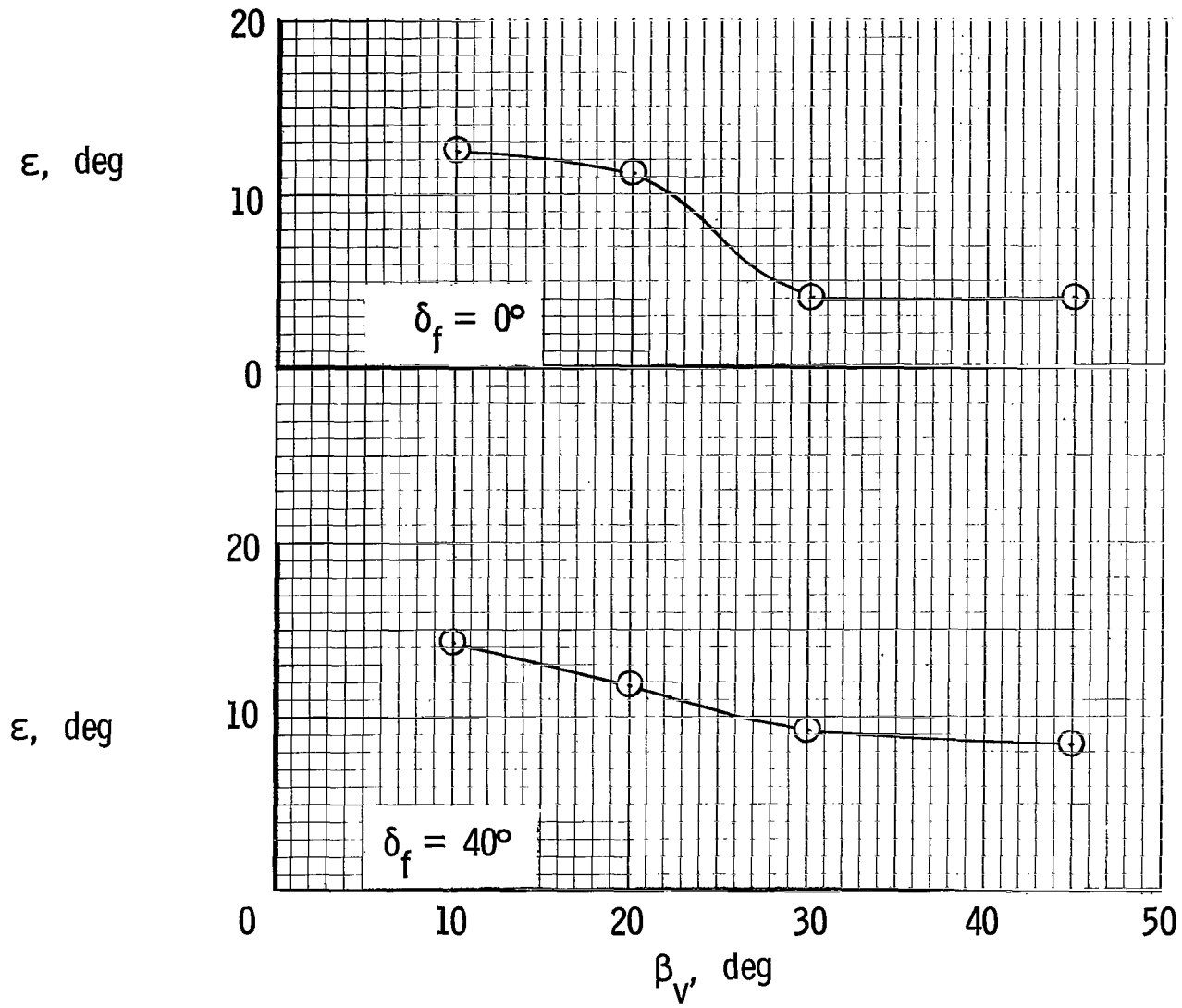

Figure 33.- Variation of downwash angle through transition speed range. Drag trimmed at $\alpha = 0^0$.

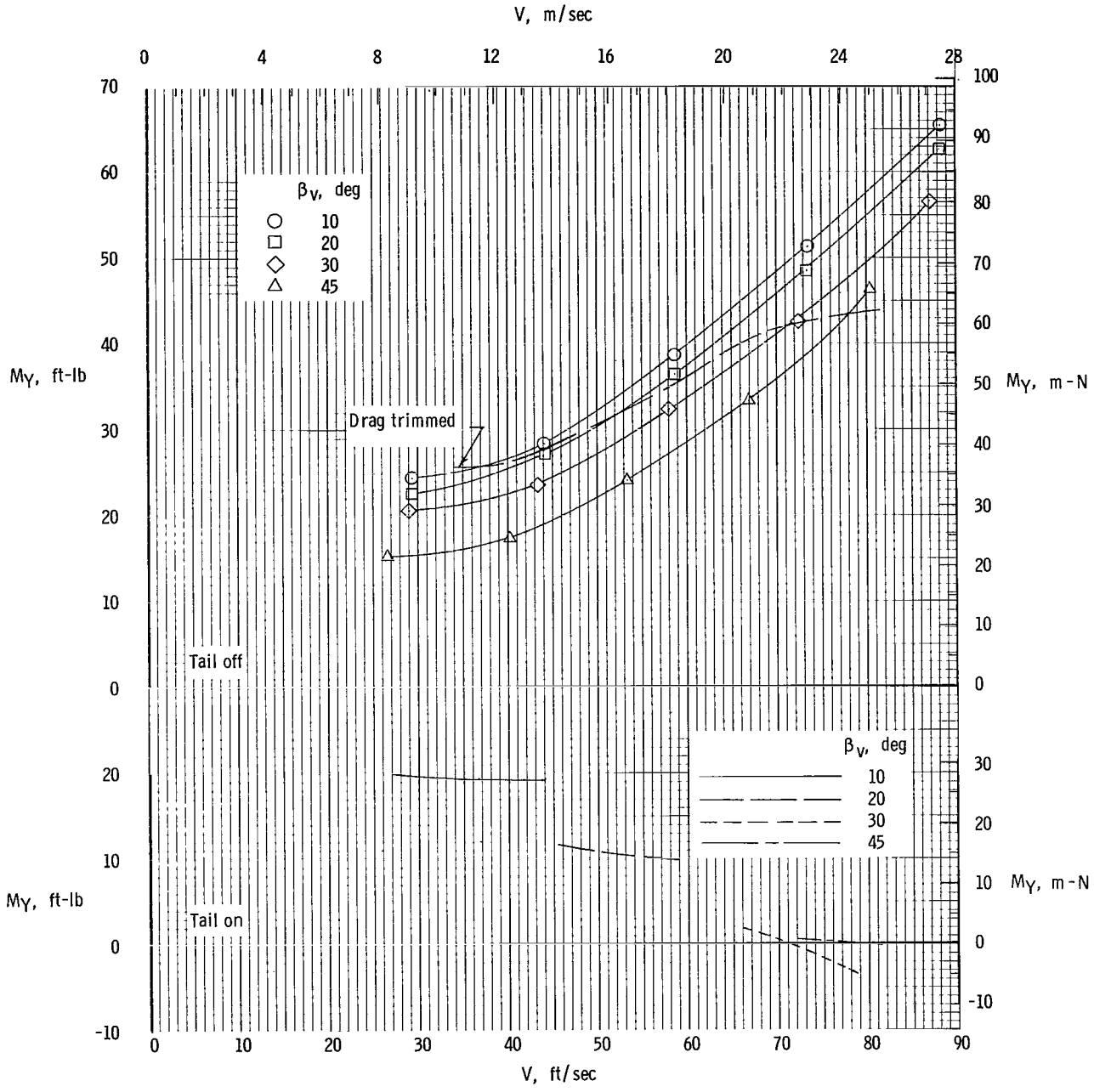

(a) $\delta_f = 0^0$.

Figure 34.- Variation of pitching moment with velocity for model with tail off and with i_t set to give minimum pitching moment in steady level flight. $\alpha = 0^0$; $F_L = 80$ lb (355 N); $S_h/S_w = 0.25$.

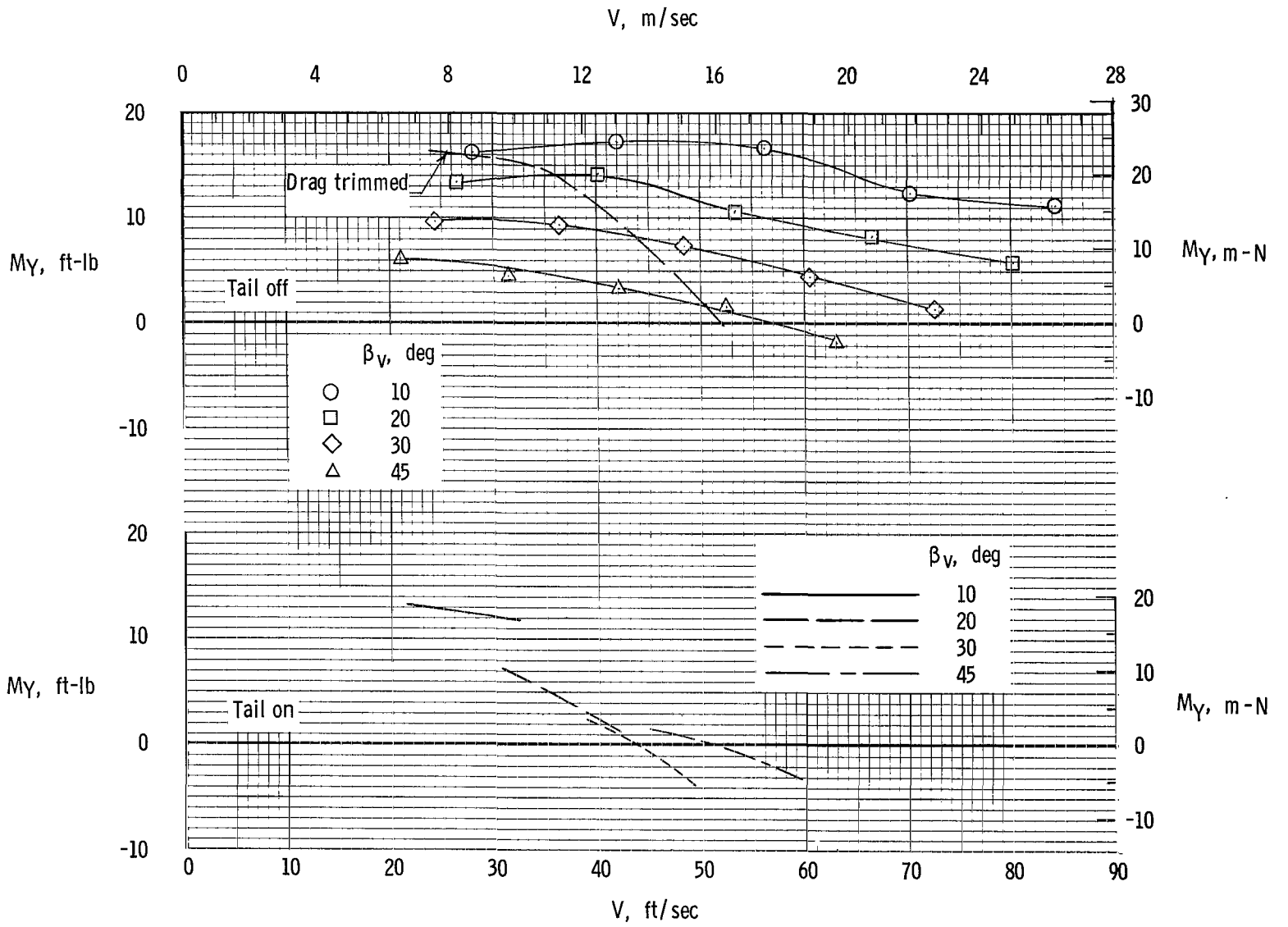

(b) $\delta_f = 40^o$.

Figure 34.- Concluded.

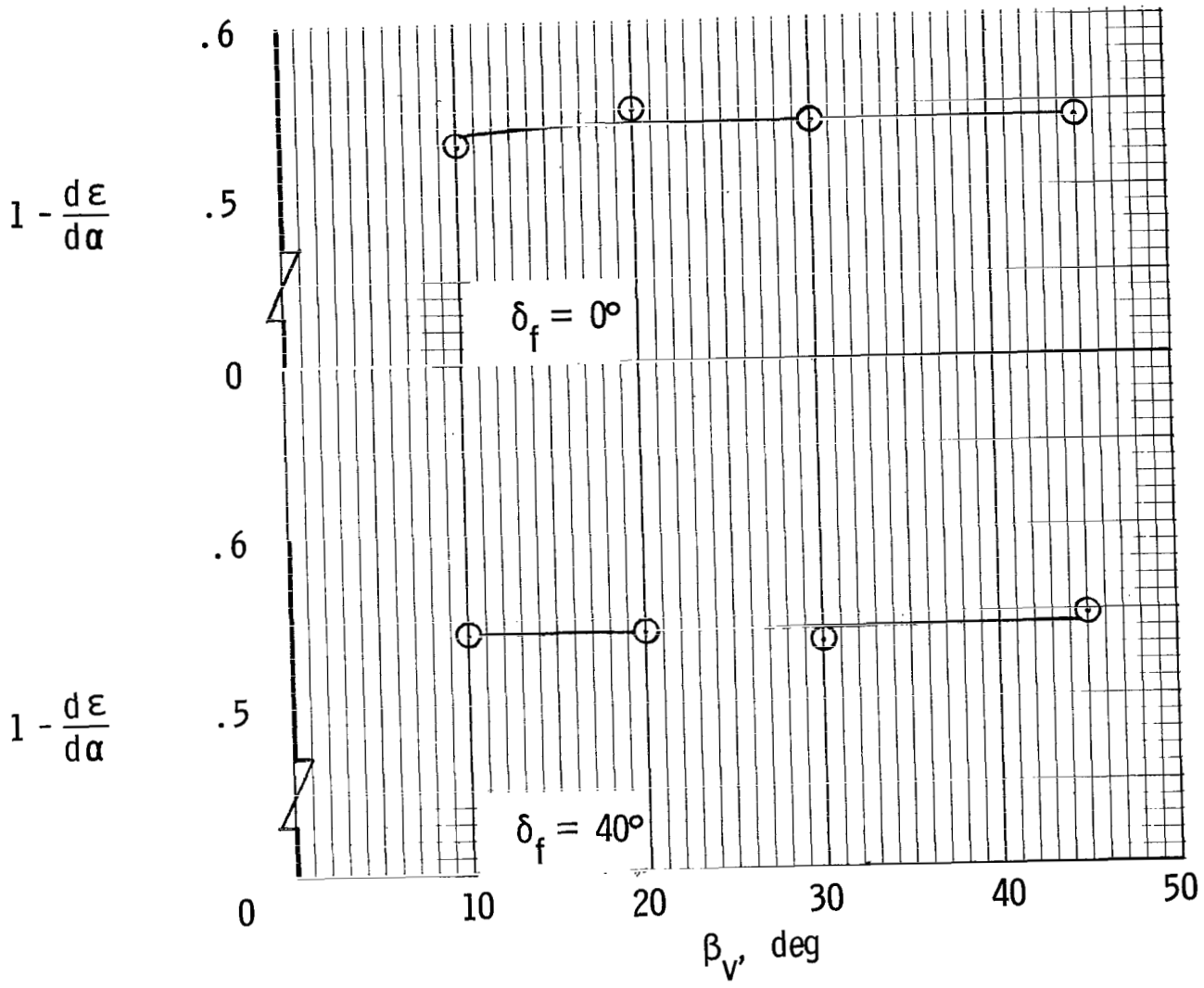

Figure 35.- Variation of downwash factor through transition speed range. Drag trimmed at $\alpha = 0^o$.

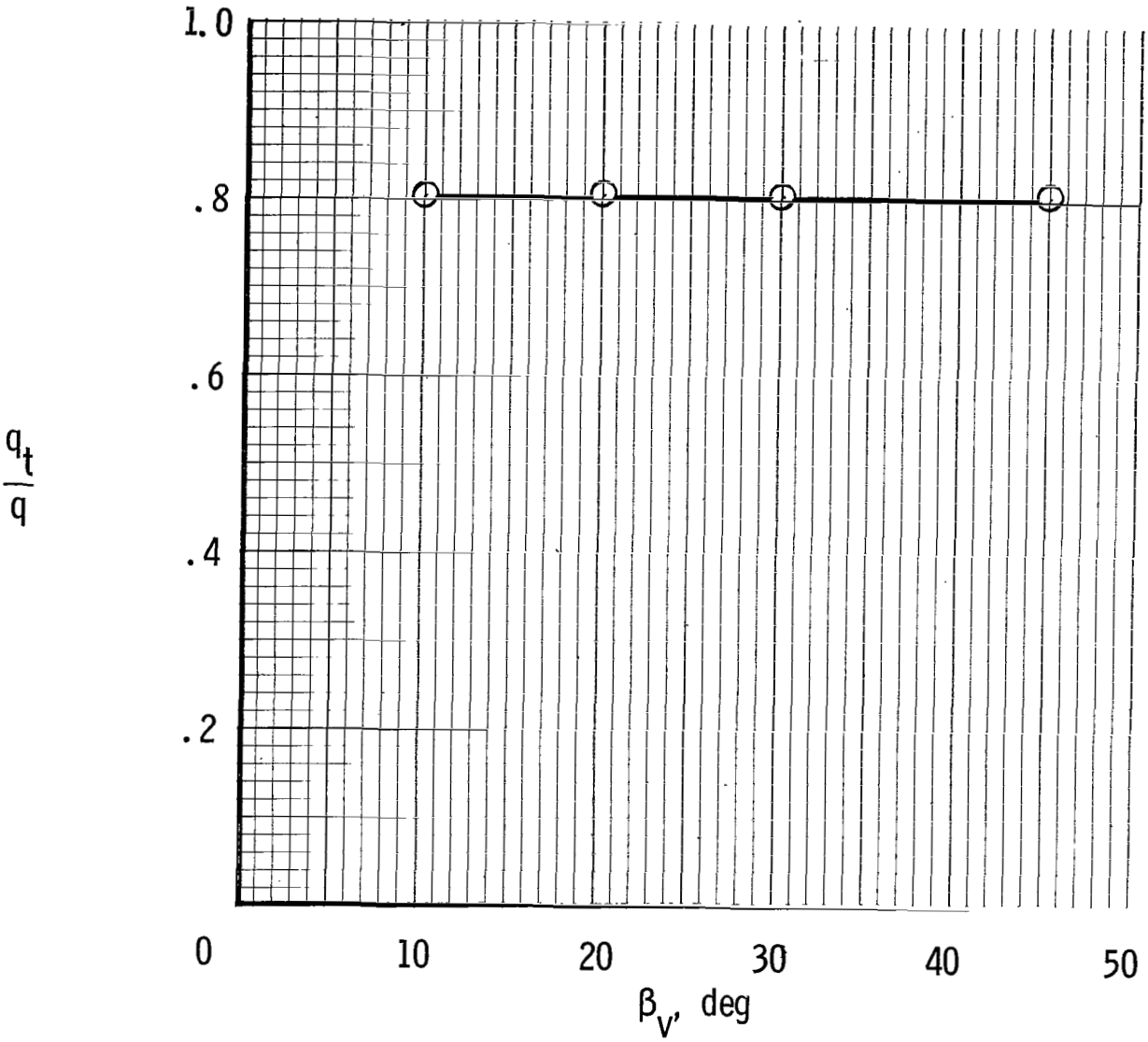

Figure 36.- Variation of dynamic pressure ratio at tail with fan-exit-vane deflection through transition speed range. $\delta_f = 40^0$; drag trimmed at $\alpha = 0^0$.

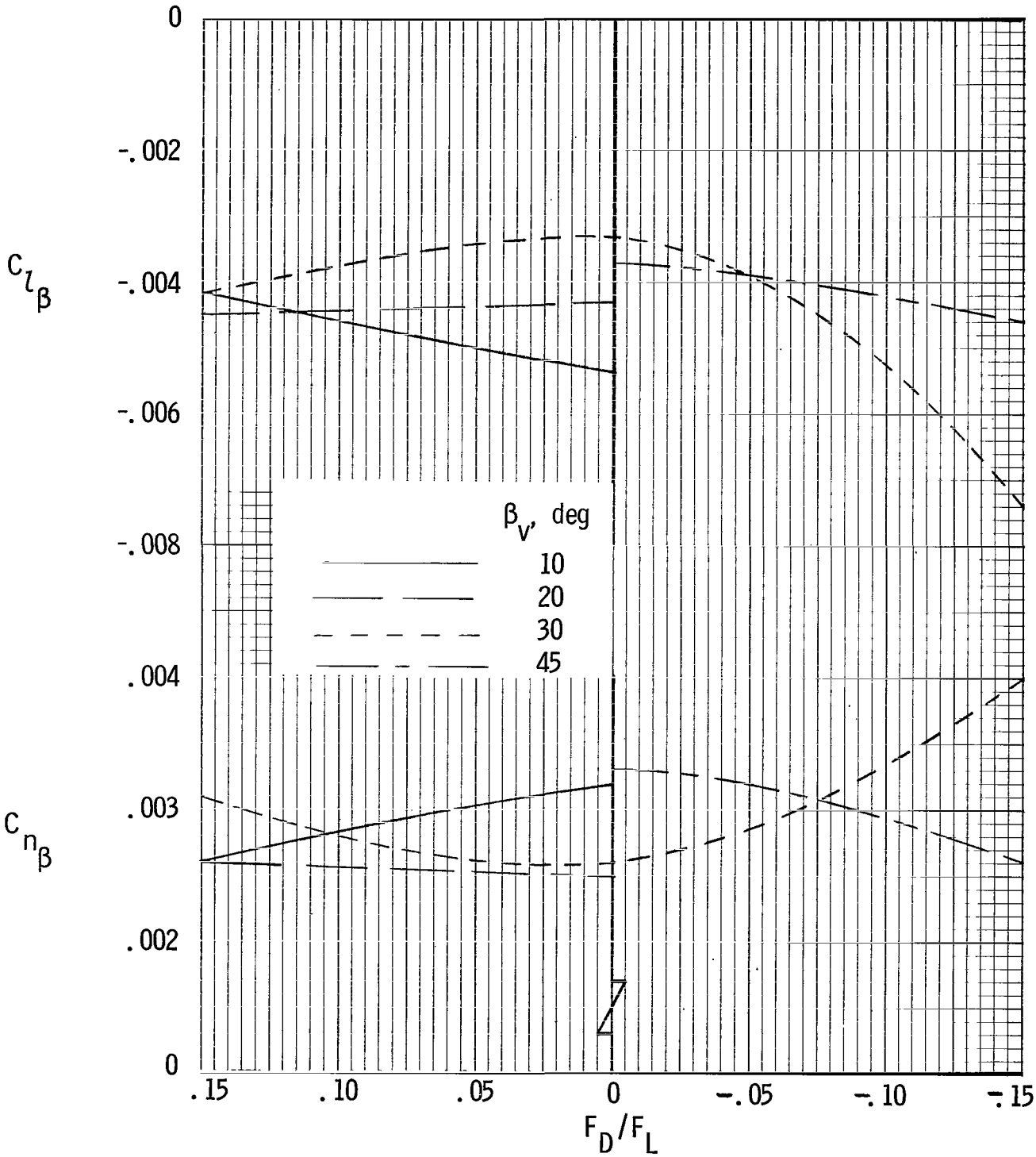

Figure 37.- Static directional stability and effective dihedral for various power conditions through transition speed range. $\delta_f = 40^0$; $\alpha = 0^0$.

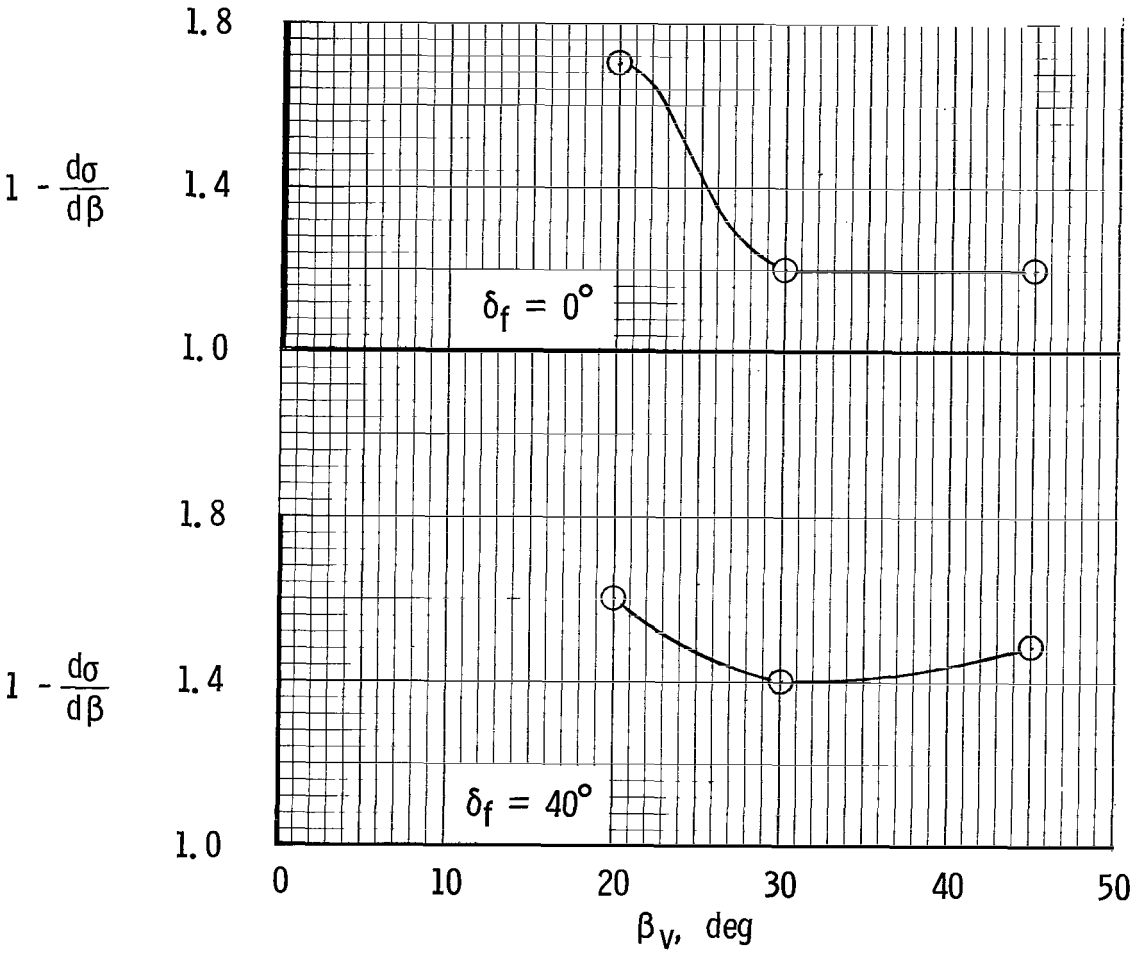

Figure 38. - Variation of sidewash factor with fan-exit-vane deflection through transition speed range. Drag trimmed at $\alpha = 0°$.

Issued 10-16-70

NATIONAL AERONAUTICS AND SPACE ADMINISTRATION
WASHINGTON, D. C. 20546

OFFICIAL BUSINESS

FIRST CLASS MAIL

POSTAGE AND FEES PAID
NATIONAL AERONAUTICS AND
SPACE ADMINISTRATION

05U 001 27 51 3DS 70212 00903
AIR FORCE WEAPONS LABORATORY /WLOL/
KIRTLAND AFB, NEW MEXICO 87117

ATT E. LOU BOWMAN, CHIEF,TECH. LIBRARY

POSTMASTER: If Undeliverable (Section 158 Postal Manual) Do Not Return

"The aeronautical and space activities of the United States shall be conducted so as to contribute . . . to the expansion of human knowledge of phenomena in the atmosphere and space. The Administration shall provide for the widest practicable and appropriate dissemination of information concerning its activities and the results thereof."

—NATIONAL AERONAUTICS AND SPACE ACT OF 1958

NASA SCIENTIFIC AND TECHNICAL PUBLICATIONS

TECHNICAL REPORTS: Scientific and technical information considered important, complete, and a lasting contribution to existing knowledge.

TECHNICAL NOTES: Information less broad in scope but nevertheless of importance as a contribution to existing knowledge.

TECHNICAL MEMORANDUMS: Information receiving limited distribution because of preliminary data, security classification, or other reasons.

CONTRACTOR REPORTS: Scientific and technical information generated under a NASA contract or grant and considered an important contribution to existing knowledge.

TECHNICAL TRANSLATIONS: Information published in a foreign language considered to merit NASA distribution in English.

SPECIAL PUBLICATIONS: Information derived from or of value to NASA activities. Publications include conference proceedings, monographs, data compilations, handbooks, sourcebooks, and special bibliographies.

TECHNOLOGY UTILIZATION PUBLICATIONS: Information on technology used by NASA that may be of particular interest in commercial and other non-aerospace applications. Publications include Tech Briefs, Technology Utilization Reports and Notes, and Technology Surveys.

Details on the availability of these publications may be obtained from:

SCIENTIFIC AND TECHNICAL INFORMATION DIVISION

NATIONAL AERONAUTICS AND SPACE ADMINISTRATION

Washington, D.C. 20546